DIELECTRIC-LOADED MICROWAVE CAVITY FOR HIGH-GRADIENT TESTING OF SUPERCONDUCTING MATERIALS

A Dissertation

by

NATHANIEL JOHNSTON POGUE

Submitted to the Office of Graduate Studies of
Texas A&M University
in partial fulfillment of the requirements for the degree of

DOCTOR OF PHILOSOPHY

May 2011

Major Subject: Physics

DIELECTRIC-LOADED MICROWAVE CAVITY FOR HIGH-GRADIENT TESTING OF SUPERCONDUCTING MATERIALS

A Dissertation

by

NATHANIEL JOHNSTON POGUE

Submitted to the Office of Graduate Studies of
Texas A&M University
in partial fulfillment of the requirements for the degree of

DOCTOR OF PHILOSOPHY

Approved by:

Chair of Committee,	Peter McIntyre
Committee Members,	Alfred McInturff
	Teruki Kamon
	David Toback
	Philip Yasskin
Head of Department,	Edward Fry

May 2011

Major Subject: Physics

ABSTRACT

Dielectric-loaded Microwave Cavity for High-gradient Testing of Superconducting Materials.

(May 2011)

Nathaniel Johnston Pogue,

B.A., Carleton College;

M.S., Texas A&M University

Chair of Advisory Committee: Dr. Peter McIntyre

A superconducting microwave cavity has been designed to test advanced materials for use in the accelerating structures contained within linear colliders. The electromagnetic design of this cavity produces surface magnetic fields on the sample wafer exceeding the critical limit of Niobium. The ability of this cavity to push up to 4 times the critical field provides, for the first time, a short sample method to reproducibly test these thin films to their ultimate limit. In order for this Wafer Test cavity to function appropriately, the large sapphire at the heart of the cavity must have specific inherent qualities. A second cavity was constructed to test these parameters: dielectric constant, loss tangent, and heat capacity. Several tests were performed and consistent values were obtained. The consequences of these measurements were then applied to the Wafer Cavity, and its performance was evaluated for different power inputs. The Q_0 of the cavity could be as low as 10^7 because of the sapphire heating, therefore removing the ability to measure nano-resistances. However, with additional measurements in a less complex environment, such as the Wafer Test Cavity, the Q_0 could be higher than 10^9.

DEDICATION

To my parents John and Christine Pogue, and my wife, Kim, for their constant support.

ACKNOWLEDGMENTS

This work is the compellation of several peoples work and support. First I would like to thank my advisor, Peter McIntyre, for teaching me how to think critically and understand how to play the game. His work ethic pushes me to excel and produce meaningful results. Because of his hectic schedule, working with him during deadlines, crises, and tense moments has given me the ability to handle such situations without panicking and retaining my rational thought process. He has allowed me to work on more things, travel to the most amazing places, and given me a broader sense of physics as a whole than any other graduate student in the department. Simply put, I wouldn't have wanted to obtain my Ph.D. with anyone else.

I would also like to give special thanks to Al "Mac" McInturff for being a constant source of wisdom, in both the scientific and personal realms. He is a great wall on which to bounce ideas and he gives critical, thoughtful replies. His stories of earlier projects have enlightened me to pitfalls which have made others stumbled over the years. Some discussions have churned up stories of shenanigans that have entertained me for hours and have let me know that even in the serious scientific world, one must alway keep one's humor and wit. Mac also has let me unload and vent about everything I was thinking, usually over a pint of Guinness on a Wednesday night.

Mac was not alone during these Guinness Guys Wednesday night sessions; Andrew Jaisle also lent a hand in advising. Andrew is source of order. Keeping things clean, keeping a schedule, and getting you stuff done are what are needed to be a productive member in a group, and how to keep progressing. Andrew has also helped in many ways especially in technical advice in design work, machining parts for projects, and making sure the job isn't just completed, but is done right.

I would like to thank Dior Sattarov for teaching me about RF, magnets, thermo-

dynamics, and every other discipline. For every question I ask him, he has an answer, and if not, leads me down the path to find it. He has taught me an enormous amount of material that is applicable to my research such as computer codes, mathematical derivations, and modeling. His work ethic puts me to shame at times, and I can only hope to be as versatile and productive as he. His modest and humble nature allows for a feeling of comfortability that makes everyone feel they can approach him with a question without judgment. I can only hope to foster this environment in a teaching scenario.

Tim and Ray have been instrumental in the design work of this project and others. Tim has been extremely useful in technical aspects of design and construction of many of the projects on which I have worked. It is universally agreed that nothing could move forward in the lab without assistance from Tim. Ray has devoted hundreds of hours of his time to drawing and designing several of the ideas used in this project and others on which I have worked. All conceptual images of drawn parts and designs were made by Ray with me giving dimensions. He made these beautiful images from my terrible hand drawn sketches. Thank you.

The rest of the group has provided physical help, good conversation, scientific inspiration, and friendship over the years. Kyle Damborsky has worked with me on my ideas which have lead to a patent and a whole new direction of research in 2212. Both he and Trey Holik make the week long conferences bearable by going out, exploring the area, and general mischief, as long as there are no foot races across HEB parking lots.

This goal could not been achieved without my committee who have been guiding me through this process since the beginning of my masters degree. Teruki Kamon, my master's advisor, called me several times during the night before my master's defense to make sure that I was up and still working on it since I only had 24 hours to

create the entire presentation due to a scheduling conflict. He still keeps in touch and makes sure my research is progressing. Phillip Yasskin, who was also on my Master's Committee, always makes sure that I clarify all the details that could be confusing in my work. Dave Toback was the first professor when I arrived that went out of his way to talk with me. He told me about the high energy research that was underway at A&M over lunch, which probably led me down this accelerator research path.

The Jefferson Lab team that helped me put this project together was spearheaded by Charlie Reece and Bob Manus. Bob Martin built the majority of the parts and Gary Slack advised and stamped the cavity. Carlton Joiner helped me assemble the cavity numerous times, and Steve Dutton helped me greatly with the thermometry. I would also like to thank Pete Kushnick for getting my cavity cold even when it seemed impossible. I would also like to thank Peter Kneisel, Gigi Ciovati, Larry Philips, and Charlie Reece for their constant input and advice as to the course of experimentation.

I would also like to thank Sandy Smith for making sure that I always do things that I am supposed to do, like register for classes after I forget for a couple months, or turn in that little piece of paper that allows you to graduate. I would also like to thank Nick Diaczenko for teaching me to keep a clean shop, to never J-walk (ha!), to watch out for moldy sandwiches, how to improve my golf game, and that every good tool has a story so take care of it.

I would also like to thank Daniel Bowring, Paul Mattione, Ryan Bodenstein, and all the rest of the Jlab Social group for entertaining me and filling my nights with friendship, humor, and the occasional pub crawl over the 9 months I was at Jefferson Lab. I would also like to thank the Jefferson Lab Residence facility for housing me on a frequent sporadic basis and for not smelling like a musty old shoe like the other places that I stayed in Newport News.

I could never have made it through this process without Kim, Mom and Dad,

Grandpa and Dolores, Grandma Pogue, Uncle John and Lisa, and the entire Pogue clan: Ted, Nadine, Cindy, Ginny, Craig, Kyle, Roger, Justin, Paul and the rest of the cousins. I also would not have made it through if I didn't have such a close set of friends/co-workers here in College Station: Sheldon Campbell, Abram Krislock, Tyler Morrison, Chris O'Brien, Kyle Damborsky, Trey Holik, David Haubrich, Elizabeth Sooby, Kevin Resil, The Bee Creek Frisbee Group, The Nerd Frisbee Group, Vonda, Kelly, Melissa, Abid, Ty, Mike, another Mike, Matt, another Matt, Charlie, Sam, John, Jim, Karie, Don, Mark, Jonathan, Tristan, Adam, and numerous other people.

This could not have been done without all of these people and I am immensely thankful for their support and friendship over this time.

TABLE OF CONTENTS

CHAPTER Page

LIST OF FIGURES

FIGURE Page

FIGURE Page

FIGURE Page

FIGURE Page

FIGURE Page

FIGURE Page

FIGURE Page

FIGURE Page

FIGURE Page

FIGURE Page

FIGURE Page

CHAPTER I

INTRODUCTION

A superconducting dielectrically-loaded RF (Radio Frequency) cavity has been designed to be a small sample testing device that quantifies the performance and qualities of advanced materials that have the possibility to enormously benefit the accelerator community. Particles accelerators are very important not only high energy applications but are used in nuclear reactors, for medical therapies, to create isotopes, and materials testing. The main goal of accelerator design is to have higher energy, in a physically smaller design, and reduce the cost.

The large colliders can cost as much as 16 billion dollars and be as large as 52 miles in circumference. If the size were to be cut in half by increasing efficiency of the accelerator, it would be a monumental cost savings. It is through the Wafer Test Cavity that it is hoped to subject advanced superconducting materials to high magnetic field and analyze their properties. If these films produce the effect they are theorized to create, many collider's sizes could be reduced by half or more. Not only would such a sample test device evaluate new technology, it would give the community for the first time the ability to make a series of measurements that are comparable. This would narrow down the causes of many problems that have plagued the industry for 40 years. By just understanding the sources of breakdown, it would be known which impurities, procedures, and materials need to be avoided thereby increasing the productivity, increasing the success rate of high performance, and reduce cost.

The Wafer Test cavity accomplishes these lofty goals by having a large sapphire located at its heart that acts as an electromagnetic lens, focusing the field onto the

---

The journal model is Physical Review D.

sample up to 3.75 times the critical limit (maximum magnetic field sustainable) of the interior of the cavity itself. This dissertation will provide a detailed description of the design, modeling process, construction, and operational parameters for the Wafer Test Cavity and the standard method of RF cavity construction today. In this dissertation the impact of such a sample test system on the community will be expounded on as well as the future technology that will dominate the industry. The feasibility of such a cavity is dependent on the large sapphire required. Therefore it will also be presented within this document the properties of large crystals of sapphire at a variety of temperatures, and how these properties can adversely affect the capabilities of the Wafer Test Cavity. The series of experiment will illustrates the successes and faults of the design, construction, and procedures used. From these results conclusion will be drawn about phenomenon observed, lessons learned, design, future experiments that can be performed, and the feasibility of meeting the design parameters of the Wafer Test Cavity.

A. Motivation

A high energy linear collider is a large machine whose purpose is to accelerate particles and collide them with other particles to give a brief glimpse into the past. In both linear and circular colliders, the RF cavity is the component of the collider that gives the beam the kinetic energy necessary to produce the particles of interest at the intersection point. In the case of the linear accelerator, the RF cavities are the main components in the whole machine. The ability to reduce the cost of these cavities, increase production rates, and increase performance are at the focus of research at this moment. The results of this investigative research will make or break a potential large budget project.

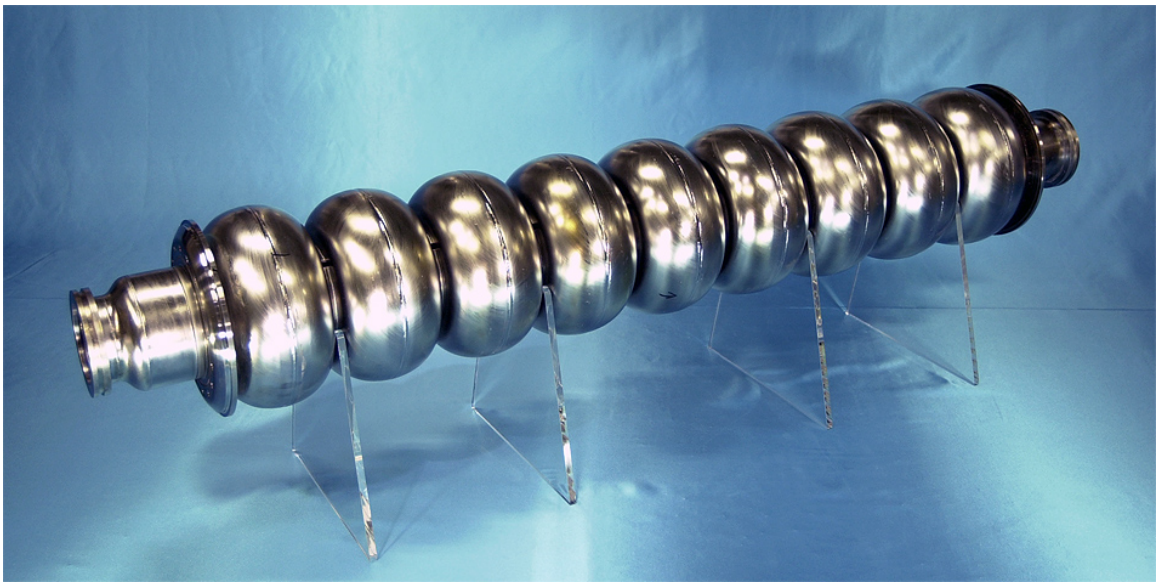

FIG. 1. The first ICHIRO 9-cell cavity produced at KEK [1].

Several superconducting linear colliders for electrons have been constructed such as CEBAF at Jefferson National lab and a few X-ray free electron lasers (XFELs). By using superconducting cavities rather than copper cavities the amount of power required to generate field with in the structure is drastically reduced, yet along with that great benefit comes several problems. The cost of these structures is high, around 100,000 dollars, and creating consistently high accelerating gradient cavities is difficult. This problem must be addressed in order for a TeV electron-positron collider (International Linear Collider, or ILC) to be built.

The backbone of the ILC is the Niobium 9-cell cavity, Figure 1. One unit of linac consists of 32 9-cell cavities contained in eight cryomodules powered by one klystron. The cryomodules hold four cavities and keeps them at 2 Kelvin during operation. The klystron, a large microwave amplifier, brings power from the outside world to the cavities. In the case of the ILC, approximately 500 of these units are required.

The size and shape of these 9-cell cavities are attributed to the ability to couple

energy to each cell, reduce the risk of higher order modes (HOMs) that can deflect the beam, beam effects such as wakefields, and the convenience of commercially available products. But all cavities are designed to have the appropriate frequency and spacing so each particle bunch passes through each of the cavities' cells at the correct phase or time to be continually accelerated down the rest of the linac. The acceleration gradient the cavity produces is a function of the shape, field, processing, and material used. The means by which to produce high accelerating gradient (above 35 MV/m) routinely in 9-cell cavities has not been found. Therefore significant research has been devoted to increasing gradient, reducing cost, and increasing production success rates.

B. Single Cell - The RF Laboratory

The manner in which research is done is not on such large structures as the 9-cells, but rather single cell versions as shown in Figure 2. Each one of these cavities is comprised of a cell, where the energy is stored, and two beam tubes that allow the beam to pass. The junction where the beam tube meets the cell is called the iris. The equator is where the two halves of the cell meet, which is usually indicted by a large weld.

When performing research the cavity is operated generally in the fundamental mode, or lowest frequency, which is the TM_{010} mode. In this mode the electric field, shown in Figure 3, is located on the axis in the center of the cavity, providing maximum acceleration. The highest surface electric field is located on the iris. The magnetic field on the other hand has its maximum at the equator, see Figure 4. Both locations of these maxima will be of great importance momentarily.

There exist two figures of merit that are used to gauge the performance of an

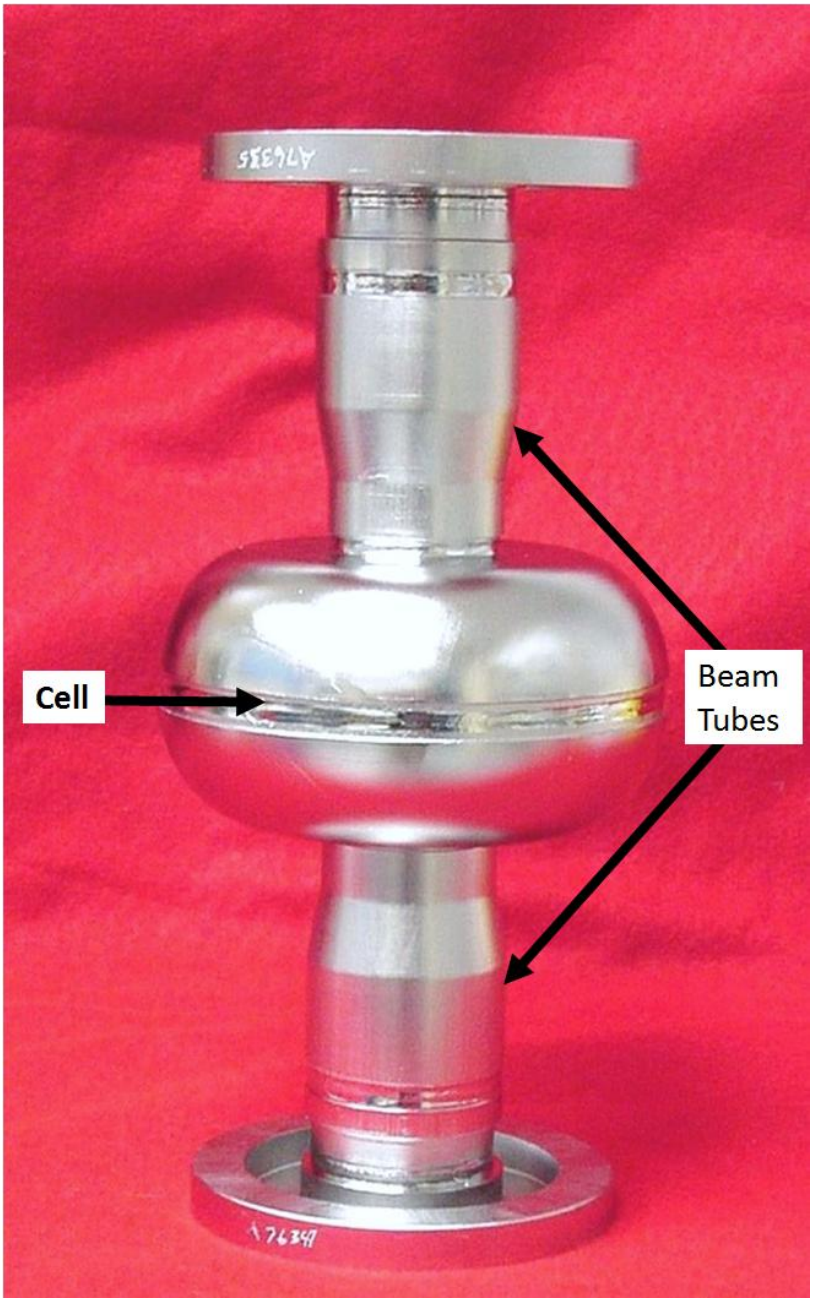

FIG. 2. Image of a single cell cavity made from a single crystal of Niobium. This cavity performed better than the ILC design goal. Courtesy of Thomas Jefferson National Lab [2].

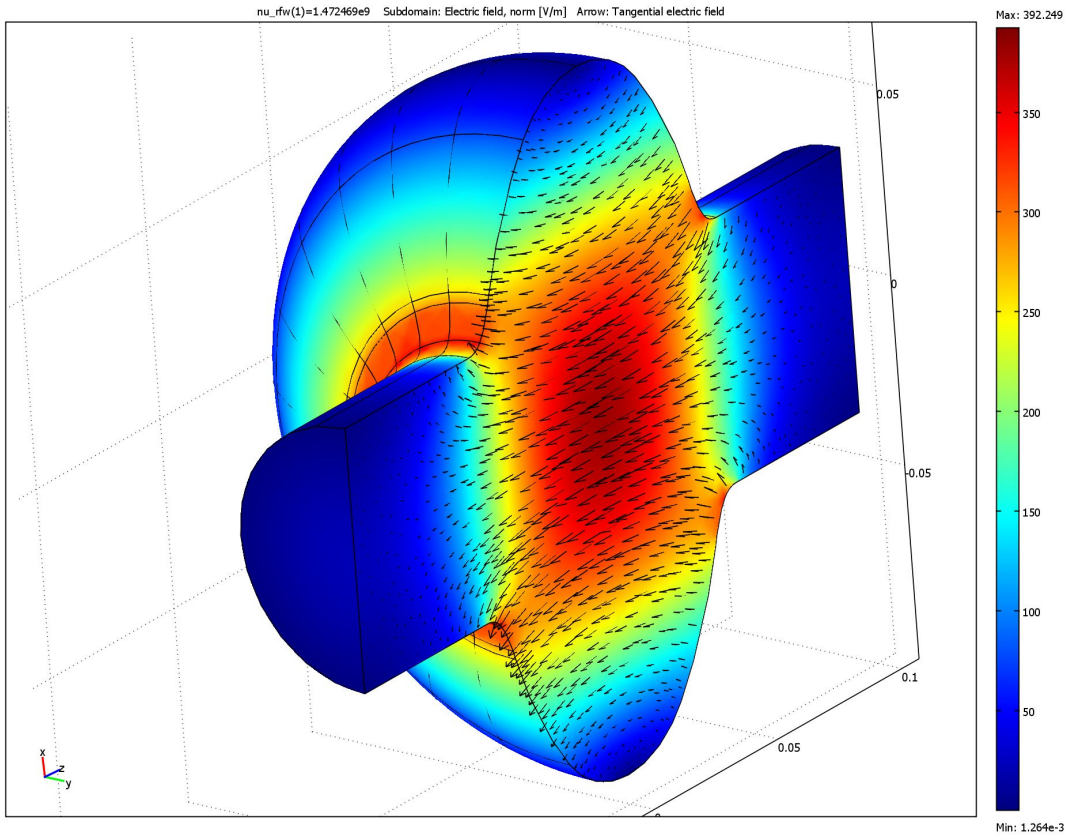

FIG. 3. The electric field of the TM_{010} mode inside a CEBAF single cell cavity. The electric field points across the cavity along the axis with the largest concentration of field on the axis at the equator. The arrows indicate direction of the field and the strength is represented by the false color.

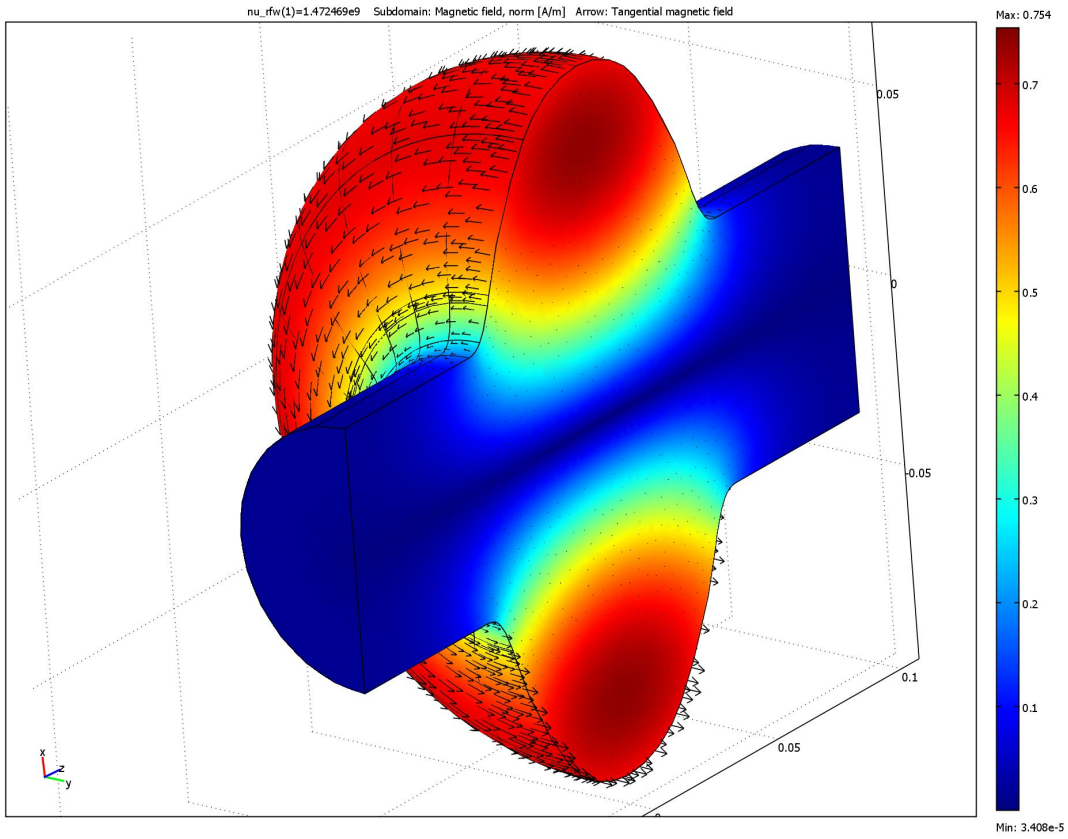

FIG. 4. The magnetic field of the TM_{010} mode inside a CEBAF single cell cavity. The magnetic field circulates in an azimuthally symmetric pattern with highest concentration at the equator.

accelerating cavity: the average accelerating gradient, E_{acc}, and Q_0. The cavity cell has a specified length, l, and therefore takes a finite time, t_{cell}, to pass through the cell. Defining one period of the RF as t_{RF}, in order for the particles to be in phase

$$t_{cell} = \frac{t_{RF}}{2} = \frac{l}{c} = \frac{\pi}{\omega} \tag{1.1}$$

must be held true. Here c is the speed of light and ω is angular frequency (cycles/sec). Integrating the time varying electric field inside the single cell over the particle bunch's time in the cavity produces the average accelerating gradient.

$$<E_{acc}>= \frac{1}{t_{cell}} \left| \int_0^{t_{cell}} E(z,t)dt \right|. \tag{1.2}$$

The RF waves will ring in the cell for a time, just like sound waves in a bell. The efficiency, or how long the bell will ring, is referred to as the Q_0 of the cavity, or quality factor. This is the number of cycles the cavity will ring. It is defined as

$$Q_0 = \frac{\omega U}{P_{diss}}, \tag{1.3}$$

where U is stored energy (J), and P_{diss} is the power dissipated (J/s). The relationship between E_{acc}, Q_0, and the field shape of the cavity is determined by Maxwell's equations. In most cases this process of solving Maxwell's equations is now handled by computational programs such as Superfish, Microwave Studio, Vector Fields, and COMSOL due to the complexity. Once the fields are solved, the stored energy in the cavity can be calculated using

$$U = \frac{\mu_0}{2} \int_V |\mathbf{H}|^2 dV = \frac{\epsilon_0}{2} \int_V |\mathbf{E}|^2 dV. \tag{1.4}$$

This is true only if the integration is over the whole cavity. This statement is not true if the integration is only over a portion, or subdomain, of the cavity. This method of integrating over subdomains will be seen in Chapter 2. The power dissipated can

similarly be calculated using

$$P_{diss} = \frac{1}{2} R_s \int_S |\mathbf{H}|^2 dS, \tag{1.5}$$

where R_s is the surface resistance. It is the sources of dissipation that truly limit RF cavities accelerating gradient and the efficiency. When the cavity has a localized point where superconductivity is lost, the cavity is no longer able to function. Therefore it is important to understand how to keep the cavity from going normal.

1. Superconductivity

The reason for the choice of superconductivity is the immense savings in power. Performing a simple analytical calculation for a pillbox cavity (see Appendix), it can be shown that the superconducting cavity uses 1865 times less power than a copper version. Hence, the immense interest in superconducting cavity research, for it makes large projects economical.

Superconductivity was discover by Heike Kamerlingh Onnes in 1911 [3]. Since then, immense knowledge has been gained regarding it properties and capabilities. The most commonly used superconductor in the RF field is Niobium. It is the element that has the highest magnetic field tolerance and temperature tolerance before superconductivity is lost. Niobium is a Type II superconductor, as are some alloys, A15 materials, intermetallics, and ceramics, meaning that it has two critical limits. The first critical limit (Niobium has the highest first critical limit of any element) is where flux begins to penetrate the surface of the superconductor, or

$$H_{c1}(T) = \frac{\Phi}{4\pi\mu_0\lambda^2(T)} \ln\left(\frac{\lambda(T)}{\xi(T)} + .08\right), \tag{1.6}$$

where Φ is a single flux quantum, or fluxoid. Here λ is the London penetration depth, or how deep the magnetic field will penetrate the surface being exponentially sup-

pressed to 1/e the original value. Another important parameter within the equation above is the coherence length, ξ. The coherence length can be thought of as the distance over which the superconducting currents, or Cooper Pairs, can communicate. A Cooper pair is two electrons with opposite spin that are bound together as they travel through the conductor. Normally a pair of electrons would repel, but the pair of electrons interacts with each other through the lattice structure which is mediated by lattice vibrations. The interaction reduces the energy of the pair. Overall the kinetic energy increases but the potential energy decreases by a greater amount making the lattice mediated bond energetically favorable. These Cooper pairs therefore flow without resistance on the surface layer of the superconductor, until the pair's communication is broken by a grain boundary, defect, or fluxoid that passes between them. Hence a smaller coherence length allows for higher magnetic fields to be applied, until the density of fluxoids is so high they break the communication, causing the cooper pairs to break and the conductor to go normal. This threshold is the second critical limit, or

$$H_{c2}(T) = \frac{\Phi}{2\pi\mu_0\xi^2} \tag{1.7}$$

If the coherence length and the London penetration depth are known as a function of temperature, then both critical limits can be calculated for any temperature below and near the critical temperature T_c.

Thus three parameters establish the criteria for the superconducting state: T_c-critical temperature, J_c-critical current density, and H_{c2}-critical magnetic field. These critical parameters create a volume over which the material is superconducting. The boundary between the normal and superconducting state is the critical surface. The performance of the material is therefore limited to the interior of the volume; as a result, pushing one parameter will reduce performance in another aspect, as Figure 5

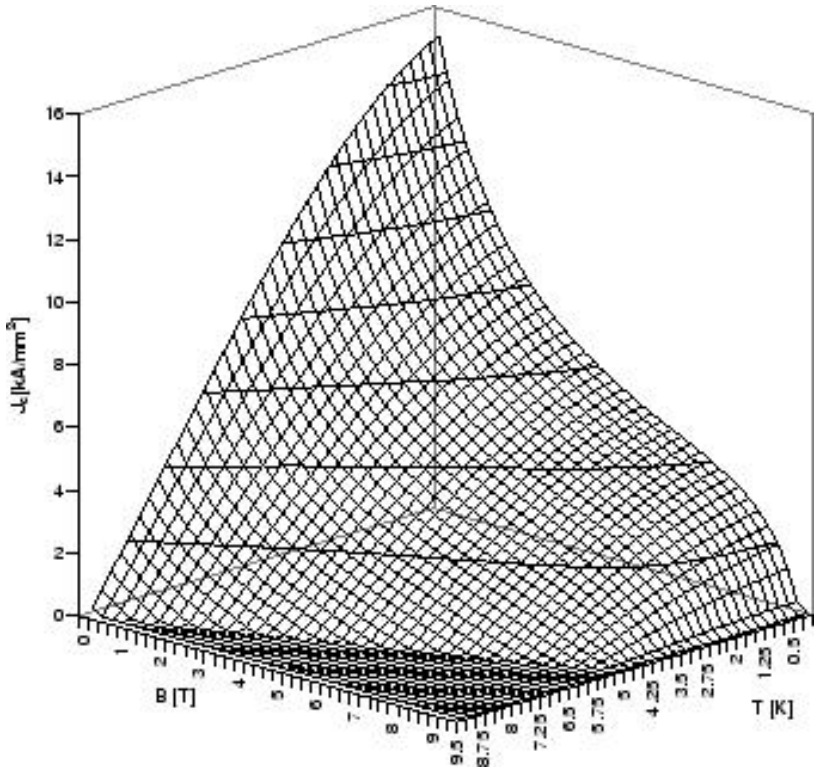

FIG. 5. The critical surface of NbTi superconductor. The temperature, magnetic field, and current density are the three parameters that form the surface [4].

illustrates for NbTi.

However in the case of RF, superheating can occur. Entropy and nucleation centers allow a metastable superconducting state to occur above the upper critical limit, H_{SH} [5].Superheating can occur because, at the GHz range of frequencies and above, the fluxoids are unable to nucleate in superconductor in one RF period. The fluxoids are unable to sufficiently form fast enough to destroy superconductivity until the magnetic field is sufficiently large to cause fluxoids to form rapidly and penetrate causing the Copper pairs to be broken. For Niobium, H_c is 2000 Oe and H_{SH} is 2300 Oe which corresponds to 50-60 MV/m [6]. Remember the gradient is not the limiting factor, but rather the magnetic field. Cavities have been constructed that could produce over 220 MV/m [7]. This is due to the geometry factor and other non-

material based aspects. Hence, there is no fundamental limit to the electric field that a RF cavity can produce. The only limitations in an ideal world are the magnetic field, current density, and temperature.

2. Resistances and Limitations

Unlike DC resistance, RF resistance is only zero at zero degrees Kelvin. The Cooper pairs move without resistance but inherently have mass. From the electrons inertia there is a lag in the flow of the pairs compared to the field. Hence the pairs do not perfectly screen out the field, and allow the field to penetrate a certain depth. The penetrating field pushes the normal electrons in the conductor back and forth generating heat. Therefore there is always a resistance in RF cavities. This resistance is generalized as

$$R_s = A_s \omega^2 e^{(-\frac{\Delta}{k_B T})}, \tag{1.8}$$

where A_s is a material dependent constant. Note that the energy gap's value, Δ, asymptotically approaches the 0 Kelvin value of the energy gap when T is below $T_c/2$, and therefore can be used in this expression. However this limits the accuracy to below $T_c/2$.

To keep the resistance down, the total number of normal electrons needs to be kept to a minimum. This is done by keeping the temperature near 0 K where all electrons are paired. Most cavities are cooled to around 1.9 K for economic reasons. The heat conduction of superfluid liquid helium is coincidentally greatest at this level.

As stated earlier, the value of A_s in Eq. 1.8 is greatly dependent on the material properties such as: ξ, λ, v_F (Fermi velocity), and mean free path [8]. For Niobium, the most common superconducting RF material the resistance is

$$R_{s_{Nb}} = \frac{2 \times 10^{-4}}{T} \left(\frac{f}{1.5} \right)^2 e^{(-\frac{17.67}{T})} + R_0. \tag{1.9}$$

where R_0 is the residual resistance. The equation provides a good fit to data given in Figure 6 up until the temperature becomes very low. At this point, the residual resistance becomes dominant, which cannot be taken into account by the BCS theory [9]. The residual resistance is caused by a variety of mechanisms. The first and foremost causes of residual resistance are defects and impurities in the material. These may come from the raw material, manufacturing, welding, etching, cleaning, or a variety of other sources, as Figure 7 shows [10].

Thermal breakdown, or quench, is caused when a localized area, usually a defect or impurity, of the superconductor is heated above the critical temperature or a localized area of high magnetic field above H_{c2}. When the area becomes normal, it rapidly dissipates the energy stored in the cavity, causing the normal area to grow. The determination of whether or not a defect will cause thermal breakdown depends on many parameters. The size and resistance of the defect plays a major role, as does the thermal conductivity of the material used, the quality and treatment of the material, and preparation of the material. At the moment, there is no means by which to connect the cause of the defects to the performance of cavities. This is why a short sample test system is necessary to make the direct connection between cause and effect of these defects.

Other sources of resistances and field limitations can come from surface chemistry performed, trapped DC flux from the earth magnetic field, thermo-electric generated flux being trapped, multipactoring, and field emission. Mulitpactoring is where electrons are emitted from the surface and are accelerated back at the walls causing more electrons to be emitted, thus leading to an avalanche effect as shown in Figure 8. This phenomenon usually occurs in between 50-2000 eV [11]. The ability for each electron to produce additional electrons is based on Secondary Emission Coefficient (SEC). The energies at which the coefficient is greater than one indicates the where each

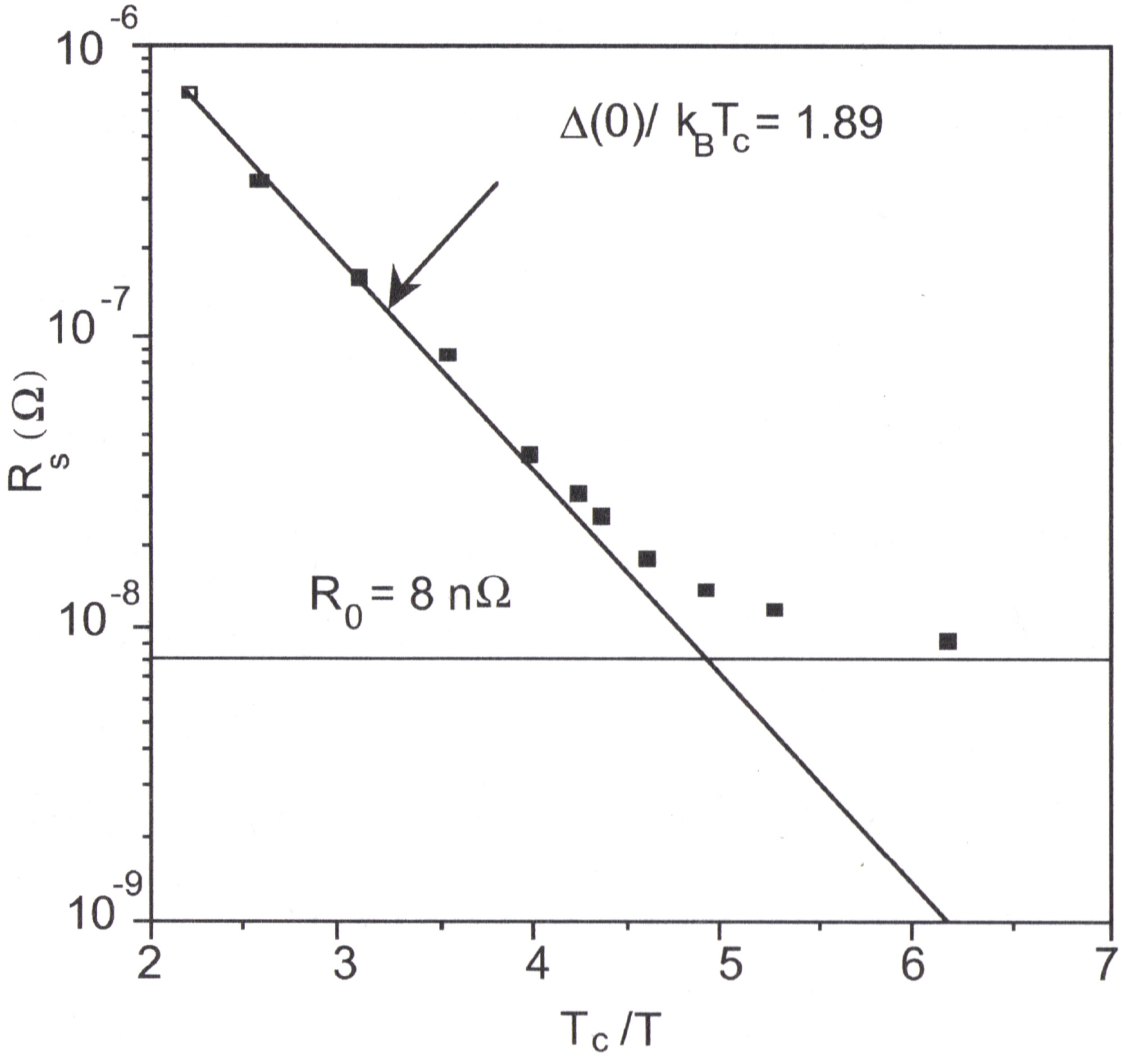

FIG. 6. Surface resistance data for a Niobium 1.5 GHz single cell cavity plotted with the BCS theory prediction for Niobium. The horizontal line is indicating the value of the residual resistance. Courtesy of Wiley-VCH Verlag, reproduced with permission [9].

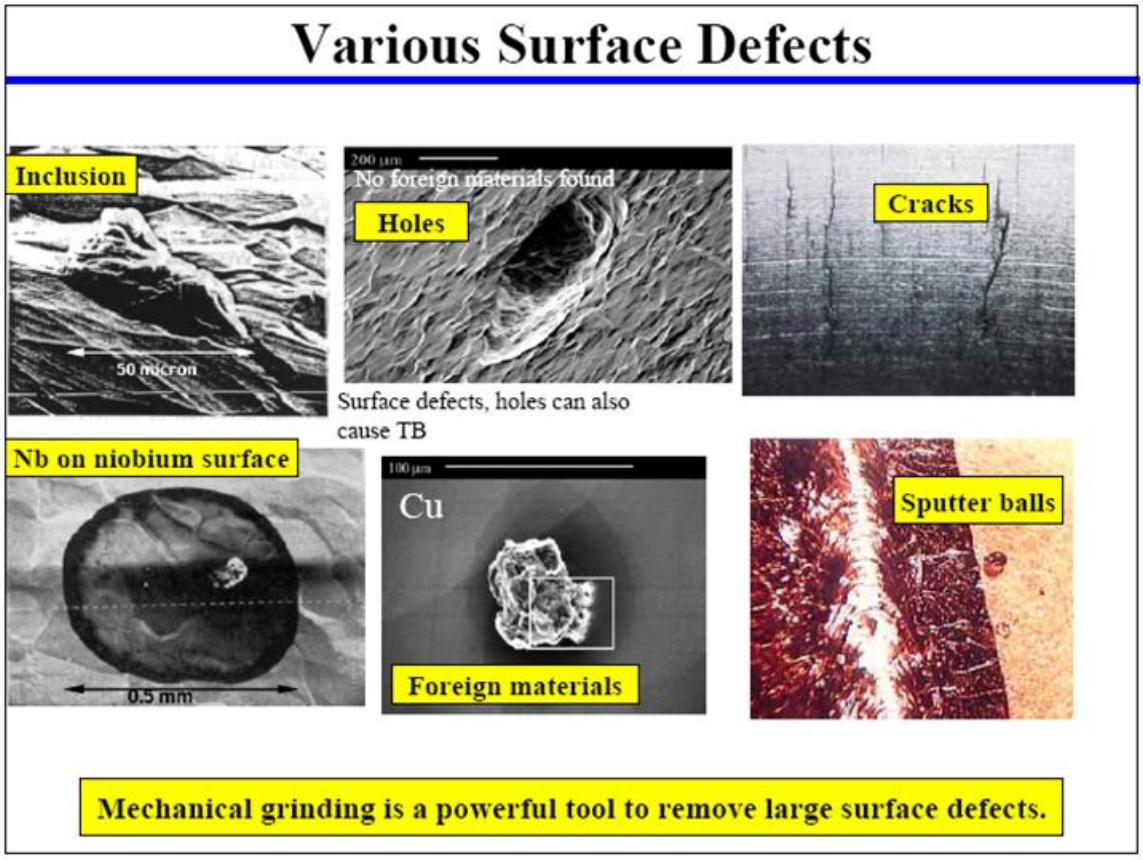

FIG. 7. Various surface defects that cause breakdown of the fields in the cavity and increase residual surface resistance [10].

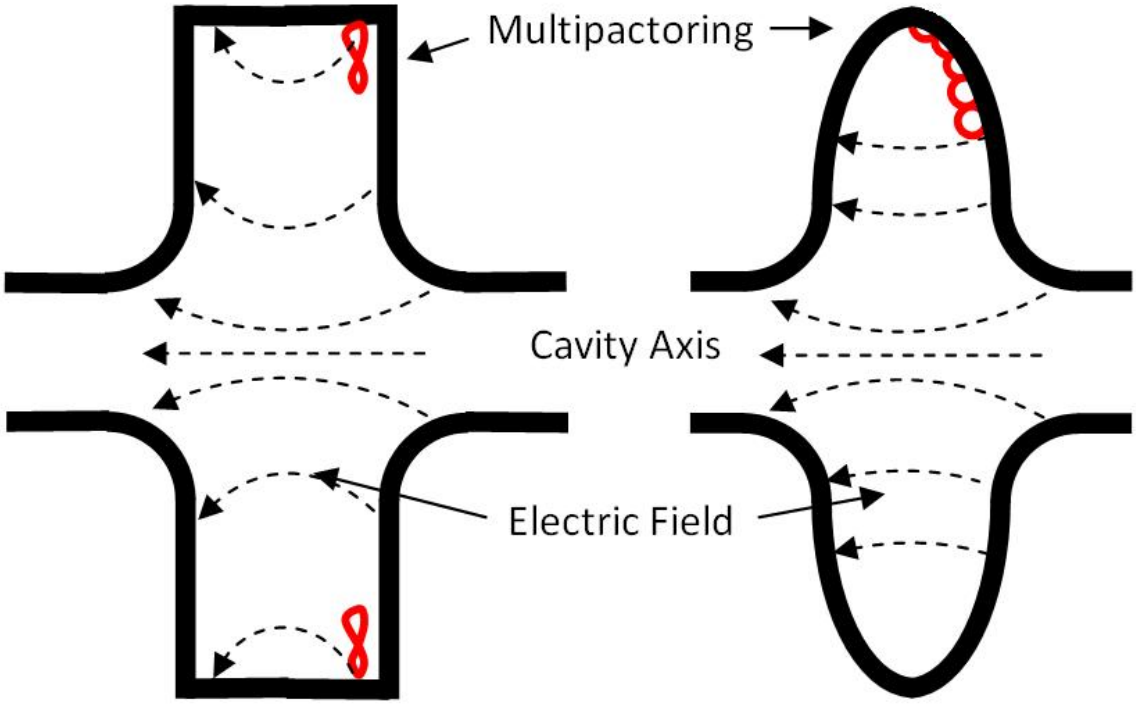

FIG. 8. Multipactoring can be a serious concern in rectangular cavities. Electrons are accelerated into the wall releasing an avalanche of electrons heating the surface and causing a quench. Problem is eliminated by elliptical shape where the charges are moved to a location of zero electric field [12].

electron is multiplied. Several SECs are given in Figure 9. Current elliptical cavities resolve this problem by shaping the cavity so the emitted electrons move according to the electric field towards the equator where the electric field is zero, stopping the avalanche which causes quench.

In some cases, field emission occurs. This is the process where electrons are removed from the surface and are accelerated with such energy that they remove a non-negligible amount of energy from the cavity and slam back into the wall. In some cases, this causes thermal breakdown; however, sometimes the cavity can recover. Field emission is a problem because up close the surface appears jagged. No matter how well the etching process performs, surface undulation will occur, creating surface

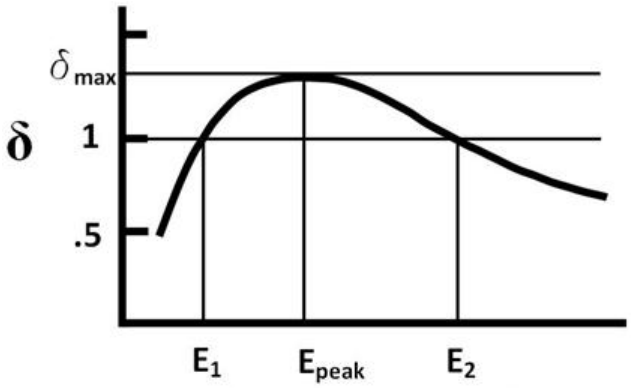

Substance	δ_{max}	E_{peak}	E_1	E_2
Ag	1.5	800	200	>2000
Al	1	300	300	300
C (diamond)	2.8	750	None	>5000
Cu	1.3	600	200	1500
Fe	1.3	400	120	1400
Nb	1.2	375	150	1200
Pb	1.1	500	250	1000
Ta	1.3	600	250	>2000
W	1.4	650	250	>1500
NaCl (layer)	6.8	600		
NaCl (crystal)	14	1200		
NaI (layer)	5.5			
NaI (crystal)	19	1300		
Al_2O_3 (layer)	2-9			
SiO_2 (quartz)	2.1-4	400		

FIG. 9. Table shows the Secondary Electron Coefficients (SEC) for various materials over an energy distribution. Data was taken from the CRC Handbook 90th edition [13].

peaks and depressions. When a large potential exists, charge will be pulled from the surface, and in the case of field emission, arc back to the surface causing immense heating and quench.

All of these factors and conditions can cause the loss of superconductivity. Therefore great care must be taken to avoid such issues. These phenomenons though have not been sufficiently linked to one process, contaminant, or defect.

C. Cost and Performance

These concepts and factors have been extensively studied for the last 50 years; yet, to date, the community still struggles to understand the inner working of RF superconductivity and cavity production. With all of these experiences, significant leaps have been made in creating high gradient cavities. However, the average of the cavities is below the acceptable threshold necessary for large multi-billion dollar collider projects, Figure 10. Moreover, an understanding for why high gradient cavities are not consistently produced is not available.

For the International Linear Collider the proposed budget is 16.2 billion dollars, which is at the extreme limit of public affordablility. The capital cost of such a collider is the cavities, cryomodules, and power systems. By choosing superconducting technology the cost of power required has been suppressed by about 2000 times. However the cost of the cyomodules and the cavities themselves are quite high, around $100,000 in just fabrication cost of the cavity. The operating cost is utterly dominated by the power supplied to the cavity to maintain the high accelerating gradient, E_{acc}, and keeping the cavities at 2K.

It is therefore very important to innovate existing technology to reduce the capital and operating costs. If it were possible to increase the gradient consistently to twice

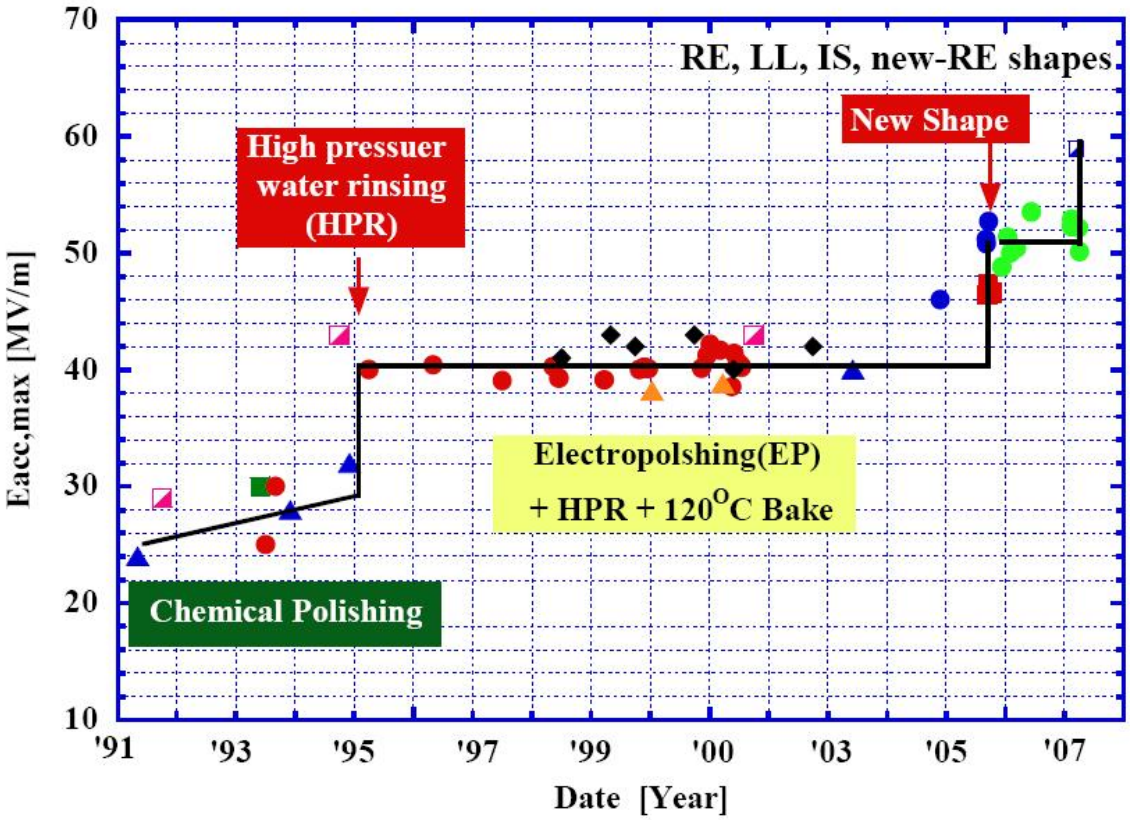

FIG. 10. Current state of high gradient cavities in the SRF world. Note these points are champion cavities, the average gradient of all cavities produced is still only 27 MV/m. Industry is now improving to the average of the national labs but increased reproducibility is required. The International Linear Collider requires at least 35 MV/m cavities to operate at an 85% peak field to reach 500 GeV[14].

the level with the same Q_0, or efficiency, then the linac could be half the size. This would reduce the capital cost and the operational cost by half.

D. Superconducting Heterostructures

Such an improvement of gradient and efficiency comes from thin films research. It is generally known amongst the RF community that thin films on the interior of superconducting cavities are the future of the industry. The reason why is these microfilms have been theorized to increase the critical magnetic field limit of a surface. As Figure 11 illustrates, Gurevich theorized that by applying thin films of insulators and Type II superconductors thinner than the penetration depth, the bulk conductor is shielded from the surface magnetic field [15]. Simultaneously the Q_0 is enhanced as well, leading to an overall increase efficiency. Knowing that

$$P_{diss} \propto \frac{E_{acc}^2}{Q_0}, \tag{1.10}$$

an accelerating cavity with such coatings would have a gradient twice as large with Q_0 four times larger, putting the total losses equivalent to that of uncoated cavity operating at half the accelerating power. This is therefore the same operational economic cost per meter for twice the performance.

It is difficult though to form these films in the proper succession with the purity and surface bonding necessary. Several national labs are endeavoring to make such films: Argonne National Lab, Fermi National Lab, and Jefferson National Lab, as well as Texas A&M University. At the accelerator research lab at Texas A&M, cluster instrumentation is being assembled to form such layers with the quality and precision required.

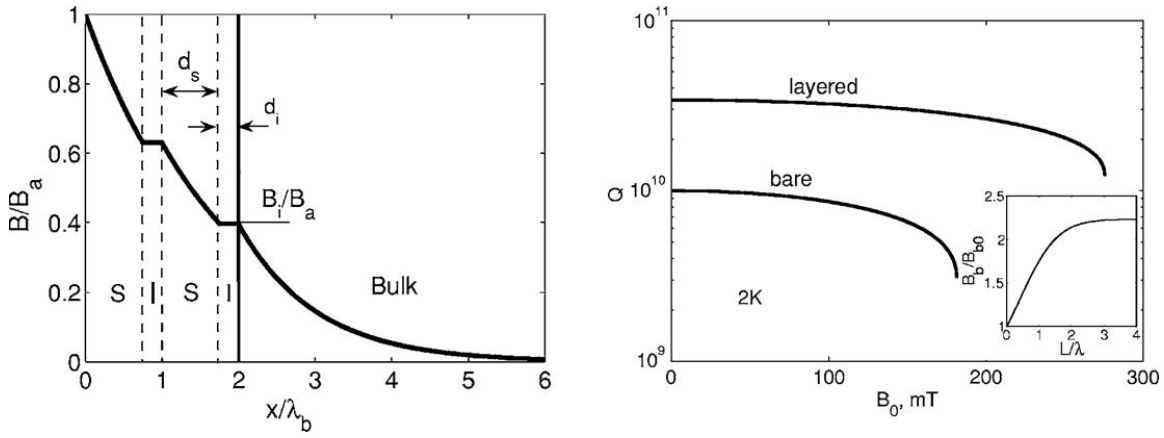

FIG. 11. Left: Alternating layers of superconductor (S) and insulators (I) are placed on bulk Niobium. The layers effectively magnetically shield the bulk niobium from the RF. In the case above, an accelerating cavity with these layers would have a gradient more than twice as large as an equivalent uncoated cavity. Right: The Q is also increased by adding these heterostructures; in the specific case above the Q is increase by a factor of nearly four [15]. Copyright 2006, American Institute of Physics.

E. Material Test Cavity

There is the lack of a reproducible manner in which to test materials, processing, manufacturing, and polishing. The current method is to construct a cavity, perform a recipe, and test. The first test may produce a cavity whose limit is 30 MV/m, the next cavity's limit is 45 MV/m, and the next is 20 MV/m. Each cavity is unique and therefore not comparable to the others. That is why a short sample test cavity needs to be constructed to determine the best procedure to reliably create high gradient cavities.

More importantly, in order to test this new realm of RF technology, the standard testing method must go beyond the limits of Niobium. Therefore a Niobium cavity was designed to push the limit of the magnetic field on a 6 inch wafer sample to approximately 4 times H_{c2} of Niobium. This is accomplished by using a dielectric to

focus the fields on the sample while operating in a TE_{010} mode.

F. Sapphire's Characteristics

The most critical aspect of the cavity is the dielectric, a HEMEX sapphire from Crystal Systems. An anticipated loss tangent of around 1×10^{-9} would allow high Q operation and measurements of surface resistance of the sample. These measurements were taken on small samples used in whispering gallery cavities. The loss tangent has been measured and perfected for such small crystal but never before has there been a measurement on the loss tangent of a specimen of HEMEX grade sapphire as large as 2 inch diameter, 4 inches long.

The performance of these large crystals needs to be investigated to adequately state the performance parameters of the Wafer Testing cavity, which utilizes such a dielectric to create the desired field profile. If this is accomplished then the RF community will truly have a sample test system that will allow reproducible measurements and be a great instrument to locate sources breakdown and limitation. Finally it will allow thin film researchers to rapidly get feedback on the quality and properties of their films, and provide information to foster increasingly strong magnetic fields on the surface of the those films/cavities.

CHAPTER II

DESIGN AND COMPUTATIONAL MODELING

A. Wafer Test Cavity

The Wafer Test Cavity must meet specific criteria if it is to answer many of the questions that still persist in the SRF world. The first is to create a reproducible environment. The second is to provide a field over a large surface area. Third, it is necessary to create fields larger than the limit of niobium to test advanced heterostructures. To meet these demands a TE_{01} cavity was designed to operate at 1.3 GHz. The frequency was chosen to mimic the environment SRF cavities would see in the ILC. The design of the wafer test cavity is not unique and took many of the strengths of preceding TE_{01} cavities, and steered away from the faults.

The basic concept of a TE_{011} mode is illustrated in Figures 12 and 13 for a CEBAF cavity. Figure 12 shows the electric field intensity and the direction of electric field. Figure 13 illustrates the electric field is azimuthal in nature. The magnetic field is most intense in the center, where the highest energy density is also located.

This mode is then stretched and distorted to place the fields on the surface in ideal locations. The number of cavities dedicated to achieving these goals is a testament to the difficulty of obtaining this potentially extremely useful field profile.

1. Predecessors

Over the past several years, over 16 different TE_{01} cavities have been constructed. Several have reached the sensitivity required to measure the resistance of the material, however many are not designed to test large surface areas. In all cases, high field has not been obtained. The highest field achieved on a sample was 64 mT. This is about

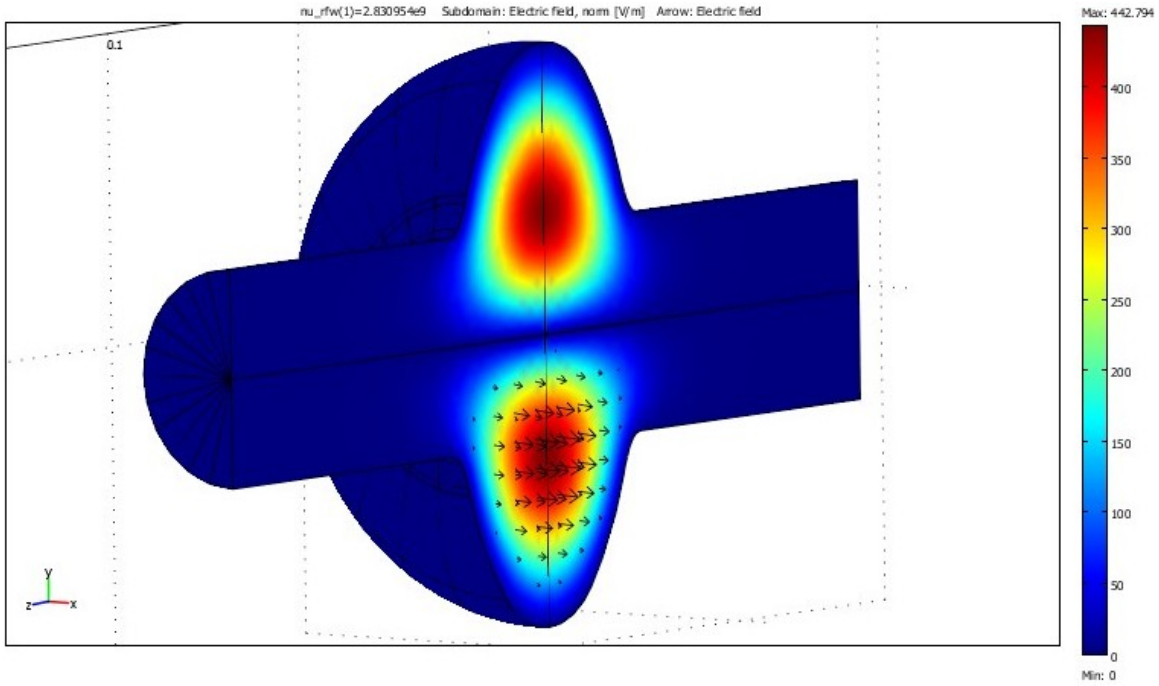

FIG. 12. The electric field of the TE_{011} mode inside a CEBAF single cell cavity. The electric field circulates around azimuthally with the most intense part of the field located in a toroid on the equatorial plane of the CEBAF cavity.

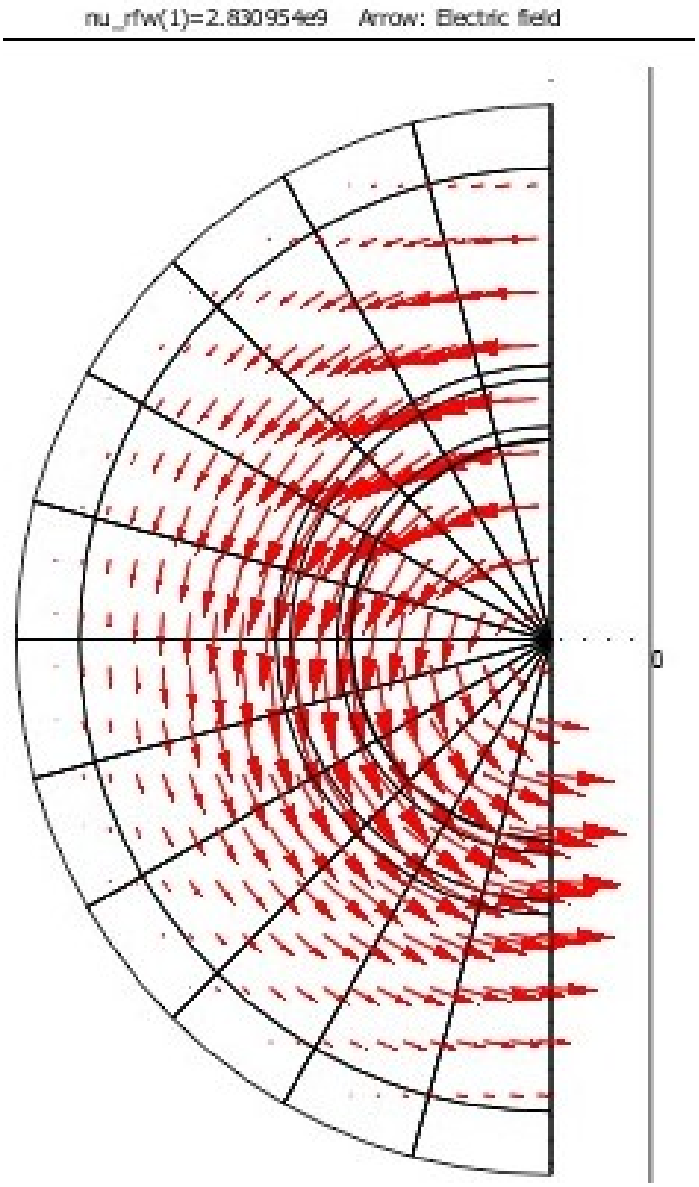

FIG. 13. The field circulates azimuthally along the entire axis of the cavity.

a third the theoretical limit of Niobium. In most cases the frequency is also higher than accelerating cavities. For the design of the Wafer Test Cavity, three cavities were drawn from heavily to produce high field, good sensativity, and operate at an accelerator frequency.

a. Cornell

An early cavity found was created at Cornell [16]. The field was focused on an elevated platform. The field peak was located on the ring, but the field concentration was an edge effect. This method does not provide a stable uniform enhanced field and only tests a minuscule sample area. The operating frequency of this cavity was 6 GHz and had a Q_0 of 1.5×10^8.

The success of this design was the coupling strategy. The couplers feeding the cavity are simple and robust. The coaxially lined loops are able to easily couple to the TE_{011} mode. The simplicity of the design is a great advantage over waveguides and other input devices. This coupler design was also used by Peter Kneisel in a similar cavity; it did not have any issues with coupling or breakdown that plagues many TE_{01} cavities. It is important that one couples magnetically rather than electrically for best performance.

b. SLAC

The conceptual design of the Wafer Test cavity was spawned during a conference in which Christopher Nantista of SLAC was presenting a copper cavity to test RF samples [17]. The overall design was quite advantageous for many reasons. The mushroom shape was able to focus the RF on the bottom surface (sample) producing a field profile that placed the maximum magnetic field peak on the sample surface with a peak 57% of the maximum on the cavity wall.

The problem with this design is that the operating frequency is 11 GHz. The current frequencies utilized for accelerating cavities are between 1.3 and 1.5 GHz. From Equation 1.5, the surface resistance is proportional to f^2 when R_{BCS} is much greater than R_0 (i.e. 8 $n\Omega$). Knowing the area will scale as $1/f$ in a multi-cell cavity, the resistance will have a linear dependence. So a lower frequency at first glance is more beneficial. However, as the frequency drops below 300 MHz, R_0 becomes the dominant term and gives the power dissipation a $1/f$ dependence. Taking these limiting cases creates an optimal range to achieve minimum losses. If this were the only parameter defining the frequency, then from size and cost considerations one could find a suitable choice.

This does not take into account wakefields which have strong frequency dependence. The iris size (radius of iris, r) of the cavity is inversely proportional to the frequency, while at the same time the longitudinal wakefields created by the beam passing through the cavity are proportional to $1/r^2$, and transverse wakefields are proportional to $1/r^3$. This creates a f^3 dependence of losses due to wakefields. This prompts us to choose a lower frequency within the range specified above. Analyzing all these different parameters and optimizing for best performance and gradient, 1.3 GHz is the closest frequency that has klystrons readily available.

Establishing the cavity at a 1.3 GHz operating frequency will suit the needs of the community, but the size of a SLAC shaped cavity would be enormous. The sample size would be 17 inches in diameter, and therefore the size is much too large. Another method must be found. The simplest solution is to dielectrically load the cavity to decrease the size. The SLAC cavity shape is quite beneficial for focusing the peak field on the sample, but the waveguide coupler and size constraints do not make it a candidate as it stands.

c. JLab

The Jefferson National Lab TE_{01} cavity developed by Phillips uses a dielectric to decrease the frequency of the cavity [18]. The design places the sapphire rod down the center of the cavity. There are several unresolved issues with the design of the cavity [19]. The first testing of the cavity showed a Q_0 of only 10^7. As to the exact cause of this is currently unknown.

Several other problems occurred as well. The waveguides that feed power to the cavity are located across from each other. This geometry has led to possible cross talking across the port, leading to a misinterpretation of data acquired. This may be a serious problem with the design. Another design challenge with this cavity is parasitic modes. The TE_{01} mode has a close lying dipole mode only 70 MHz away. This is only a one percent difference in frequency. Great care must be taken in tuning the cavity, and therefore it would be very beneficial to have a cavity whose azimuthal mode has a large separation from the closest parasitic dipole mode.

d. Others

Several other groups have created TE_{01} cavities ([20],[21],[22],[23], and others - see Figure 14). Taking what was learned from these previous attempts and utilizing the strengths of each, the goals that are wished to be obtained have been met in the design the of the Wafer Test Cavity.

2. Modeling Wafer Test Cavity

The basic design is similar to the SLAC cavity described above in which the mushroom shape is utilized. For ease of construction, the top of the mushroom cavity consists of half a TESLA cell. The cross section of the TESLA cavity contains an area along

f (GHz)	A_{Sample} (cm^2)	A_{RF} (cm^2)	$R_{Sensitivity}(\Omega)$	B_{max} (mT)	Reference paper for Cavity
8.6	0.9	0.9	1.00E-05	Very Low	Allen et al. MAG-18 1983
3.5	127	127	1.00E-09	2	Kneisel et al. ASC 1986
5.95	20	0.2	<1.50E-05	?	Moffat, Rubin et al. 1988
.17 - 1.5	~1	~1	2.00E-06	64	Delayen et al. Jour. Super., 3, 1990
1.5	4.9	2	1.00E-09	25	Liang, et al. RSI 1993
1.5	12	2	1.00E-06	60	Mahner, Weingarten 8th SRF 1997
7	1	1	1.00E-05	0.15	Andreone SRF Thin Films Wkshop 2006
0.403	44	12	1.00E-09	25	Mahner, Haebel, et al. CERN RSI 2003
0.4-1.2	44	12	?	51	Juniger et al. SRF 2009
11.4	19.6	~8	?	?	Nantista SLAC PAC 2005
7.5	20	0.8	<1.00E-7	?	Delayen, Wang, Phillips
5.95	35	35	2.00E-06	45	Romanenko Cornell SRF Wkshop 2005
34	35	12	2.00E-03	?	Martens APL 1991
.6-10	<.1	<.1	<1.00E-7	?	Oats, Moeckly ASC 2006
10	1	1	1.00E-05	?	Taber RSI 1990
3.54	22	18	?	50	Ciovati, Kneisel Jlab

FIG. 14. Listed are the preceding TE_{01} cavities built to create test beds. The compilation provided above was collected by Charles Reece [20].

the profile that is straight or flat. In the straight narrow band, two holes are cut 180 degrees apart from each other. The edges are then bent and shaped into a nipple. This protrudes the material up off the flat, making the edges of the nipple point perpendicular to the surface.

Similarly a flat disk, with the same diameter as the half cell, has a hole cut into the center. The interior hole edge is shaped into a nipple so the material has a smooth corner. A cylinder of the same diameter as the inner hole is then welded to the flat creating a top hat shape. The half TESLA cell is then attached to the inverted top hat, making the mushroom shape. The sapphire is suspended in the center of the cavity through the top of the half cell as Figure 15 shows.

The cavity is run in the lowest order azimuthal mode, TE_{011}. The size of the cavity has been decreased using the sapphire to 1.3 GHz. The geometry of the sapphire was shaped to allow the top hat cylinder diameter to be smaller than 6 inches and yet place a significant field concentration on the sample surface. The 6 inch sample is a standard silicon chip industry machine size. The chip industry devices can produce thin film layers reproducibly on a regular basis. This cavity allows the smooth integration from thin film creation to thin film evaluation.

As Figure 16 illustrates, the cavity is producing an azimuthal current, as well as circulating radial magnetic field lines in a toroidal fashion, Figure 17. Figure 18 highlights that the magnetic field is indeed radially symmetric as anticipated, and locates the maximum field on the bottom sample surface. The intensity profile, Figure 19, shows the field on the surface is approximately four times larger than anywhere else on the niobium cavity surface.

The fields, electric and magnetic, are mostly localized within the sapphire. The sapphire acts as a lens and focuses the fields on the sample. Note that the dielectric is 4 mm off the sample surface to reduce any risk of multipactoring. The risk

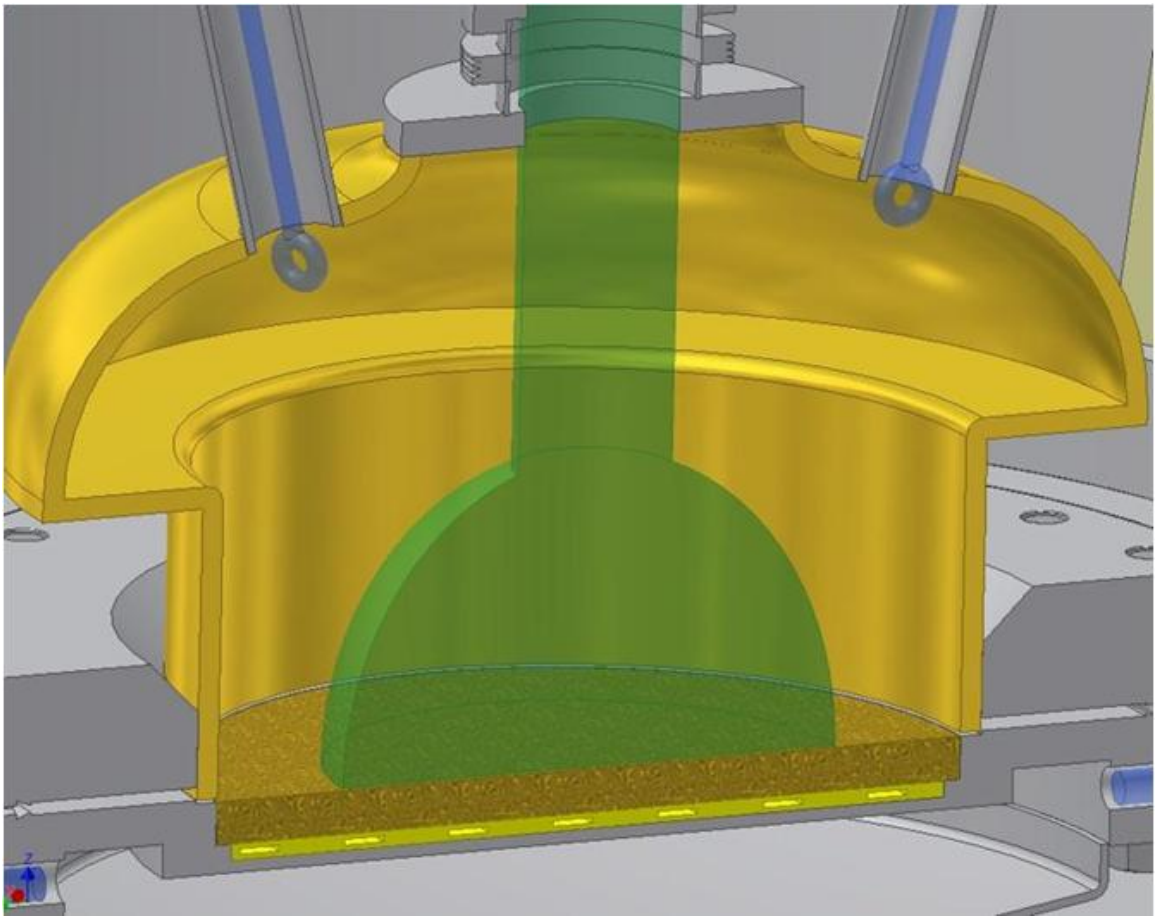

FIG. 15. Model of the Wafer Test cavity with sapphire located in the center, including the base illustrating the resistor bank for quench positioning. The two antenna ports flank the sapphire on the flat ring of the TESLA half cell which are attached to the smoothed nipples on the flat. These are the major components of the cavity.

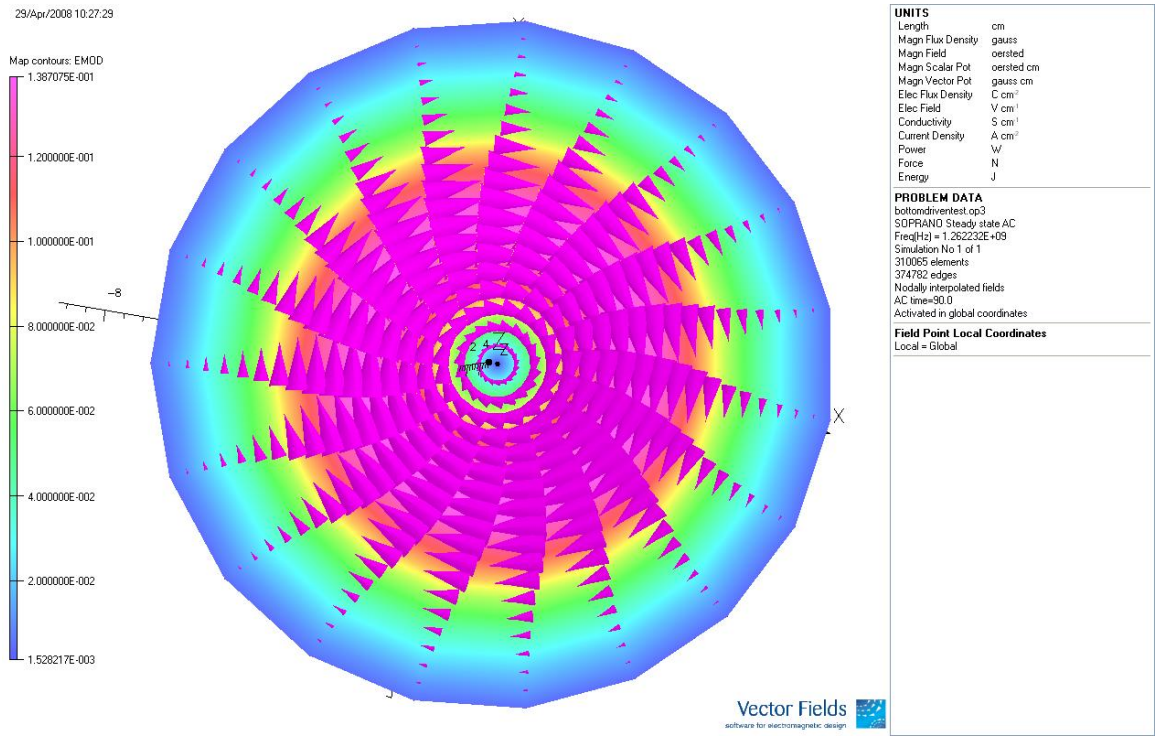

FIG. 16. The electric field circulating around the axis of the cavity in the TE_{011} mode above the sample surface. This eliminates any problems of electrons being pulled off surfaces.

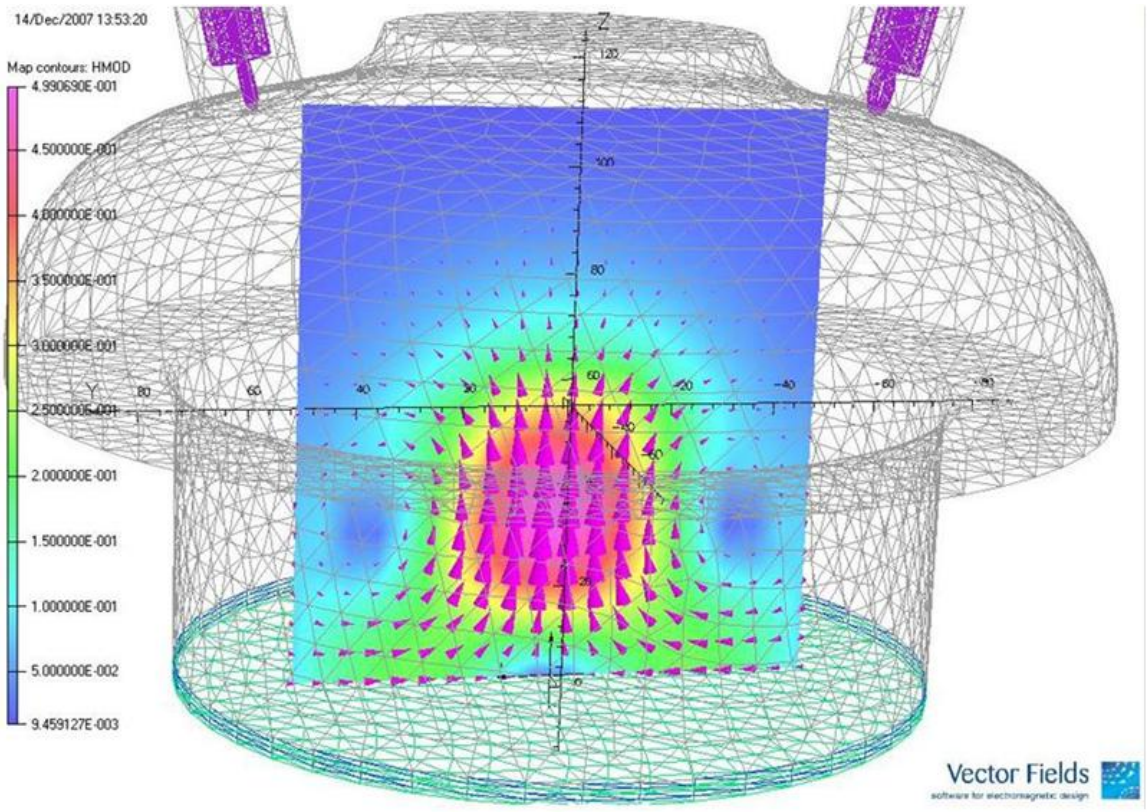

FIG. 17. The magnetic fields rotates in a toroidal manner in the radial direction of the cavity. Note the most intense field is located within the volume occupied by the sapphire.

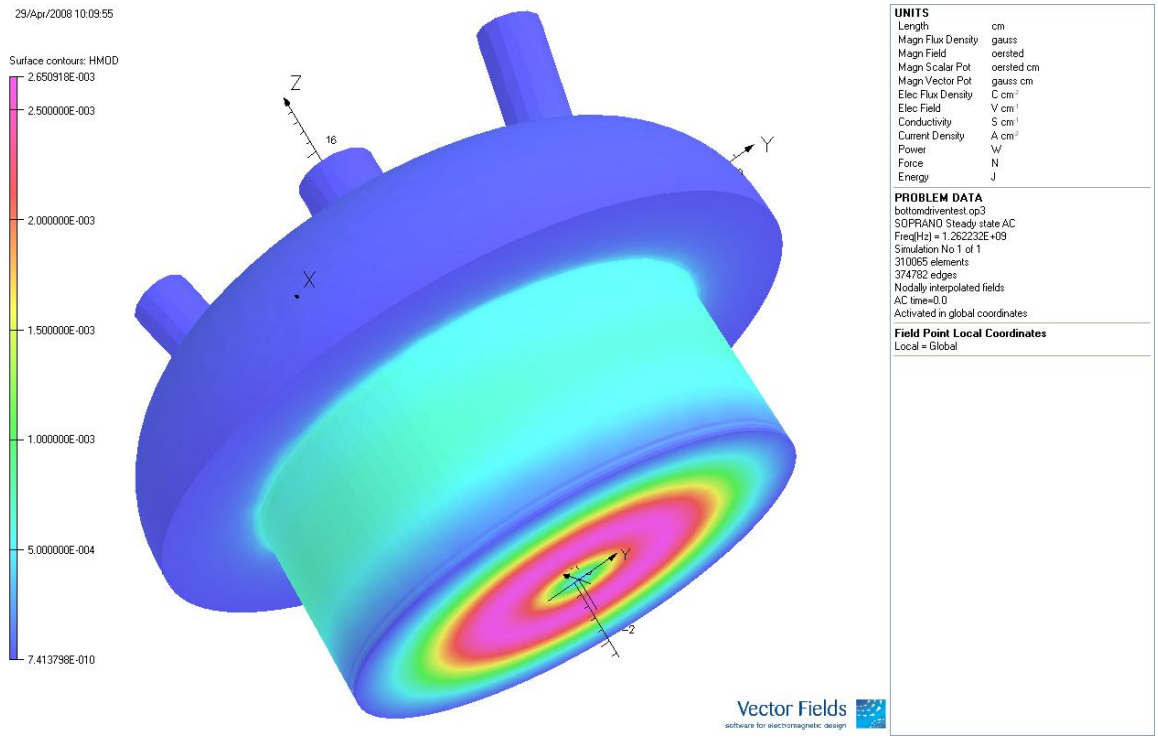

FIG. 18. The magnetic field located on the cavity walls. The false color plot determines intensity of the field. Note the concentric nature of the field on the sample surface. Also the most intense spot is located on the sample surface.

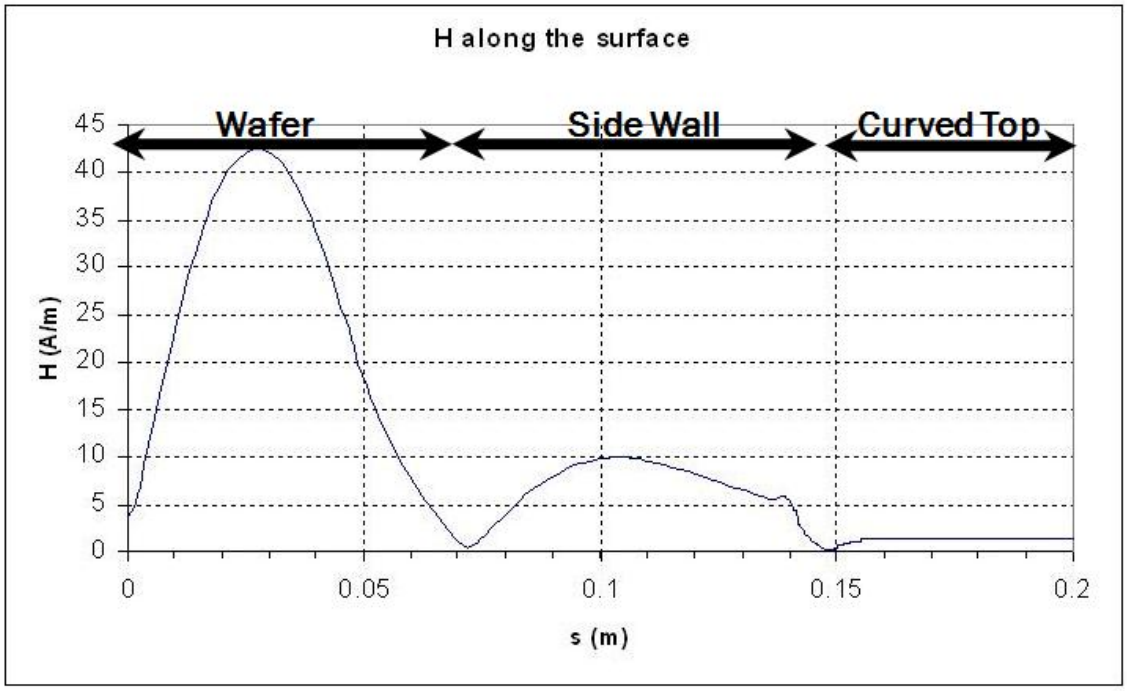

FIG. 19. The magnetic field located on the cavity walls. Zero is located at the center of the sample and goes to the junction of the sample and cavity, indicated by the sharp drop in field. It then proceeds up wall of the test cavity to the top. The most intense spot on the cavity wall is four times less than the peak on the sample surface.

is non-existent because the electric field is azimuthal and therefore the electric field will never be perpendicular to the surface of the dielectric. But since the sample is a perfect conductor, the boundary condition dictates that the surface field must be perpendicular. The perpendicular field is very localized and should not be strong enough to pull electrons off the surface, but the sapphire was elevated as a precaution. The height of this offset can be changed by altering the length of the bellows that holds the sapphire to the top of the cavity. Altering the spacing between the sapphire and the sample was modeled and no significant benefits or detractions were seen. Therefore the offset sensitivity is extremely low. Modeling of these fields was performed using eigenvalue and steady state solvers provided by Vector Fields and COMSOL.

The method of coupling power into the cavity was quite an undertaking. Several different methods were analyzed. The model chosen can be seen in Figure 17. These coaxial loop couplers fulfilled the requirements and are minimally invasive to the cavity. There is a large work of experience with these couplers ([16], [22], and [23]) and they should perfectly couple to the TE_{011} mode. The key is to couple magnetically rather than electrically. Therefore the orientation of the loop is critical. The coupling of each loop can be adjusted to create one input coupler and one probe. The individual control should provide excellent matching.

The basic concept of the cavity is complete. The construction of the cavity is quite simple using standard materials located in the Jefferson lab SRF facility. The cavity walls are made of RRR grade niobium. All the seams are electron beam welded, and the baking and chemical procedures are the same as for accelerating cavities. The sapphire is attached to the cavity through a flexible stainless steel bellows which allows the position of the sapphire above the sample to be adjusted. The bellows has two stainless steel flanges welded to each end. A similar, but thicker flange made of NbTi

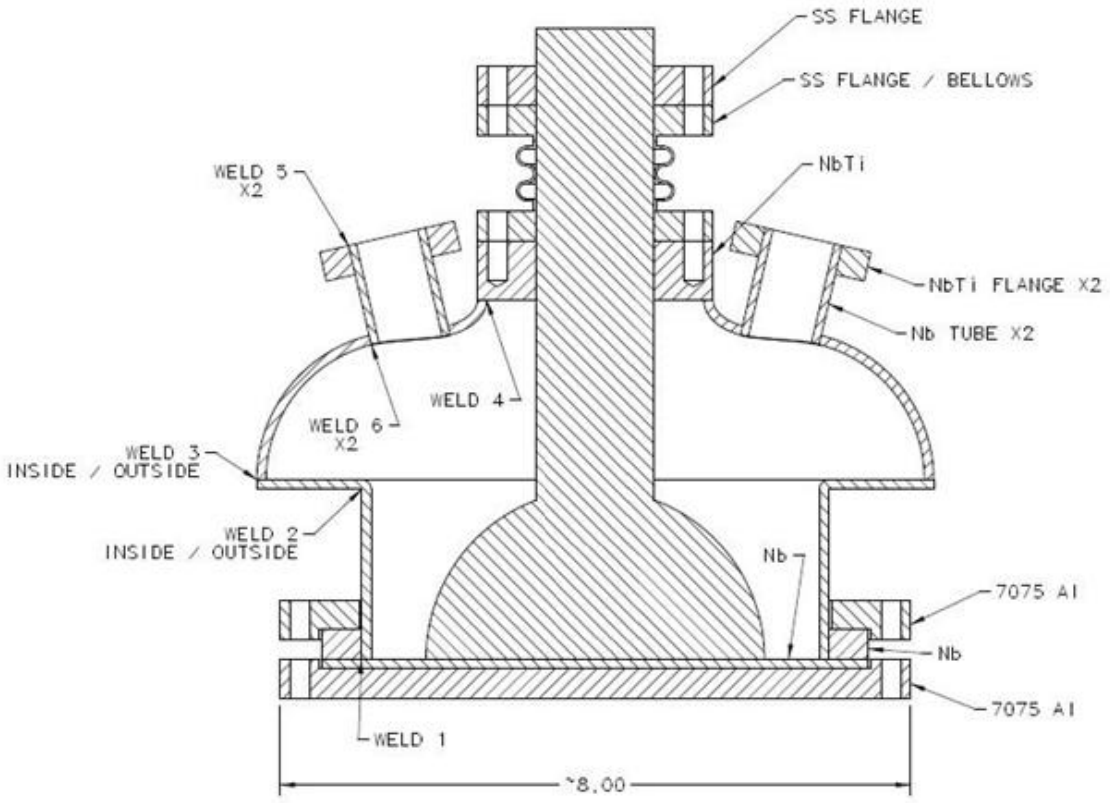

FIG. 20. Mechanical drawing of the Wafer Test Cavity indicating materials used for each piece and order of the welds.

is welded to the top of the mushroom cavity. This allows the bellows to be anchored to the cavity structure. Each flange has a hole through the center approximately the same size as the sapphire shaft. At the top flange of the bellows, a 45 ° bevel is placed on the upper edge of the center hole. This is mirrored on the capping flange that is located on top of the bellows assembly. The two 45 degree angles provide a beveled pocket for an indium wire seal. The wire is pinch pressed against the sapphire as the flanges are tightened down. This creates a soft, sturdy, superfluid helium tight seal that rigidly locks the sapphire into place. The coupler ports are comprised of Nb, and NbTi as Figure 20 shows.

The bottom of the cavity is held with two flanges. The wafer is placed inside the

bottom flange. The back side of the wafer will be coated in Apiezon N grease. The thermal conductive properties of the grease as a solid are excellent and should allow for nice thermal contact between the wafer and the cradle flange. It is important to have robust cradle flange. When a vacuum is pulled on the interior of the cavity it will cause the sample to bow inward, if not sufficiently structurally supported. An indium wire will be placed between the wafer and the niobium flange creating the helium tight seal as well as the RF seal. As usual the interior will be under vacuum and the outside will be immersed in superfluid helium.

Thermometry similar to Figure 21 will be placed on the bottom of the cradle as a means of detecting locations of heating. The cavity will be able to measure the Q_0 through the antennas, as well as mark the location of the heating anomalies. Through these two methods, the analysis of the data should shed some light on the parameters that must be optimized to provide quality material and surface chemistry for superconducting RF cavities.

All of the modeling for, and the performance of, the Wafer Test cavity rely on the quality and the properties of the sapphire. The sapphire is quite large and is very expensive, on the order of $50,000. Since the success of the cavity is so heavily dependent on the sapphire, a test of the sapphire is needed to ensure that the quality is high enough to perform the tasks needed. The constraints placed on the cavity are as follows: operate at 1.3 GHz, have a Q_0 value between $10^9$and 10^{10} in value, and not have its properties vary dramatically with temperature. To reduce cost and to ensure the sapphire is excellent quality, a test system is needed to measure these properties. The Dielectric Test Cavity was designed to use a smaller sapphire and test these important parameters as well as obtain experience in working with RF equipment.

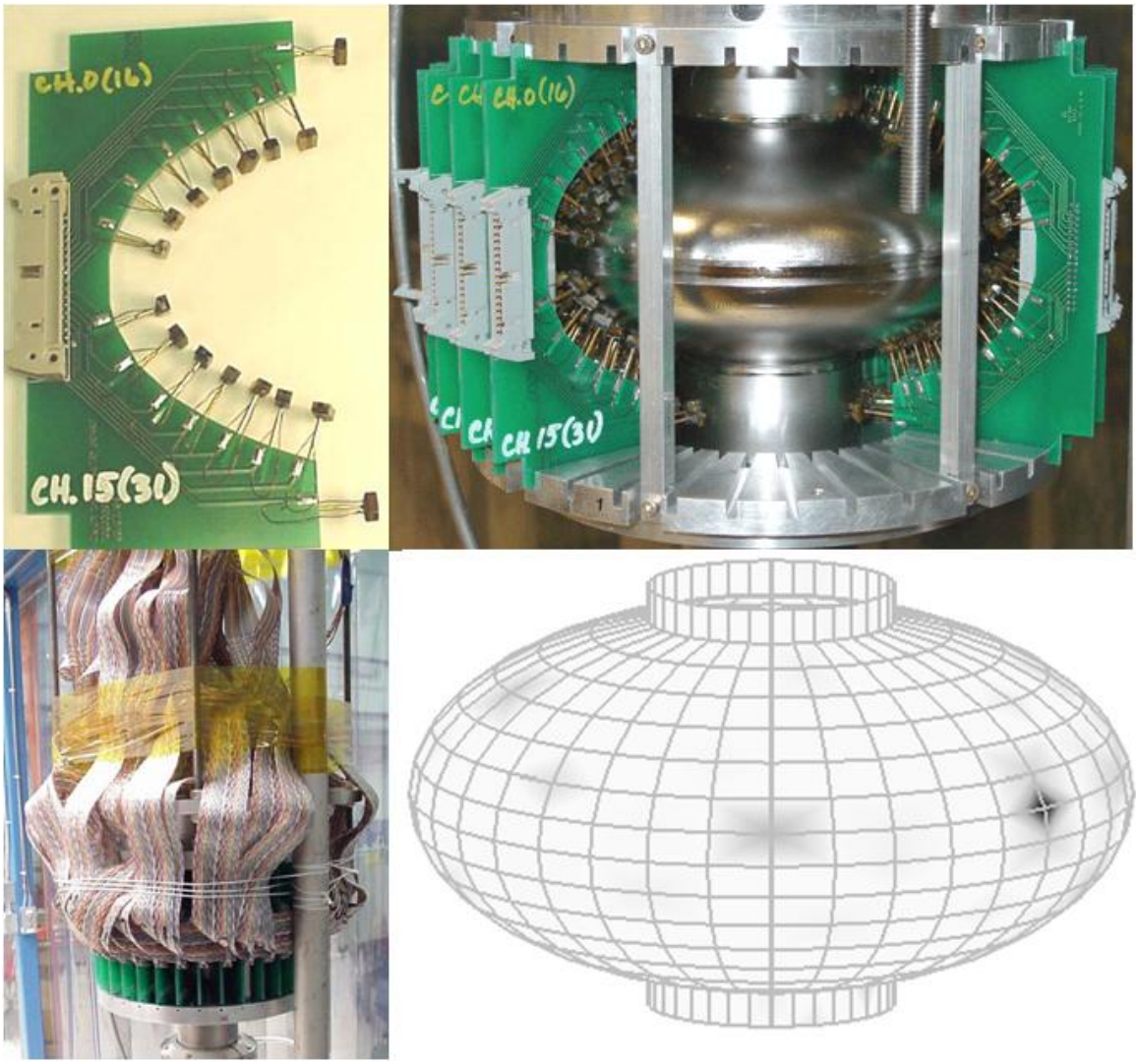

FIG. 21. Upper Left: The thermometry shown is for a single cell cavity. The thermometers used in this particular set up are 576 Allen Bradly resistors that have the capability to measure an eighth of a Watt [24]. These resistor have a range between 10 Ω at 300 K to around 3 $k\Omega$ at 1.9 K. These particular models will reach 22 $M\Omega$ with 5% tolerance into the mK range. For the wafer cavity, a flat resistor bed would be created that mates to the bottom of the cradle flange. Upper Right: Full set of resistor panels placed around the cavity. Lower Left: The electrical lines attached to the resistor plates. Lower Right: The computer read out of the thermometry during the triggering of a quench.

B. Dielectric Test Cavity

The purpose of Dielectric Test Cavity is to learn about the dielectric properties of sapphire at a reasonable cost. To minimize cost, a CEBAF cavity was used as the primary design. This is the predominant type of cavity that is used in the Jefferson Lab accelerator. The difficult aspect of such an experiment is to determine the amount of dielectric needed to measure the quantities accurately. At the same time a method to hold the sapphire in the cavity, as well as the means by which to measure these unknowns, had to be designed. After significant trials and thought experiments, a design was completed using Vector Fields, COMSOL, and Autocad Inventor programs.

The sapphire length was chosen based upon two parameters. First, the majority of the sapphire would encompass the intense region of the field generated. This parameter is dependent on the dielectric constant of the sapphire. The dielectric constant determines how much the fields will shift in the cell. The dielectric constant is axially dependent and varies with temperature. A series of measurements have been made on the different axes of sapphire over a wide range of temperatures, Figure 22. COMSOL allows for asymmetric dielectric constants and larger computational runs. The dielectric constant used for the c-axis for all the models was 11.34, and 9.27 was taken as the value for the a-b plane since the temperature the cavity will be predominantly tested at is 2 K.

With accurate dielectric constant numbers, the second parameter for the length of the sapphire was analyzed, the holding fixture. The cost of the sapphire increases with the size of the crystal, therefore the smaller the crystal the better. The limiting factor is the fields on the sapphire holding apparatus. The field generated from the cavity will leak down the beam tubes because the sapphire will draw the field towards it. Hence the length was set based upon the decay of the field down the beam tube,

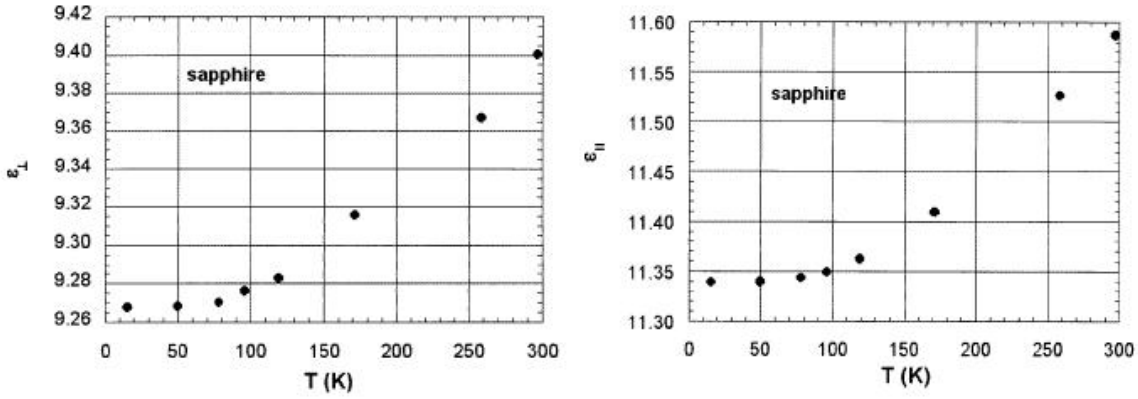

FIG. 22. Illustrates the dielectric constant of sapphire as a function of temperature perpendicular and parallel to the c-axis. Axes a and b are perpendicular to the c-axis [25]. Copyright 1999, Institute of Physics.

and the field on the holder.

After a series of developments, the final cavity design was completed. This design shown in Figure 23 contains all of the major components of the cavity excluding the couplers. The side port was added at the last minute due to a discussion with Peter Kneisel and Gigi Ciovati. The coupling was originally designed to be located on the same end flange. In almost all cases in the RF work, the input power antenna is located on the end flange of the beam tube. The pick up probe is on the opposite beam tube flange, on opposite side of the cell. In this configuration the fields must travel down the beam tube, resonate in the cell, and then travel down the opposite beam tube to the pick up probe. This then is truly measuring the transmitted power.

The two antennas on the same flange could lead to cross talking between the two antenna. The probe, instead of reading the decay time of the cell, could read the power coming from the antenna as well as the decay of the cell. This would decrease the Q of the cavity. It was therefore necessary to separate the antennas and attempt to remove the direct line of sight from one antenna to the other. The initial design

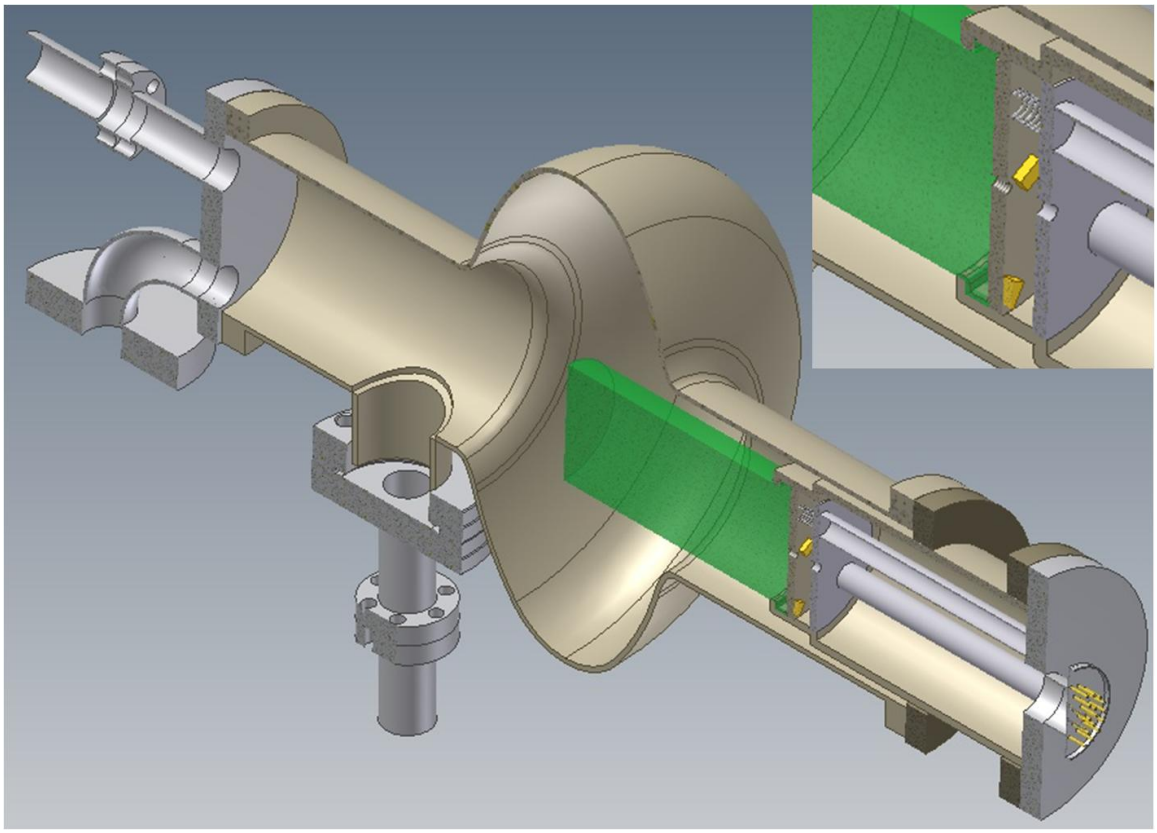

FIG. 23. Final design of the cavity. The left end contains the vacuum flange which holds both the vacuum port and an RF port, which is off center, for an antenna. The side port was attached after construction began to eliminate the possibility of cross talk of the two antennas, which would have been both located on the vacuum flange. Now one antenna is located off center on the side port. On the right, the sapphire (green) is held by a reactor grade niobium holding fixture. On the rear of the sapphire (upper right), a backing plate with an air escape hole is placed on the back. A groove is inserted on the backing plate allowing an indium seal to make a thermal bridge between the sapphire, backing plate, and holding fixture. The backing plate has two resistors to allow for thermal measurements and the holder acts as a thermal sink to cool the sapphire. This is compressed with a spring loaded pushing fixture, holding everything in place. The cap has a electrical feedthrough for the leads to the resistors to pass through.

was to place the probe on the end flange and place the input power antenna in the side port near the iris. This should eliminate the majority of the cross talk, and since both antennas are placed off center from their respective flanges, they should couple to the TE_{01} nicely.

The input power antenna is a copper $\frac{1}{4}$ inch rod that is bent into a hook. Two of these hooks are made for testing purposes. The base of the hooks are bored and given a 4-40 thread, the top is rounded. Copper spacer rods are also made to get the coupling correct. The hook and spacer are attached to the RF feedthrough which is connected to the input power. For the probe, the process is similar. The only difference is the probe is just a straight section with a rounded end.

The deeper tapped hole on the base of the hook allows for the antenna to bottom out on the feed through. For the hook it is imperative that the leg of the hook is pointed in the azimuthal direction. During assembly, the flange will be bolted on after the hook is oriented properly. For the straight pin probe this is not an issue. The couplers are then sized to the correct dimensions for the correct coupling to the cavity.

The couplers are not needed for the RF simulations. However the inner structure of the sapphire and its holder are required. The sapphire dimensions were set at 10.5 cm in length, 5 cm outer diameter, 4.5 cm inner diameter, and a lip thickness of .5 cm. The holder, made of Niobium, is shaped to snuggly fit the sapphire within it walls. The sapphire lip keeps the sapphire from falling. The wall thickness of the entire holder is $\frac{1}{8}$ of an inch. The holder has two Niobium Titanium flanges welded to its side providing the vacuum seals. In addition three holes are drilled on the interior of the first flange to allow vacuum to be pulled on the expanse behind sapphire and holder.

On the back side of the sapphire is a niobium backing plate. The backing plate

has a groove to allow for an indium wire seal to be pressed. The indium forms a thermal conducting pathway between the backing plate, niobium holder, and sapphire. A tapped 4-40 hole is inserted in the center of the backing plate to allow for the removal of trapped gas during the indium compression, as well as a means to pull the backing plate off the sapphire during subsequent disassembly.

On the face of the backing plate pointing away from the sapphire are two thermometers. These Cernox silicon diode resistors were anchored to the plate to measure the temperature of the backing plate, which should be at the same temperature as the sapphire due to the thermal bridge formed by the indium seal. To ensure the bridge is held together, a part was machined and welded to provide constant pressure to the plate even during contraction and expansion.

This pusher system is built out of 316 stainless steel parts. The reason for the specific metal is 316 is nonmagnetic, compared to other steels. The resistors are sensitive to magnetic field and therefore every effort must be made to reduce errors. In this pursuit 316 springs were also needed. 316 steel is not a very good spring material and therefore custom spring had to be made. Three rods were attached to a capping flange that forms the outer vacuum seal and includes a 8 pin electrical feed through for the resistors to connect to the outside world. The other end of the three rods has another thin plate with the 3 springs welded to it. So when the flange bolts are tightened and the springs compress, it places a constant load on the backing plate, which will allow the thermal bridge to stay intact.

The other side of the cavity contains both the side port, with an off center RF feedthrough, and the end port. The flange at the end of the beam pipe contains a hole with a pipe elbow transitioned to a vacuum line. It is located at the bottom of the cavity, when hung vertically, to pull out particulates filtering to the bottom via gravity. This indium sealed flange also contains the other RF feedthrough. The

design of all the major components has been completed. Slight alterations were made in certain dimensions to be prudent in material usage without degrading performance.

Using COMSOL, a full electromagnetic model was generated using a standard CEBAF cavity. To simulate this cavity only the interior surfaces need to be examined. It simplifies the problem greatly to only have the model require the outer holder surface, sapphire, backingplate, indium seal, and interior of the cavity. The holes located in the holder are ignored because of the size and location. The fields will exponentially decay traveling down the thin ring to first holder flange. The holes are quite small and therefore no field of any measurable value will penetrate them and dissipate on the resistor chamber. Note the side port addition must be added to the model to ensure the correct field distribution and frequency. This side port does add an asymmetric component to the cavity and therefore a half geometry is required compared to a small slice. Figures 24, 25, and 26 show the fields at 1.875 GHz, which is the TE_{011} mode for the loaded cavity.

To find what is expected for the Q_0 of the cavity the loss tangent, $\tan\delta$, must now be taken into account. The loss tangent of vacuum is non-existent and any residual gas in the cavity is assumed to not have any effect. However the sapphire, as can be seen from field shape, has a significant effect on the cavity. Therefore the relationship between the loss tangent and Q must be understood.

Referring to Equations 1.3, 1.4, and 1.5, the equation for Q_0, where U is the stored energy and P_{diss} is the power dissipated, can be more elaborately written as

$$Q_0 = \frac{\omega\mu_0 \int_V |\mathbf{H}|^2 dV}{R_s \int_S |\mathbf{H}|^2 dS}. \tag{2.1}$$

Now that the sapphire has been introduced, the stored energy needs to be divided into subdomains and the lost power expression is incorrect. In the stored energy equation it is assumed that the entire volume is integrated. Since there are two subdomains

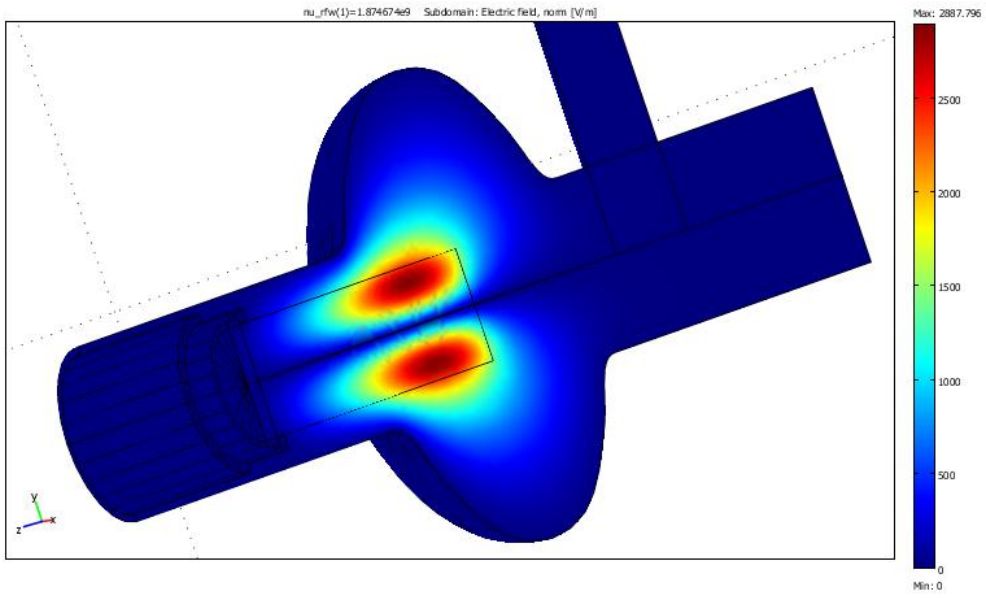

FIG. 24. Electric Field of Dielectric Test Cavity. The electric field points azimuthally and the field is almost entirely located within the sapphire, whose outline can be seen the in center. The cavity is operating at a 1.875 GHz frequency with little field on the surfaces of the cavity and the holder.

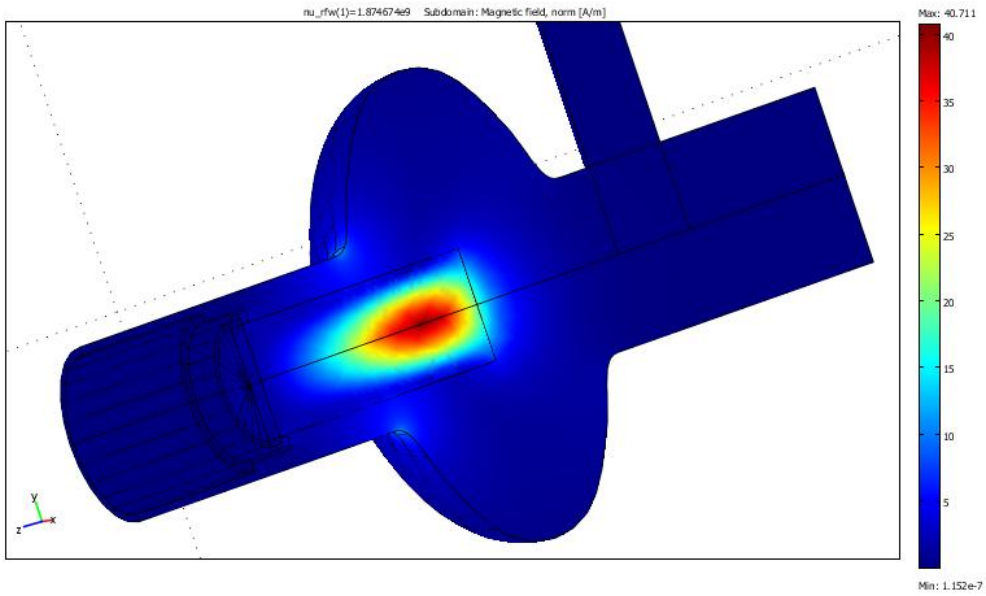

FIG. 25. Magnetic Field of the Dielectric Test Cavity. The magnetic field is located within the heart of the sapphire with only a slight bit of leakage to the iris.

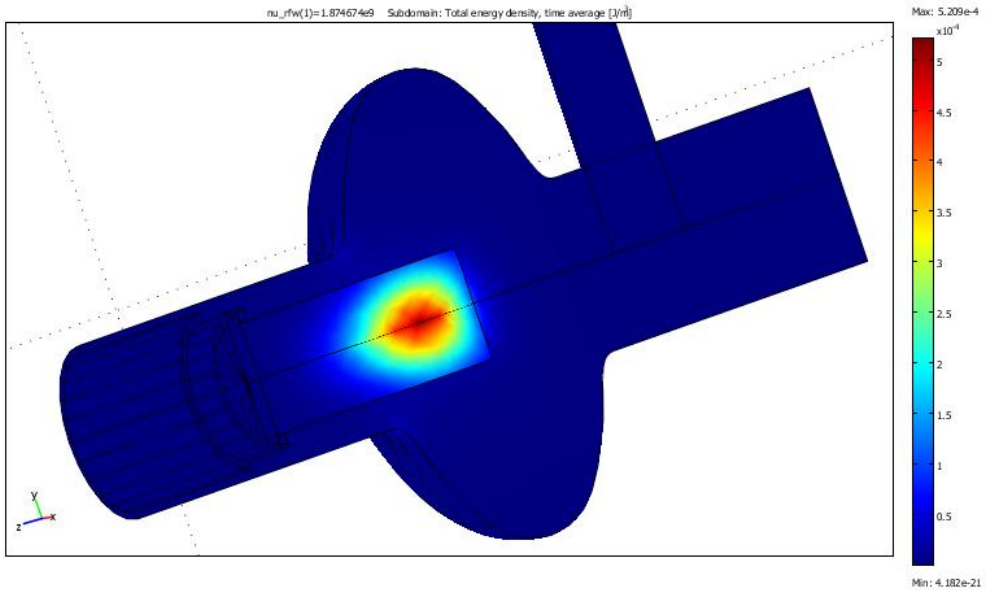

FIG. 26. Energy Density of the Dielectric Test Cavity. The energy is time averaging of the electric and magnetic fields. The energy is clearly a superposition of the previous two images. The energy is stored towards the end of the sapphire almost entirely. Therefore if the losses in the cavity should be completely dictated by the loss tangent of the sapphire.

within the cavity, each must be summed over individually. The electric and magnetic fields vary with time and are not spatially dispersed in the same manner, a averaging must occur when finding the energy located within each subdomain. Hence forth, U will be the sum stored energy of all domains within the cavity, and E_{die} will be the stored energy within the sapphire, both are time averaged.

The losses on the surface of the cavity will be calculated in the same manner as was done in the empty cavity, but an extra term needs to be added in the losses to reflect the loss tangent of the sapphire. This is easily performed.

$$P_{diss} = P_{rad} + P_{sap}, \tag{2.2}$$

where P_{rad} is the losses on the walls due to radiative effects and P_{sap} is losses created by the loss tangent of the sapphire. The power dissipation in the sapphire is proportional to the frequency, the loss tangent, and the amount of energy located within the sapphire volume. Therefore

$$P_{sap} = 2\pi f E_{die} \tan\delta \tag{2.3}$$

and

$$Q_0 = \frac{\omega U}{P_{rad} + 2\pi f \tan\delta E_{die}}, \tag{2.4}$$

Now that the appropriate equations are derived, it is straight forward to find the expected Q_0 for a specified loss tangent. The COMSOL models provide the frequency, stored energy, and the field distribution. Then using Eq. 2.4 and these calculated values, it is possible to draw several conclusions about the cavity using the loss tangent as the only variable parameter. In order to get an estimate, several material properties need to be known. The niobium and indium resistances are needed at 2 and 4.2 Kelvin to get an accurate estimate of P_{rad}. Using data provided by Gigi Ciovati for a random high Q_0 CEBAF cavity, the niobium resistance is approximately 600 $n\Omega$ at 4.2 K and

21 $n\Omega$ at 2 K. For the indium, the story is much more complicated. The Cryogenics Handbook [26] states that room temperature resistivity is 8.19×10^{-8} Ωm. Using the ratio given of .0015 ρ/ρ_{273} at 4.2 K, the resistivity is therefore 1.2285×10^{-10} Ωm. However the resistance is needed, not the resistivity. This can be easily found using the definition of resistance in an RF setting, Eq. A.5, and simplifying.

$$R_s = \sqrt{\pi f \mu_0 \rho}. \tag{2.5}$$

This is equivalent to one divided by the skin depth times the conductance. However this expression above is much more useful, which allows the direct computation of the indium resistance of 9.5352×10^{-4} Ω at 4.2 K. The handbook does not have the resistivity of the indium below 4.2 Kelvin. The only value below the transition temperature found was at .82 K [27]. Using Figure 27, the resistance of indium can be found at 1.875 GHz, 9.5352×10^{-6} Ω. This is a reasonably accurate value to use for these calculations, but the impurities are not specified and could have a adverse effect on the indium.

The surface impedances of the two materials seeing field are now known, the Q_0 can be calculated as a direct relationship to the field distribution and loss tangent.

$$Q_0 = \frac{\omega U}{P_{In_{rad}} + P_{Nb_{rad}} + 2\pi \ f \tan\delta E_{die}}, \tag{2.6}$$

To get the P_{rad}s, the magnetic field on each part is found by using the COMSOL model to integrate over the intensities. Once the fields are integrated, multiply the appropriate resistance of the material and divide by two, for the time averaging, to get power dissipated. The magnetic field losses on the walls are the second largest form of loss other than the sapphire (assuming that the sapphire's loss tangent is high).

From Figure 25, the majority of both the electric and magnetic fields are located

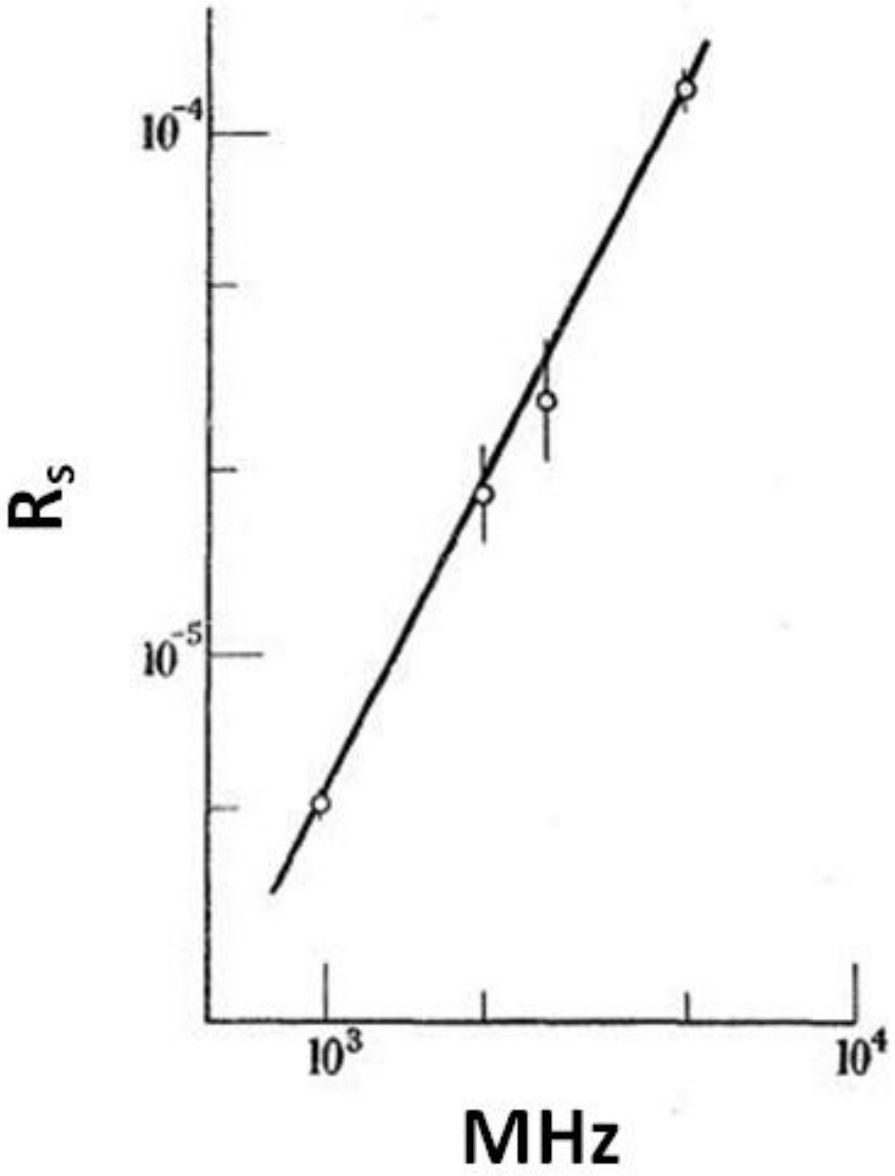

FIG. 27. The resistance of indium at .82 Kelvin over a frequency space of .5 to 10 GHz. The operating frequency is 1.87 GHz, therefore the resistance is approximately one hundredth of the measurement at 4.2 K [27].

within the sapphire. The electric field is parallel to the surface and therefore no electrons should be stripped off the surface. At the center of the sapphire, the highest magnetic field is 40.711 in arbitrary units. On the cavity surface itself the highest field is on the sapphire side iris, which sees 10.899 units of magnetic field. The second highest field is located on the niobium holder's lower curved surface on the support lip and has an intensity of 5.166 units. These locations are the highest magnitudes of field but not necessarily the highest loss areas for it is the integrated area that dictates the losses.

The Q_0 is a now a direct function of the choice of the loss tangent. It expected that the loss tangent of the sapphire would be between 1×10^{-8} and 1×10^{-10}. As Figure 28 illustrates, the loss tangent of sapphire can be extraordinarily small. There is a temperature dependence but, on the range of 2-4 K, it is relatively small. In previous test cavities, such low loss tangents are not seen. One reason for that is paramagnetic resonances. These are impurities within the sapphire lattice, such as Cr^{+3}, Fe^{+3}, Ti^{+3}, and Mo^{+3}, that will resonate and dissipate energy in the lattice at frequencies above 7 GHz [28]. There have been several papers showing that the loss tangent can be very small, such as 2×10^{-10} [29],[30]. However, these samples are extremely small, on the order of 1-2 centimeters. The lowest measurement ever made, by Buckley, was the only measurement to be completed by calorimetry, where as all others were performed with resonators. Rabi Wang has performed measurements on relatively large crystals (2 inch diameter, 2 inches tall) and has seen losses on the order of 1×10^{-9} for both the 4.2 K and 2 K measurements [31]. This is approximately half the size of the sapphire that will be incorporated by the dielectric test cavity.

The dielectric loss tangent is therefore frequency dependent, temperature dependent, and orientation dependent. The orientation dependence comes from the crystal lattice itself. The loss tangent parallel to the c-axis is different than the a,b-axis.

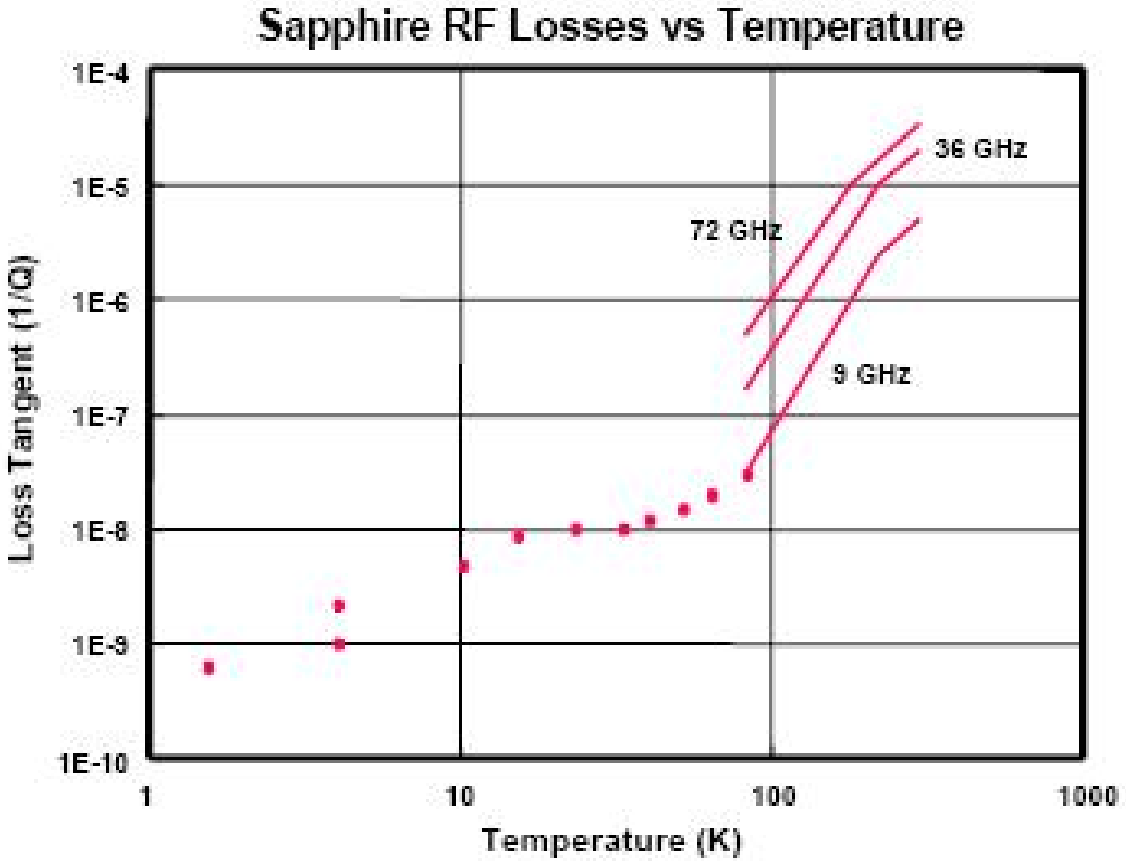

FIG. 28. Loss tangent of sapphire as a function of temperature and frequency. The mechanism for the loss at low temperature is conjectured to be paramagnetic resonances. These resonances should disappear at lower frequencies [32].

Q of the cavity with varying loss tangents					
loss tan	1.00E-08	5.00E-09	1.00E-09	5.00E-10	1.00E-10
Q at 4K	1.09E+08	2.00E+08	5.94E+08	7.88E+08	1.07E+09
Q at 2K	1.20E+08	2.40E+08	1.19E+09	2.34E+09	1.05E+10
Losses in sapphire compared to total losses in entire cavity					
loss tan	1.00E-08	5.00E-09	1.00E-09	5.00E-10	1.00E-10
Sapphire loss 4K	90.69%	82.97%	49.34%	32.75%	8.88%
Sapphire loss 2K	99.85%	99.71%	98.55%	97.14%	87.15%

FIG. 29. Upper: The Q as a function of loss tangent is located in the upper table. Lower: Table shows the percentage of dissipated energy in the sapphire compared to the total losses in the cavity as a function of loss tangent.

The difference between the two can be as large as a factor of two. The parallel axis has the lower loss tangent but neither the parallel nor the perpendicular is the loss tangent that is of interest. The direction that is under observation is the loss tangent on the azimuthal direction since the field is a TE mode. This quantity has not been measured recently with new sapphires made with updated refining processes but in the past has fallen between the parallel and perpendicular loss tangent values, and not expected to change. The a,b,c-axes values are quite recent, and therefore these values can be used more reliably to compare with this cavity.

The Q as a function of loss tangent can be summed up in Figure 29. Most of the energy is located within the sapphire and a wide range of loss tangents are plausible. The Qs shown are also very reasonable compared to known data about SRF cavities and therefore is an accurate approximation as to what is expected.

These Qs are what will be expected in the experimental procedure. Most important "take away" is that with this development the loss tangent can be calculated from the Q measurements taken experimentally.

CHAPTER III

EXPERIMENTAL SETUP AND PROCEDURES

The construction of the sapphire test cavity began at Jefferson National Lab (JLAB) on February 4th of 2010. The niobium sheet used for the project was purchased from either ATI Wah Chang or Tokyo Denki. The niobium was RRR grade material, rather than reactor grade material which is more common because it is used in nuclear facilities. RRR, or Residual Resistivity Ratio, is defined as

$$RRR = \frac{\text{resistivity at 300 K}}{\text{resistivity at low temperatures above } T_c}. \tag{3.1}$$

The RRR requirement for JLAB is 250 or better. The details of the material assay are different at every facility and one must look for the specific demands in content. Reactor grade niobium is less expensive than RRR grade niobium, but less refined in its composition. As a result, the quality of the reactor grade material is lower than that of the RRR material. The reactor grade is generally not used for cavities, but is often used for beam tubes and other fixtures. The reactor grade material is a harder material therefore requires different methods to machine it. The difference between the two materials in terms of RF performance is not known, and there is no existing scientific evidence that proves that one material causes a significant change in performance compared to the other material. RRR can be affected by processes such as rolling and stamping, but also by the type of impurities. Therefore, the RRR figure of merit is not consistent. Two different materials containing distinct impurities could both receive the same RRR classification because one material was given more mechanical work than the other material. Hence, each billet of RRR niobium is unique; the content and RRR are never the same. An alternative definition of RRR could be the measure of processing performed on the material, but not the inherent

characteristic regarding superconductivity.

The material used for the formation of the sapphire test cavity at Jefferson National Lab was small grain RRR sheet. Small grain material is much easier to work with than large grain material because the grains are randomly oriented. In the niobium crystal, the lattice is more easily worked in one direction versus another. In large grain material, internal stress can build up, leading to deformity when shaping the metal. In small grain niobium, this long-range order is bypassed and allows more flex in the metal during shaping.

Two disks were made out of $\frac{1}{8}$ inch thick RRR Niobium material. The outer diamter was machined to $9\frac{3}{8}$ inches and a $1\frac{3}{4}$ inch hole was cut in the center. The discs were hydraulically formed using a 7075 Aluminum (aircraft aluminum) stamp and dye. Aluminum was used in order to address the concern that some of the steel could embed in the niobium and the carbon in the steel could leak into the material during a heat treatment. This alloy of aluminum was also used because it has a higher tensile strength than steel and therefore little to no deformation, but also Aluminum is easier to cut and shape compared to steel.

To stamp the parts in the press, lubrication is needed to prevent tearing. The dye, stamp, and plate are rubbed by hand with a generic motor oil. If the potential for contamination by the carbon migrating from the steel dye into the bulk was already a cause for concern, using hydrocarbon oil as the lubricant would exponentially exacerbate the issue. Perhaps the oils during compression are being stored in the bulk in pockets, penetrating through the slip planes, or seeping through grain boundaries during deformation. The realm of magnet manufacturing has seen a similar problem. Mobil 1 was used for years as a lubricant during the wire drawing process. All attempts to completely cleanse the material of the lubricant were unsuccessful. A single monolayer persisted on the surface of the wire. Hence, a different lubricant may be

needed. Several industrial companies produce lubricants for a variety of purposes. Contact has been established with such a company that makes a lubricant with a solvent that will completely remove any residual molecules.

To create the half cells the disks were inserted between the dye and stamp. Then the assembly was placed inside the press, followed by engaging the press until the pressure gauge reached 100 tons. It was held at this pressure for approximately 3-5 seconds and was then released. The niobium was then removed from the dye and stamp, then wiped down with a rag to remove excess oil, see Figure 30. In general, the method for production of a cavity is to coin the irises after the initial stamping. A "coining" fixture is needed to ensure that the iris is shaped properly. However, the coining fixture was not found for the CEBAF shape.

After stamping occured, the formed cells are then trimmed at the machine shop. The cells were placed in a fixture where they were cleaned with alcohol and methanol. Then, the two half cells were placed between machined dyes. The excess material on the irises' and the equators' edges was machined off. Special OSG powdered metal end mills were used during the machining of the niobium. The reason for such a specialized cutter was because of the E-beam weld. Niobium is an extremely abrasive material. It is quite soft, harder than copper, but work hardens slower than copper. These unique properties are the reason for the non-standard tooling. When a standard cutter breaks, it takes large pieces of the mill tool bit. If this occurred while machining niobium, the shard would embed itself in the material surface.

Steel and high-speed steel are the materials used in the standard cutter and are much harder than the niobium. If a shard enters the material, during welding, steel will explode and high speed steel will vaporize because of the non-metallic elements in the steel. Carbide tools are especially bad since the material is not eaten away by the chemical cleaning process (acid etch) and will remain in the material. During the

FIG. 30. Image of two half cells created directly after the pressing. Note that the center of the holes and lips of the iris are not symmetric. This asymmetry is most likely due to the material sliding in a preferential direction.

chemical cleansing processes, the tool shard is generally too large to be adequately removed. The powdered metal bits, during a break, fracture into extremely small pieces. These powder sized particles are easily removed by the acid etch. If the foreign fragment is not removed prior to the E-beam welding, a hole will be blown in the cavity, which will have to be patched. These patches are tentatively useful.

Once the excess material was removed, the mill was then brought to the exterior of the edges for a weld preperation cut. From the interior of the cavity's equator to the outside, the thickness must be $\frac{1}{16}$ of an inch for the butt weld. The tolerance for the weld prep was plus or minus .003 inches. These criteria are necessary for the ebeam welder to make a consistent butt weld across the equator and iris. There is some debate as to whether or not this "weld prep" is even necessary to give a uniform weld.

The interior of the equator was slightly machined to ensure there was a smooth radius flowing into a flat at the joint. This procedure was performed using a half inch high speed stainless steel ball end mill. Great care was put into the research of the powder bits; it is strange that the location that is most crucial for RF performance (source of most breakdown) is often machined with stainless steel tool bit. The two half cells after machining came out within four thousandths of an inch of the specifications.

A beam tube with a side port was cannabalized from a previous cavity to be used for the dielectric test cavity. A piece of reactor grade niobium was used for the other beam tube. A single half cell and the beam tube with the port were then cleaned by the chemistry lab.

In general, the procedure for cavity fabrication is as follows. The parts are degreased then given a buffered chemical polish, or BCP. A BCP is a chemical etch using hydrofluoric acid, nitric acid, and phosphoric acid in a 1:1:1 ratio. After the

pieces are etched they are rinsed with 16 MΩ water (note all water used at this facility is 16 MΩ). Then the parts are high pressure rinsed (Figure 31). This is done by a rod with holes is inserted along the axis. The parts are then rotated and moved up and down, insuring that the jets adequately rinse all surfaces. The rinse lasts approximately an hour for a single cell moving at 4 mm a minute vertical while under constant rotation. For a 7-cell cavity, the rinse is around 4 hours. A constant flow of water is always used, even when not in operation, to deter bacterial growth inside the sprayer.

The acid used was poured back into its original container from whence it came and stored for the next usage. The acid can only be used for about 20 minutes, or 20 single cells. All of the Niobium and additional material eaten away by the acid is accumulated in the acid– hence the finite lifetime. It is important to note that since a large amount material was removed, it might be possible to contaminate the cavity by recycling the acid over and over.

Once the high power rinsing was completed, the part was dried using filtered nitrogen. Once dry, the pieces were then placed in an ultraclean nylon tube bagging and the ends were sealed. In the end state, the piece is located in a clean bag filled with nitrogen, waiting for further processing.

At this point the parts are cleaned and given to the welder. It is important to where gloves during removal from the bag since the oils on your fingers can adversely affect the welding process of the niobium. The parts are then checked for bumps, dings, or burs that would prevent the two surfaces being welded from meeting each other. If such defects occur they are removed.

The parts being welded to one another are placed together and a rod is inserted down the center of the axis. Two aluminum plates are used to set the fixture, one of which was spring loaded. The spring loaded Aluminum plates, anchored to each side

FIG. 31. High power rinsing device that moves up and down as the water jets rotate about the axis.

FIG. 32. Fixture is inserted through the parts to insure proper alignment. Pressure is applied through a spring loaded plate to keep the faces together and to handle the expansion and contraction of the metal during the welding process.

of the rod, are used to apply quite a bit of pressure to the parts, as shown by Figure 32. The spring compensated for the expansion and contraction of the material during heating from welding, and the cooling down from the Nitrogen purge.

The end of the fixture, a rod, is inserted into the chuck of the ebeam welder axis control base (Figure 33). All items in the chamber must be stainless or aluminum. The oils used in pumps and other mechanical parts must be vacuum type oils. It is possible for oil to backstream down the vacuum line; however, an alarm will sound, and all parts within the chamber are scrapped.

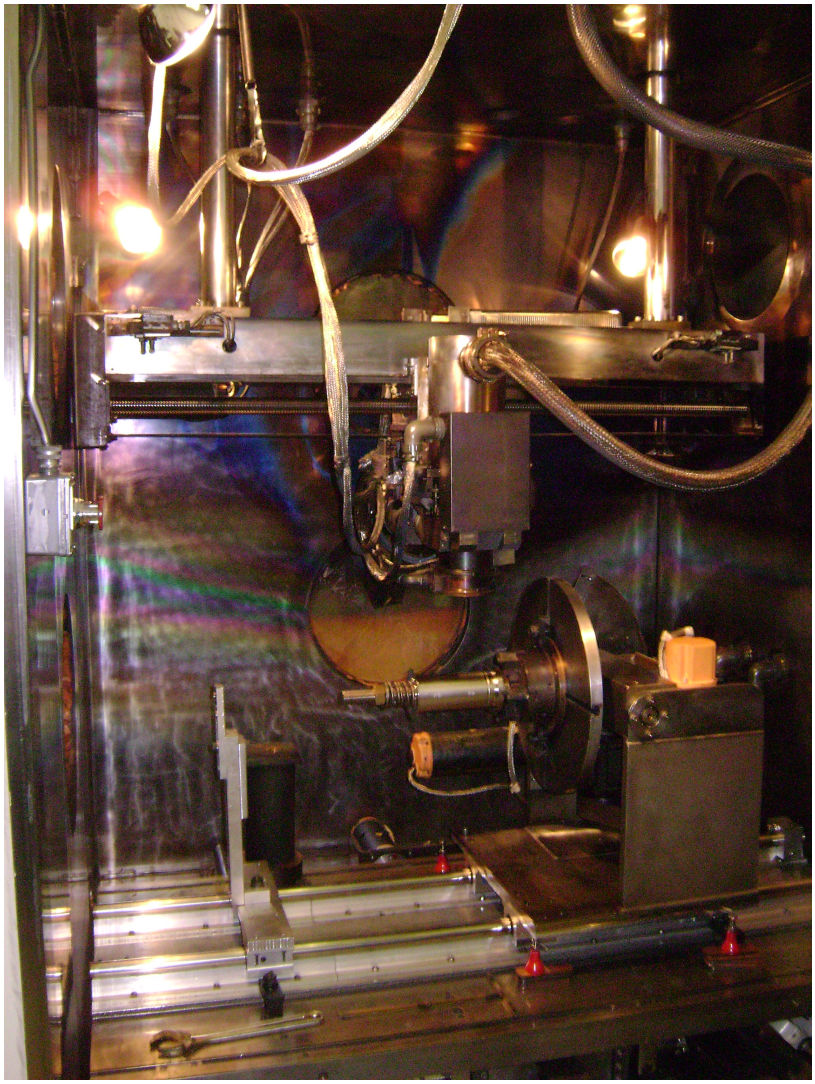

FIG. 33. Sciaky 6-axis E-beam welder located at Jefferson Lab. Pictured here is the vacuum chamber open with the beam tube inserted for welding.

There are several possible sources of contamination that could occur in the E-beam welder machine. One source of contamination is the insulation on the wiring may outgas. Even though the lubricant in the pumps is vacuum oil, there is oil in the bearings of the motors and chucks for turning the piece located within the welder's vacuum chamber. These oils may outgas during pressure changes and heating.

Once the setup inside is complete, the chamber is sealed and brought down to 7×10^{-5} torr. Once the chamber is under vacuum, APTs, or Axis Position Table points, are taken. Several APTs were taken around the circumference of the joint. These APTs act as markers for the welder as it traveled. Between each APT, the welder traveled in a straight line. If a part was curved or complex, many APTs must be taken around the joint in order to be properly welded. For 3D welds such as the side port, as many as 40 APTs will be taken.

After the position is established, four tacks are made on the surface. These tacks are necessarily made before the welding process, because as the piece is welded and heated, the material will want to deform. The tacks anchor both pieces to each other to eliminate motion in the joint. During the welding process, the part is rotated and translated rather than the electron gun. The beam liquefies an area of the material by rastering the beam in a small ellipse. The ellipse axes are aspected with a 2.75:1 ratio. The beam creates plasma in the metal and allows the beam to travel through the entirety of the material. Therefore, the spot where the welding occurs is a plasma-molten liquid mixture. The gun is always held approximately 6 inches from the weld during the tacking and welding processes.

The first weld to be done was an inside-outside weld. This type of weld is done using two half penetrations welds, one on both sides of the joint. This weld gives a nice smooth surface to the joint on the exterior; but more importantly, it gives a smooth joint on the interior. The weld prep makes the joint, as previously stated,

$\frac{1}{16}$ or .0625 inches thick. The half penetration weld goes .040 inches deep so the two welds indeed overlap.

Once the weld is completed, a ten minute period is provided to let the gun cool down. Then, the ebeam chamber was filled with dry nitrogen gas for approximately two minutes. The part being welded is currently at 2000 degrees Celsius and is quite active in an electrochemical sense. It is interesting that Argon is not used instead of nitrogen. The reason for this is the large volume of gas that is used per day. Using argon would be expensive. It has been seen though that the content of Nitrogen near the welds is quite high. The niobium is quite active and could be absorbing the gas at these temperatures. Perhaps using argon to cool down would make a difference in performance. Once cooled off, the part is usually removed from the welding chamber at 100 degrees Fahrenheit; it is warm to the touch.

It is worth observing both the smell of the air after the weld chamber is opened and the color of the walls. The odor has been referred to as the smell of tallow; the author has described the odor as smelling like a Chamois leather. It is not understood why the smell occurs.

The interior of the vacuum chamber is spattered with niobium vapor creating thin films of over the interior surface of the welder. As described earlier, the windows must be replaced to make the interior visible because of this deposition. The walls reflect the light in various ways. A rainbow of light comes of the walls, indicating a wide variety of niobium oxides and nitrides are forming at varying thicknesses. Before the advent of the E-beam welding, TIG welding was used in most applications. It was the experience with TIG welding in vacuum that the intense light produced caused the stainless walls of the chamber to outgas the water it absorbed. As to whether or not this occurs during e-beam is unknown.

During a full penetration weld, or two half penetration welds, the material in

the direction perpendicular to the weld will shrink by .016 inches every time a weld is made. At the location of the tacks from the outside weld, it appeared that a full penetration weld occurred during the half penetration weld. This appeared to be an interesting observation to the welder. An intriguing research opportunity would be to mark the location of the tacks and compare those locations to those of quench sites along the equator. Perhaps there is a correlation.

To cut down on time, it has been brought to the author's attention that the welder could ignore the weld prep altogether and weld the $\frac{1}{8}$ inch material directly. The beam tubes are done in this manner, but all the other welds are not. This is another legacy of Cornell. It could be a cost savings to just weld the material without the weld prep and check performance. In addition, the concept of e-beam assisted diffusion welding of two Niobium pieces has been contemplated. This could be done using the fixtures made for stabilizing the half cells during final equator weld. The two half cells could be pressed together using large springs. Then, using a low power high speed passes, the material would heat up rather uniformly across the whole equator. The heat and pressure combined could diffusion weld the material together. This process has been used on a variety of materials with excellent results. An RF cavity was constructed using diffusion welding, but other parameters in the cavity limited its performance, and the process has since been abandoned [11].

Sometimes during welding, as mentioned above, a hole can be blown through the material. Figure 34 shows a 7 cell cavity where a hole was blown through the iris. There are several mechanisms that can cause this to occur, such as a gun arc or contamination.

The parts are cleaned again after each weld, After the flanges were attached to the beam pipe and each half cell is welded to the corresponding beam tube, the interior is inspected. Looking at the interior of the two half cells, it was noticeable

FIG. 34. Image of a hole created in the final iris of a 7-cell cavity during e-beam welding.

that there were defects on the interior of the surface. The most notable defect is a pit on the half cell with the side port attached. One concern is that during polishing of the surface, the niobium might smear and possibly hide small pits. This is a potential problem in later stages when the acid might eat through the smeared layer exposing the pit. Hoping that this does not occur, the interior of the cells were polished using 120 grit flap wheel and scotch brite pad.

The two half cells were then cleaned in the chemistry laboratory and taken to the welder for the final equator weld. Using a gloved finger, which is good within about a thousandth of an inch, the equator was felt around the circumference. There was no noticeable lip, top or bottom, which could be found visually or tactilely. This meant the two cells are very symmetric and had the same shape and size. The piece was then placed in the welder. APTs were taken as usual, every thirty degrees, and 12 tacks were made. The weld was performed and inspected on the interior and exterior. The weld was considered to be a good, clean weld as shown in Figure 35.

The empty cavity was now complete, and the interior structures have to be fabricated. The Niobium backing plate, pusher plate, pusher rods, and flanges were to be constructed as designed in Chapter II. In order to finalize drawings on the holder, an accurate measurement of the sapphire had to be performed. Using a coordinate machine, the large HEMEX sapphire (which visually had a frosted look) was measured (Figure 36). These dimensions are well within the tolerances given to the manufacturer. The diameters of the sapphire were also measured to be within the specifications with excellent concentricity.

Once the sapphire's and cavity's dimensions were measured, the length of the niobium holder was cut to make sure the sapphire's end face was flush with the plane of the equator. A NbTi flange was then welded to the circumferential surface of the holder (Figure 37). In addition to the welding of the two flanges to the surface of the

FIG. 35. The equator joint after e-beam welding.

holder, the three $\frac{1}{8}$ holes were drilled into the wall to allow a means of pulling vacuum on the portion of the cavity containing the resistors, behind the backing plate.

The other pieces for the inner fixturing are shown in Figures 38 and 39. The vacuum flange and probe flange were made of stainles steel. An aluminum mock up of the sapphire was also created to rehearse assembly.

To keep the backing plate down, springs were used. The springs had to be made of 316 SS, which is non-magnetic. Springs of this sort are not easily obtainable. Stanley Spring was kind enough to provide samples of the springs, which provided adequate force. The design called for a 100-pound load when the spring was compressed to .550 inches. However once the springs were compressed, they no longer return to the original length, but provided the same load under the same length compression. The load necessary to compress the indium seal must therefore be tested to ensure the

FIG. 36. The HEMEX single crystal to be used in the Sapphire Test Cavity is shown. Note that the dull color is due to the texture. The surface was ground and not polished. If the surface had been polished, it would have appeared as transparent glass. When placed in a liquid the crystal becomes essentially transparent.

FIG. 37. The Niobium holding fixture is used to suspend the sapphire in the cavity. Holes are located in sides for evacuation of tube.

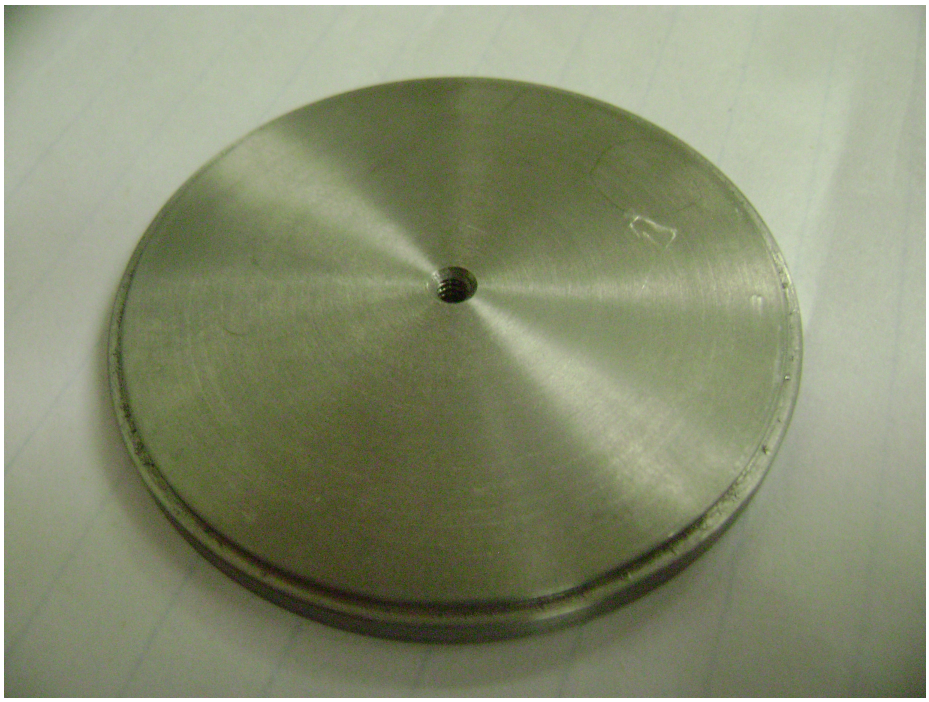

FIG. 38. The niobium backing plate has a groove on the circumference that has a .045 inch well that is recessed from the circular edge by .025 inches, giving a cross sectional area of .001125 square inches. The cross section of the indium wire is .001257 square inches, forcing the indium to flow between surfaces of the sapphire-sidewalls-backing plate intersection.

FIG. 39. This 316 stainless steel structure pushes down the backing plate with a large uniform load. It is attached to the top of the niobium holder, creating indium vacuum seal. It also serves as the means by which the thermometers are connected to the read out, via the electrical feed through at the top of the fixture.

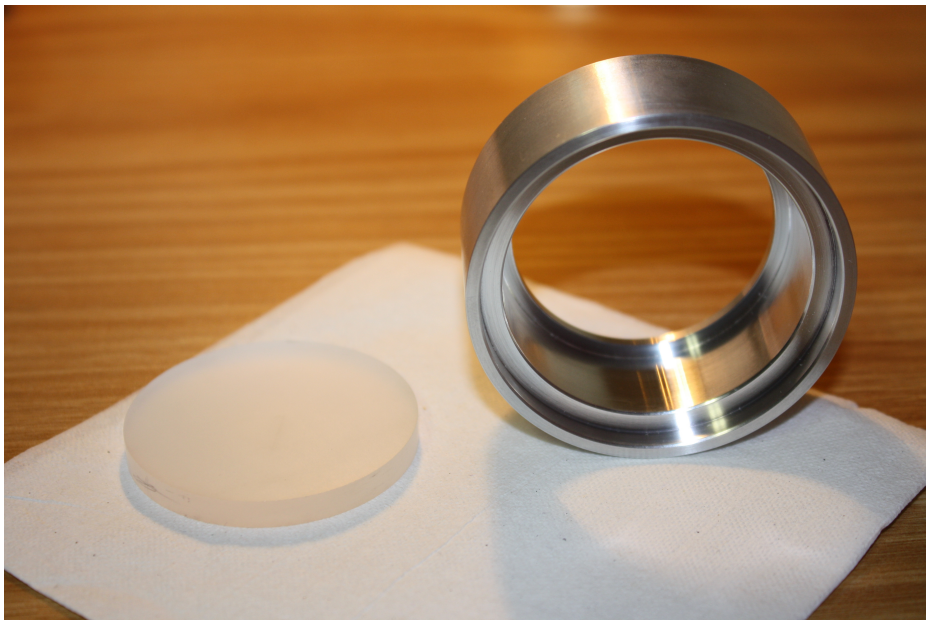

FIG. 40. Left: HEMEX sapphire puck used for indium crush test. Right: Aluminum mock fixture of the sapphire holder.

indium is crushed and if the springs can provide that load.

A. Indium Seal Test

The indium seal was placed on a mock aluminum backing plate. A shorter aluminum mock up of the sapphire holder was made to completely simulate the conditions expected in the cavity (Figure 40). A small puck shaped sapphire of the same quality and crystal structure as the large test sapphire was purchased from Crystal Systems. The thickness of the sapphire puck is equivalent to the lip of the larger test sapphire. This small sapphire was used in the test so as to ensure that the larger sapphire was not damaged during this experiment.

A .040 indium diamter wire was wrapped around the aluminum backing plate, which contained a .025 inch well with side walls recessed in .045 inches. The wire was wrapped until an overlap was created. The wire was then cut using a razor, creating

a small gap between ends. The backing plate was then set on top of the sapphire puck and inserted into the aluminum mock holder. After several test insertions, there was a great deal of confidence that the indium was sandwiched between the two surfaces. The fixture was then placed on a flat parallel which was set upon the top of a load cell. An insert similar to the pusher plate was placed inside the mock holder on top of the backing plate. Another parallel was placed on top of the whole assembly. The entire apparatus was placed in a hydraulic press, with a dial indicator resting on the surface of the upper most parallel. This set-up is shown in Figure 41. The hydraulic press was then activated, exerting force on the top of the parallel. The compression was measured by the dial indicator. The compressive distance should not exceed .015 inches, the difference between the well and the diameter of the wire. The cross sectional area of the wire is slightly greater than the area of the well. This should have led to smearing in all three directions on the gap: between the sapphire and side wall, between the sapphire and the backing plate, and between backing plate and side wall. This should provide adequate thermal contact.

The test showed that two deformations were occurring. The left (steeper) line indicated in Figure 42 is the indium forming in recesses of the backing plate intersection. The second line is the aluminum fixture slightly deforming. The rationale behind this is at around 100 pounds, the compression is .015 inches, the depth of the well machined into the backing plate. This is the threshold where one would expect to begin compressing the aluminum. From the graph, it is apparent that the test went as anticipated. After reaching 500 pounds the piston was withdrawn and the holder inspected. The load cell went to zero when the piston was withdrawn, guaranteeing that the device was still appropriately calibrated.

The sapphire was firmly stuck in the holder as expected. Using light finger pressure, the sapphire and the backing plate were dislodged from the holder. The

FIG. 41. This is the set-up for the indium seal test. Two parallels sandwich a sapphire placed in the holder with a backing plate and pushing bar placed on top of it. The entire fixture was then placed on top of a load cell, after which the entire contraption is put into a hydraulic press.

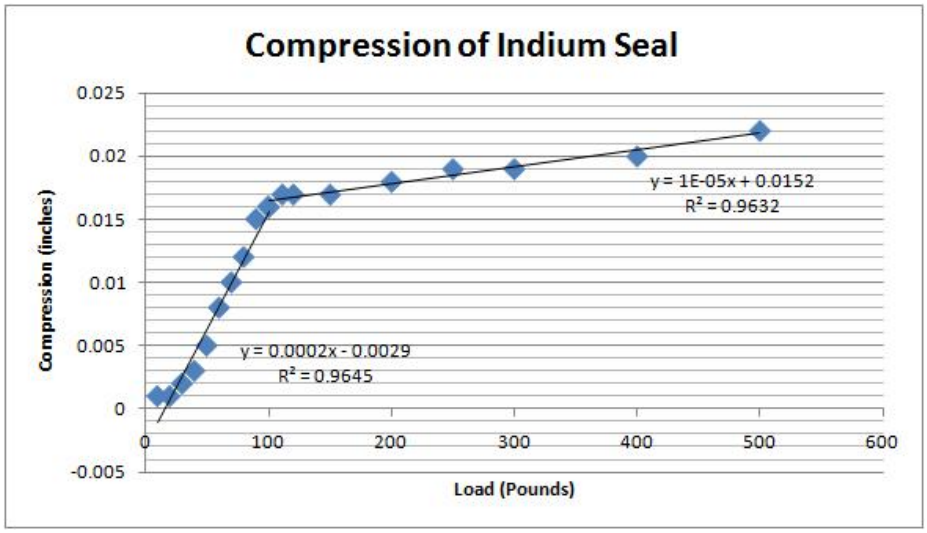

FIG. 42. Data from indium seal test. The compression appears to be of two materials. The first line indicates indium wire forming to the groove. The second (right) line is most likely the aluminum fixture yielding in shape slightly.

sapphire was then removed from the top of the backing plate with no effort. Figure 43 shows the backing plate. The shiny material with the machine marks is the aluminum backing plate and the indium ring is on the perimeter with a dull metallic gray color.

All the surfaces clearly had indium smeared on them. From Figure 44, the indium appeared to smear radially inward about a $\frac{1}{4}$ mm between the sapphire and backing plate beyond the 1.15 millimeter recess. This image also shows that there is still a step between the sapphire and the backing plate. Therefore, all the heat will be transferred through the indium seal. Some indium adhered to surface of the sapphire which was somewhat difficult to remove. Not all of the indium was removed from the surface, even though several methods were tried. It is clear that the sapphire, backing plate, and side walls were all thermally anchored to one another. This should provide the ability to cool the sapphire to 2 Kelvin and ensure the thermometers are indeed seeing the temperature of the sapphire. The conclusion drawn from the compression test was only a 100 pound load is required to deform the indium.

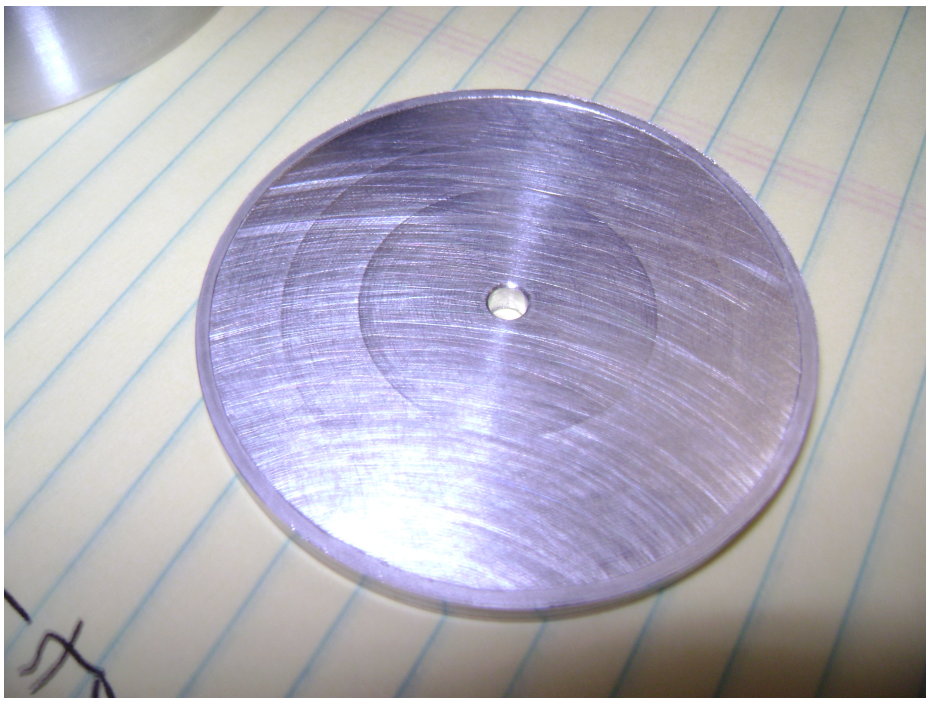

FIG. 43. Image is of the backing plate with indium ring around the perimeter. The ring has good uniformity and the small gap between ends has disappeared.

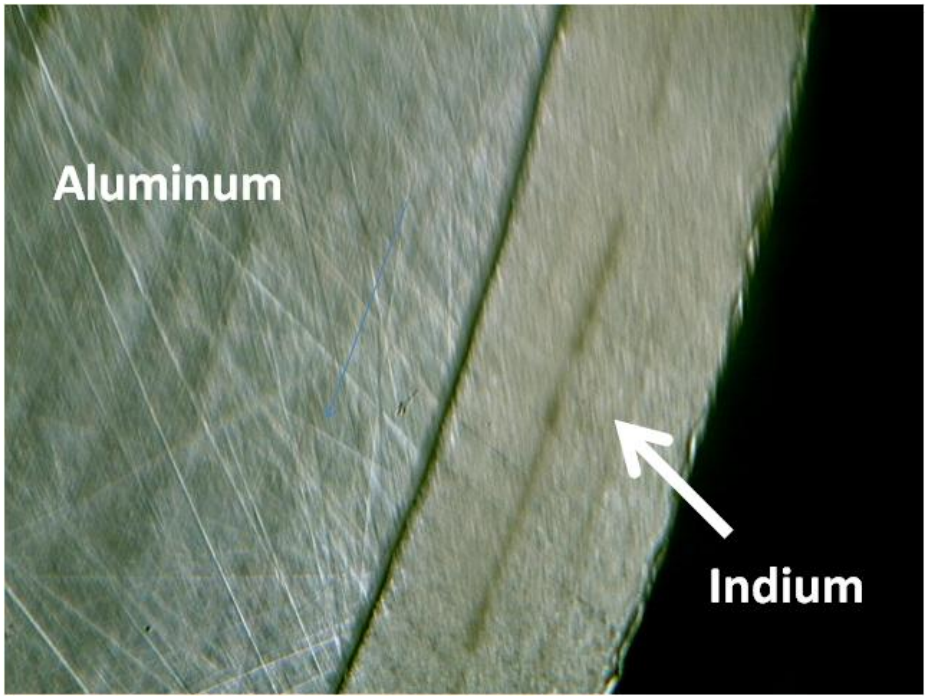

FIG. 44. Image of the indium located in the recessed well. The indium has smeared inward, creating over a millimeter width coating around the circumference of the plate, making good thermal contact between the backing plate and sapphire. Note that there is a step created by the indium overlapping the aluminum. This indicates that the indium is the only thermal bridge between the two materials.

A second test was then performed in order to make sure the springs were to specification. A load of 70 pounds was applied and the spring height became .841 inches. Therefore, it is certain that with three springs attached to the pusher plate, a load of 200 pounds will be placed on the indium joint when the springs are compressed to .550 inches, the compressed height during cavity operation. The thought of removing the springs after each use was tossed out since the load to deform the spring was high. The spring was tested again for the same load, and the height remained constant. Therefore, the springs were welded to the pusher plate and will not have to be replaced after each test.

At this point, all the structural pieces are constructed. The next step was to clean all of the parts in the manner appropriate for their materials followed by assembly and testing of the cavity.

CHAPTER IV

DATA ACQUISITION

This chapter highlights the important aspects of the data collection process. The steps completed are given in a chronological order. Each experiment's results lead to the experimental design of the following experiment.

The first experiment had poor coupling but provided the crucial surface resistance information for the empty niobium cavity. The bad coupling for the TE mode lead to the second experiment being overcoupled, yet produced the best Q measurement (2.17×10^8) of the TE_{010} mode and therefore best value for the loss tangent. This second experiment had multipactoring and hence in the third experiment the antennas were withdrawn. However contamination caused from the change of antennas created a poor measurement. In the fourth experiment, problems with cross talking lead to changing the coupling strategy again. This turned out to be a poor choice, but the network analyzer gave measured the best Q value during the entire set of experiments 3.4×10^8. However this measurement was outside the bandwidth of accuracy of the devise.

The fifth test removed all sources of possible contamination including the resistors located on the backingplate on the sapphire. This test established the level of coupling the antennas needed to have, as well as showed for the first time the sapphire was heating. The sixth test reinserted the resistors but an attempt to clean up the signal failed significantly, leading to the polishing and baking to remove defects and reduce surface area that could be attacked by water. The seventh test quantified the heating, but was no better than previous measurements. The final test filled the entire cavity with superfluid helium but material within the helium medium contaminated the interior of the cavity. The details of each of these experiments are given below with

justifications for conclusion drawn. The analysis of the data will occur in the next Chapter.

A. Bench Testing

The first step to evaluating the performance of the sapphire cavity requires a bench test. This tests the coupling parameters for the cavity and finds the resonance frequencies. The initial tests were to find the fundamental frequency and the TE_{01} mode of the empty cavity. Both the power input and probe antennas, made of welding wire, were long and protruded into the cavity. This most likely perturbed the fields, but was necessary to make sure that the fields could be found.

The cavity was found to have a frequency of 1.462770 GHz for the TM_{010} mode, or fundamental mode. This was lower than the frequency the model produced, 1.472469 GHz. After much searching, the TE mode was found, but the signal was quite poor. The frequency was 2.7969 GHz, which was much lower than expected. As to whether this was the correct mode remained uncertain even with the correct antenna orientation dependence.

A model was created that had the same dimensions as the final cavity, including the side port. This model was run on COMSOL modeling software. The side port was added to the model to see if it caused a perturbation to the frequency of the cavity. The model produced a frequency of 2.830691 GHz as Figure 45 shows. Comparing this to the previously modeled cavity without the side port, the two are quite close.

Two copper hooks were made; one .850 inches wide and another 1 inch wide made of $\frac{1}{4}$ inch copper rod. The small difference is a 10 decibel (dB) change in signal strength. The coupling could be changed by inserting extension rods on the ends of the hooks, then with a network analyzer find the correct extension for the perfect

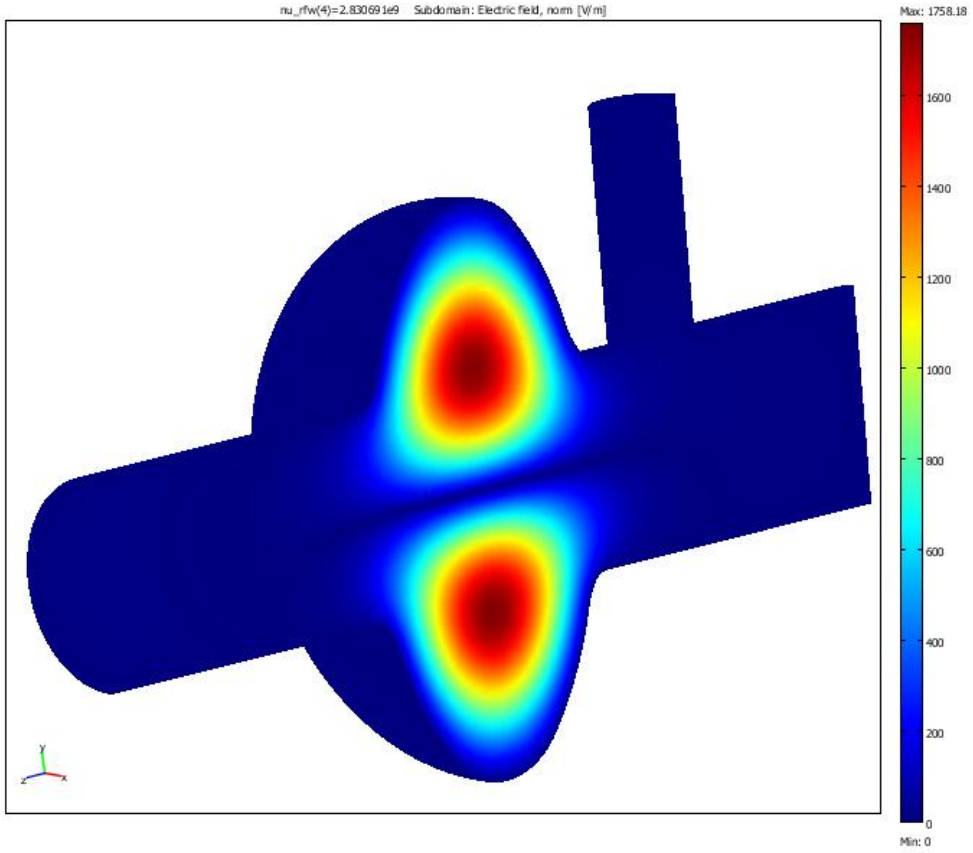

FIG. 45. The electric field of the TE mode in a half geometry of the empty sapphire test cavity, i.e. no sapphire.

coupling. Port 1 of the Network Analyzer was attached to the probe antenna made of welding wire and Port 2 was attached to the copper hook in the side port.

The network analyzer has to be calibrated everyday for temperature and humidity changes in the lab. The need for the calibration is to compensate for the losses in the cable themselves. The two respective coupling coefficients for each port can be calculated using S_{11} or S_{22}.

$$\beta_{\#} = \frac{1 - S_{\#\#}}{1 + S_{\#\#}}. \tag{4.1}$$

The normalized equation is

$$\beta_{\#norm} = \frac{1 - \frac{S_{\#\#}}{S'_{\#\#}}}{1 + \frac{S_{\#\#}}{S'_{\#\#}}}, \tag{4.2}$$

where $S'_{\#\#}$ is the value of the background which is less than and near 1, or true reflection. These equations are good only for situations where the cavity is under coupled, $\beta < 1$. In the case of the over coupling, $\beta > 1$, the coefficients are the reciprocal of equations 4.1 and 4.2. The signal for S_{22} (copper antenna) is very noisy compared to S_{11} as would be expected since the hook is smaller and coupled loosely to the cavity compared to the long protruding welding wire in Port 1. Plugging in the values for the S parameters, the coupling coefficients, β, can be found.

Next step was to look at the transmission from one port to another, or S_{21}. Using the parameter S_{21}, which is identical to S_{12}, the frequency was measured. The resonance was 2.797 GHz. The peak of the resonance has a specific width which determines the loaded Q, or Q_L. The network analyzer will automatically calculate this quantity, but is only correct if the peak is symmetric. Manual methods can be used to calculate the Q_L by measuring the width from the peak frequency to the closest -3 dB point as well as locating the linear section in the phase plot of the

signal. This is quantified as: for the -3 dB method

$$Q_L = \frac{f_{max}}{2 \times \Delta f_{3dB}}, \tag{4.3}$$

where the peak frequency is f_{max} and the width to the steepest side is Δf_{3dB} and for the phase method

$$Q_L = \frac{f_{max}}{\Delta f_{\phi \frac{90}{\Delta \phi}}}, \tag{4.4}$$

where Δf_ϕ is the angle of the linear section, which matches -3 dB point. In all cases where it was necessary to measure the cavity by all three methods, the phase measurement was always in between the other two methods' values.

The second important quantity from these measurements is the strength of the signal at maximum, or the transmitted power lost from the input port to the probe measured in dBs. This value is called S_{21} and is extremely important for determining the Q_{ext}, or external Q. The Q_0 value hoped for in this cavity is 10^{10}, but in order to accurately measure it the Q_{ext} must be similar to or higher than what is expected. The Q_{ext} is computed using

$$\frac{1}{Q_L} = \frac{1}{Q_0}(1 + \beta_1 + \beta_2). \tag{4.5}$$

where

$$\beta_2 = \frac{Q_0}{Q_{ext}} = \frac{P_{ext}}{P_{cav}}. \tag{4.6}$$

and therefore

$$Q_{ext_{Port2}} = \frac{Q_0}{\beta_2} = Q_L \frac{(1 + \beta_1 + \beta_2)}{\beta_2}. \tag{4.7}$$

However for cavities above $Q_0 > 10^5$ a more accurate definition is required. As the Q becomes increasingly large the measurement error in β_2, which will be extremely small, will adversely affect the ability to confidently set the external Q value. Therefore in

such cases

$$Q_{ext_{Port2}} = \frac{4Q_L\beta_1}{(1+\beta_1+\beta_2)}10^{|S_{21}(dB)|/10}. \tag{4.8}$$

is used. This formalism comes from the definition of S_{21}, which is

$$S_{21} = \frac{4\beta_1\beta_2}{(1+\beta_1+\beta_2)^2} = \frac{4\beta_1\frac{Q_0}{Q_{ext}}}{(1+\beta_1+\beta_2)^2}. \tag{4.9}$$

Writing S_{21} in decibels (dB) the equation becomes

$$S_{21}(\text{dB}) = -10\log\left(\frac{4\beta_1\frac{Q_0}{Q_{ext}}}{(1+\beta_1+\beta_2)^2}\right). \tag{4.10}$$

Taking both sides of Eq. 4.10 to the power 10, equation 4.8 is obtained.

Inserting the values for β_1 (large welding wire), β_2 (very small, copper hook), and Q_L, the Q_{ext} could be set to the appropriate level just by varying the length of the copper antenna. However, after reproducible measurement could not be made a new measurement technique was employed that included adding an antenna made of welding wire to a flange located where the sapphire would have been located. This setup is the standard method of acquisition for an empty cavity. This method puts one antenna on each side of the cell ensuring the signal must pass through the resonating chamber. For the duration of the bench tests the new sapphire side end flange and its wire antenna were unaltered. Therefore the input antenna's coupling was constant allowing variation of the hook antenna's length, located in the side port, to be the only parameter altering the external Q. The flange located on the end of the beam pipe containing the vacuum line, the end of the cavity opposite the sapphire's usual position, was blanked off.

The copper hook was located on Port 2 and the welding wire hook was located on Port 1 on the network analyzer. Measuring $S_{11} = .82535$ and $S'_{11} = .97598$ it was possible to calculate β_1. The value of β_1 was .0836215 and the S-parameters

for the hook on Port 2 were not measurable since the parameters were swamped by background.

The measurement of Q_L using S_{21} was completed three different ways to get an accurate value. The asymmetry in the resonant peak required averaging of several different techniques. The first method was using the network analyzer to calculate Q_L, and the second method was the measuring of the -3 dB point on the steepest side of the maximum. The third method is measuring the phase. The phase data seemed more accurate and straddled the other two methods results. The data can be seen in Figure 46.

The measurement of Q_L for the empty cavity operating in the TE_{011} mode at 2.796 GHz using all these methods and procedures described are as follows: network analyzer method produced 13004, one sided 3 dB measurement (f_{3dB} = 2.79681 GHz gave 18645, and the phase measurement evaluated to 17910 for Q_L. The phase method was used for Q_L, and utilizing Equation 4.8, the Q_{ext} was determined by varying the lengths of the coupler. As Figure 46 shows, several lengths were tried until eventually a Q_{ext} of 1.1549×10^{10} was achieved with copper antenna of sufficient height to protrude 1.380 inches into the side port from the flange. The input antenna's coupling has been established for the TE mode, yet the process is half complete.

Now the hook was removed from the side port as was the blank. The vacuum end flange was clamped on the end of the beam tube. Attached to this flange was the probe; a copper rod with a hemispherical tip, the pin. For the probe, the loaded Q was measured to be the same. This result was expected since the impact of the coupler hook being removed should have no effect on the loading of the cavity and the coupling of the welding wire input antenna located at the sapphire port was unaltered and therefore β remained constant. Once again, the signal was in the noise for the reflection coefficient of the probe as it was for the hook. The length of the probe was

Empty Case				Coupler			Probe	
Δø	Δf (kHz)	difference		dB	ΔL		dB	ΔL
5	8.88		Q_L=17910	-57.384	1.48		-39.13	0.58
10	17.5	8.62		-60.285	1.426		-66.879	-0.05
15	25.84	8.34		-61.5	1.414		-74.712	-0.105
17.5	30.06	4.22	X 2 =8.44	-61.9	1.396		-84.137	-0.225
20	34.28	4.22	X 2 =8.44	-63.27	1.38		-84.922	-0.232
25	43	8.72		Q_{ext}=1.1549*10^{10}			Q_{ext}=1.689*10^{12}	

Loaded Case-Wire antenna in coupler port						Probe	
Δø	Δf (kHz)	difference				dB	ΔL
5	123		Q_L=883			-87.491	0.325
10	248	125				-99.07	-0.01
15	376	128				-99.1	-0.095
17.5	441	65	X 2 =130			-103.83	-0.22
20	509	68	X 2 =136	Q_{ext}=1.5198*10^{12}		-104	-0.232

Loaded Case-Wire antenna in probe port				Couple	1st set		2nd Set
Δø	Δf (kHz)	difference		dB	ΔL	dB	ΔL
5	150		Q_L=693	-49.634	1.26	-24.247	2.805
10	307	157		-53.48	1.2	-48.284	1.645
15	452	145		-59.889	1	-50.307	1.32
17.5	548	96	X 2 =192			-52.678	1.25
20	630	82	X 2 =164			-62.42	0.825
						-65.191	0.815
						-69.741	0.74
						-71.3	0.68
						-72.44	0.63
				Q_{ext}=1.40023*10^{10}		-74.49	0.57

FIG. 46. The data taken to measure the external Q of the couplers, for both the empty and sapphire loaded cases.

decreased until the Q_{ext} reached 1.689×10^{12}. The probe length was decreased by such a degree that it no longer protruded into the cavity but actually was recessed into the feedthrough tube located on the vacuum flange. It was recessed .232 inches from the interior face of the vacuum flange in order to achieve the proper coupling. At this point coupling for the empty case was completed.

Additional time was available and it was possible to complete the bench test with the cavity loaded with the sapphire. The sapphire was inserted into the holder and placed into the cavity. The sapphire's current condition was uncleaned and had several gray marks on the surface from the niobium holder rubbing it during the fitting. This was not anticipated to cause any problems. A mode was found in the anticipated location but was 50 MHz off what the model predicted. It also had a close lying higher mode when shifted off axis. From the hook dependence and higher value of Q_L (673), the mode at 1.879998 GHz was guessed as the TE mode. However this frequency is 50 MHz off of what was expected, and therefore confidence is not that high in the choice.

The three different measurements determined the Q_L: Network Analyzer produced 673.2, -3 dB measurement was calculated to be 1201.03, and the phase method delivered 883.349 as its value (Figure 46). The phase value was taken as usual. The copper was pin was reduced to the point where the copper was recessed again. The same probe was determined to be appropriate for the both the empty and sapphire loaded case with a Q_{ext} of about 1.5×10^{12}. The hook length was reduced to .570 inches protruding from the flange port and the Q_{ext} was set at 1.40023×10^{10}.

B. Test 1: Empty Cavity Test

1. Assembly

Once the bench test was completed the cavity needed to be assembled. The blank, probe flange, coupler flanges, and copper antennas were given to the cleaners. The stainless pieces (blank, both flanges) were degreased in the standard manner for Stainless Steel. This entails putting the pieces in a soapy liquid while sitting in an ultrasonic agitator. The copper antennas were cleaned by the labs recipe which included an etch. This etch was a concern since 18 thousandth of an inch is a full rotation on the 2-56 screw, meaning a small etch could cause the antenna to point the wrong way. These items, after cleaning, were placed in the pass-through which is the load lock from the chemistry room to the clean room.

Peter Kneisel was instrumental in preparing the cavity itself. He measured the fundamental mode to be 1.462704563 GHz. The loaded Q was 8970.9, which is better than average (Figure 47).

Once the measurement was completed, the cavity was degreased by Peter using soap and ultrasonic agitator. It was removed from the bath and rinsed, then filled with the BCP (1:1:1) acid concoction. The acid was fresh acid, in that it had not been used prior to this cavity, and the etching process was performed at room temperature. Two four minute etches were performed, then the cavity was rinsed and then dried. A second frequency measurement was made illustrating the acid etch created a frequency shift of 483 kHz and increased Q_L to 9062, as Figure 48 shows. Using the rule of thumb for a CEBAF cavity, an 11 kHz shift is equivalent to one micron of material removed. Therefore, approximately 40 microns were removed during the etching process, or 5 microns per minute. Another BCP etch was performed for three minutes to remove an additional 10-15 microns of material after the measurement was completed to

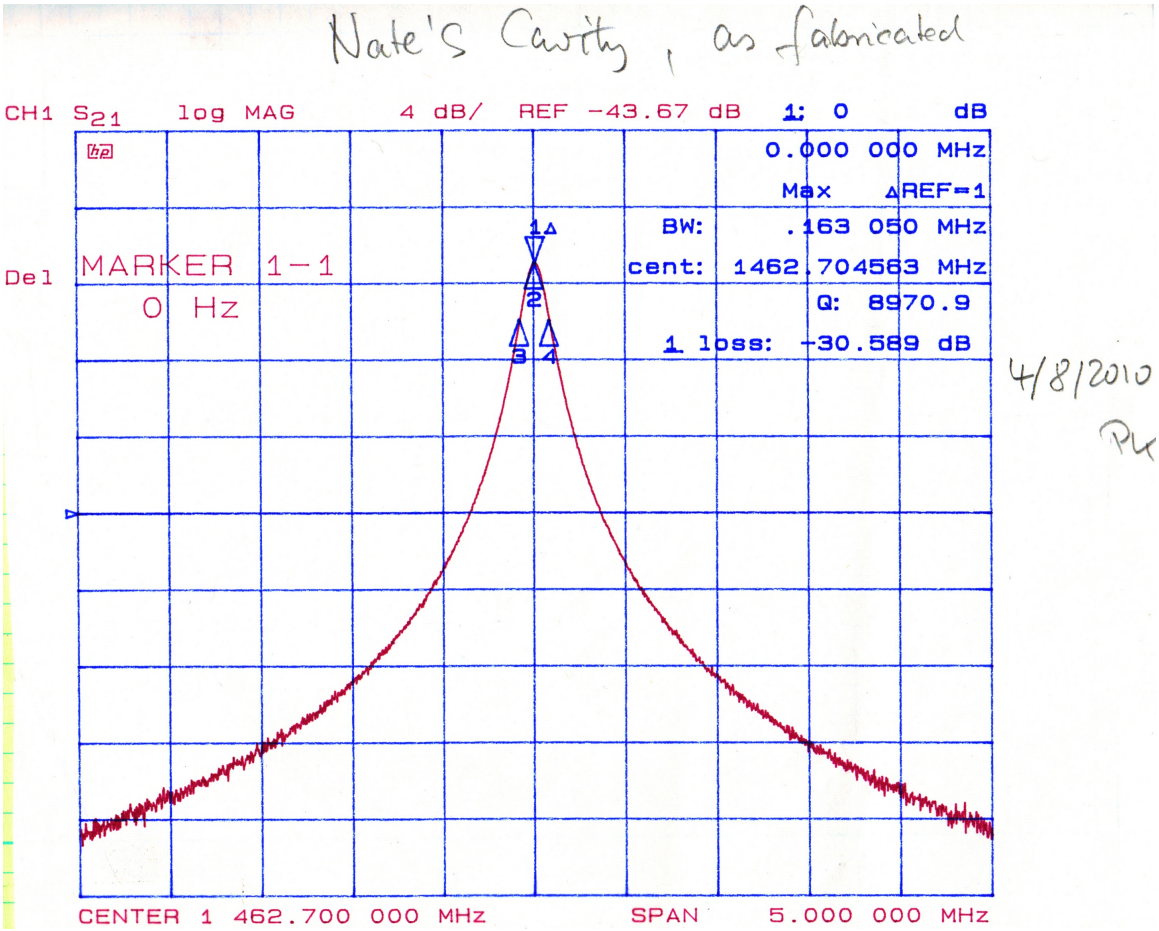

FIG. 47. The resonant frequency and the loaded Q of the fabricated cavity operating in the fundamental mode.

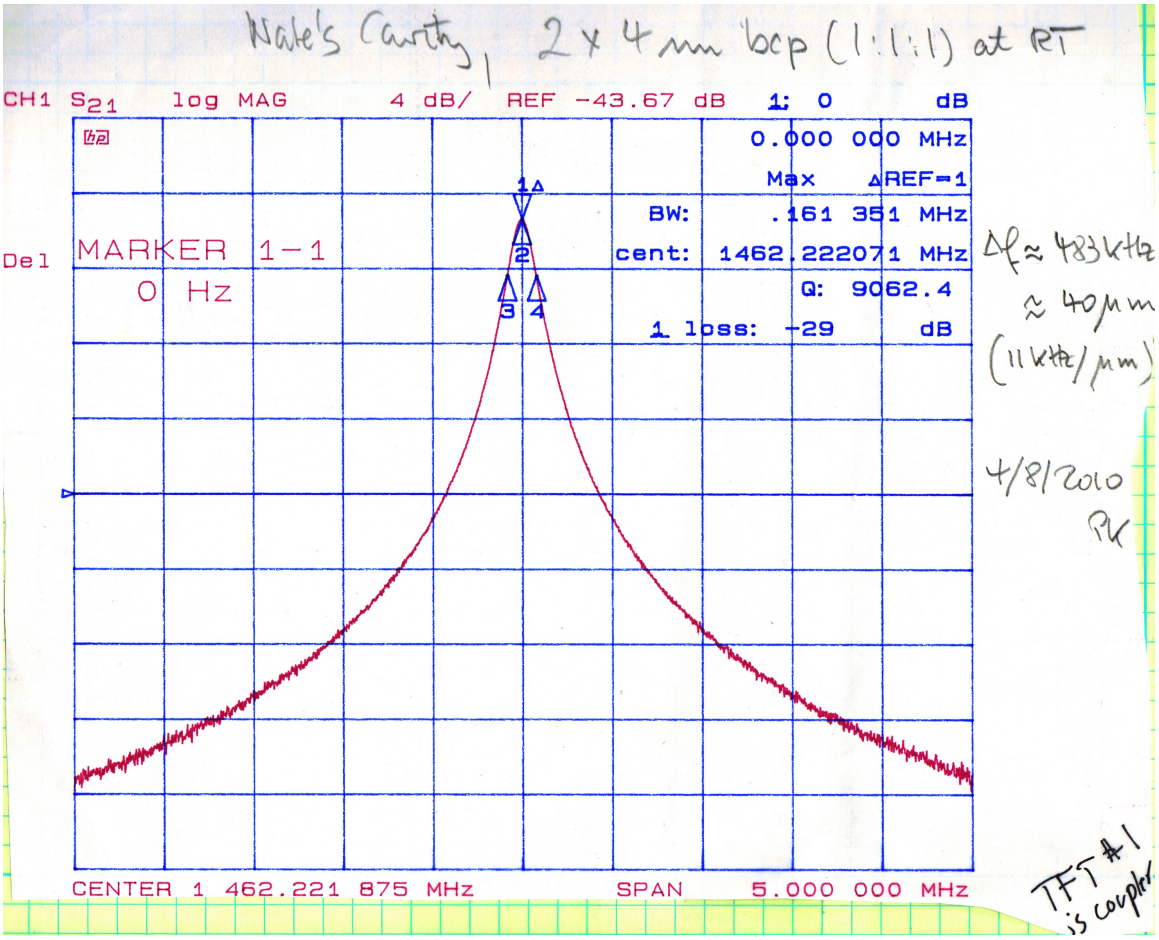

FIG. 48. After an etch, the frequency of the fundamental mode changed by 483 kHz, meaning that approximately 40 microns of material was removed from the interior of the cavity.

remove possible contamination generated during this second frequency measurement. So in total, approximately 55 microns of the wall was removed. Once the third etch was completed, the cavity was taken to the research and development high pressure rinsing device. Using 16 MΩ water, the rinse was completed in 75 minutes. After the rinse, the cavity's openings were covered and the cavity was placed in the pass-through, followed by removing the bottom flange letting the cavity dry inthe class 10 clean room.

Once all the parts were in the clean room, one of the technicians assisted in the cavity assembly for the empty cavity test. Assembling was performed in the standard manner for SRF cavities. The most delicate assembly process was the placement of the antennas. The pin was inserted without incident, but with the hook great care was put into making sure it was point in an azimuthal direction. Once assembled the umbilicals were placed on the cavity in the test stand, followed by pulling vacuum on the cavity. Once the cavity was pumped down to a level around 1.4×10^{-7} $m$barr, the cavity was then helium leaked check and passed without incident. The test stand was then removed from the clean room housing by crane and placed in Dewar 3.

2. Q_0 Measurement

The test stand was placed inside the dewar and connections for the vacuum line to the cavity were made. The test stand's RF connections and vacuum ports were attached to the test system for monitoring performance and providing power. The cavity was then brought down to 4.2 Kelvin. The frequencies of the modes were recorded and compared to the modes identified in the modeling process using Microwave Studio and COMSOL (Figure 49). According to the RF experts at Jlab, the frequency should shift approximately 5 MHz from material contraction during cooling. A program is used to find this shift for a given geometry.

Modelled modes and frequencies found at 4 K		
Modelled Frequencies (MHz)	Experimentally found modes (MHz)	Modes
1462	1464.64	TM010
1867.88	1848.99/1851.606	TE111
2039.41	2040.8/2038	TM110
2584.61		TE211
2586.5		TE211
2595.84		beam tubes
2673.16	2672.3626/2662.8561	beam tubes
2727.13	2733.499	TM210
2730.28		TM210
2780.7	2764.363	TM011
2810.53	2788.841/2788.906	TE011
2936.19	2938.67	
2955.34	2944.28	
	2955.645	
	3032.35	
	3037.7	

FIG. 49. Modes of the cavity as modeled compared to those that were found experimentally.

From Figure 49 it can be seen that the TM modes are essentially located at the correct frequencies. The TE modes however appear to be shifted 20 MHz lower than expected. After discussions with several people, it was concluded that the cavity shape could be deformed slightly. The shaping of the structure in the stamp could have lead to a non-exact copy of the design shape. Also the coining fixture was not used during the construction of the cavity, so it is known that this cavity does not have the exact design shape, but whether or not it is the cause for such a shift is unknown.

Now that the cavity is cooled to 4.2 K, the Research RF system operating between 1 to 4 GHz was needed to measure the Q_0 of the cavity. The setup and calibration procedures were simple once understood.

For most of the calibration, only a network analyzer and a power meter are required. Before calibration, the temperature of the dewar must be stabilized so that the frequency does not fluctuate due to microphonics. After gathering the calibration data the radiation shield (Figure 50) should be closed, the security gates around the installation need to be locked, and security system armed.

All the data gathered can now be processed into calculating the calibration coefficients that are used in the Q_0 calculation using a time decay measurement. Once again this is done to understand the losses in the system itself so as not to be attributed to the cavity. The values of these coefficients are shown in Figure 51 for all eight tests. The calibration must be done at each temperature because the resistances will change in the RF lines, though not by much.

Scanning the frequency space with the network analyzer under high resolution, the TE mode was unable to be found. The next step was to locate the TM_{010} and compare the performance to a standard cavity. The frequency of the TM_{010} mode was 1.464636 GHz. The Q_0 of the cavity was 2.38×10^8, with Q_{ext} of the drive antenna

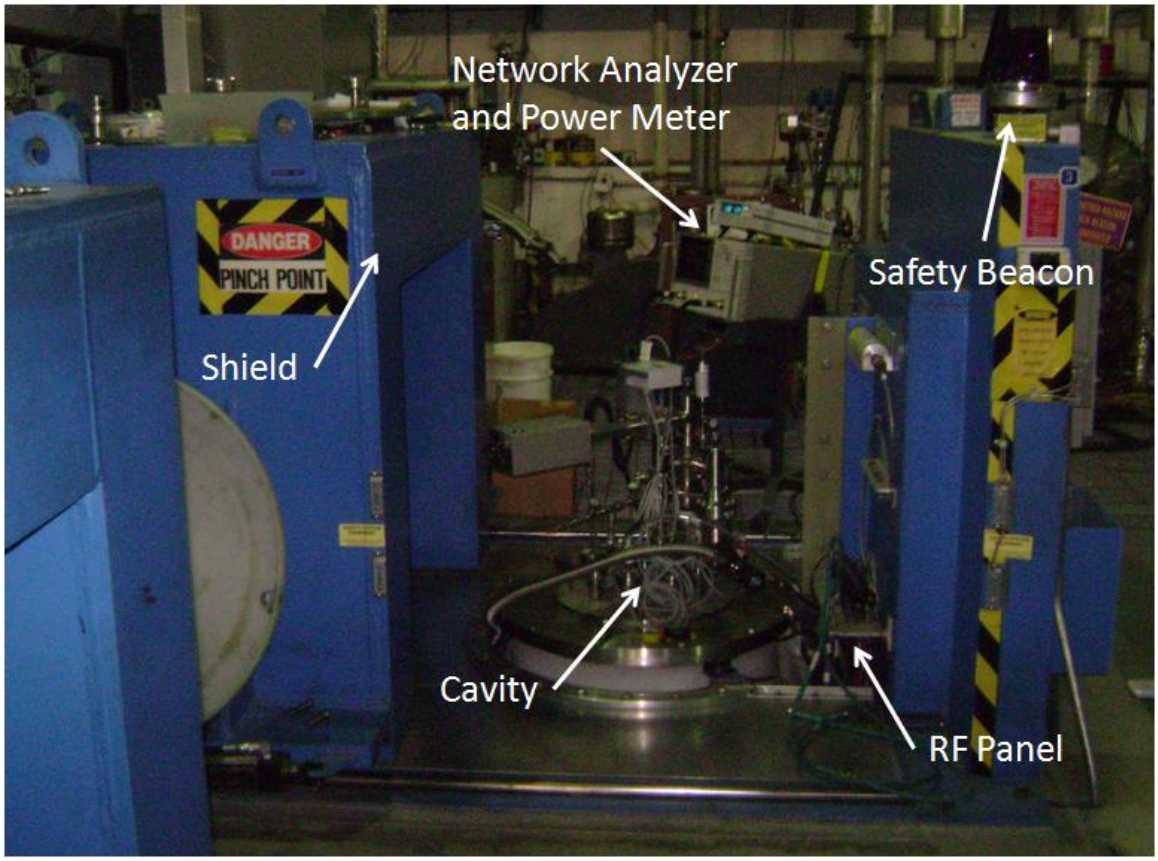

FIG. 50. This image shows the shield containing the dewar which holds the cavity. The shield is hydraulically pushed over the dewar. The network analyzer and power meter can be seen in the background as well as a visual security beacon notifying personnel of a possible radiation source.

	Temp/Mode	Cincident	Creflect	Ctrans
Test 1	4K TM010	96.28	487.30	5.76
	2K TM010	96.95	487.30	5.76
	2K TM011	314.06	2065.00	67.60
Test 2	4K TE010	145.31	1325.33	44.04
	2K TE010	145.31	1325.33	44.04
Test 3	2K TE010	105.84	774.00	5.71
Test 4	RF system could not establish lock			
Test 5	2K TE010	90.70	1193.55	5.57
Test 6	2K TE010	155.57	969.41	6.07
Test 7	4K TE010	113.80	1308.00	9.80
Test 7	2K TE010	113.80	1308.00	9.80
Test 8	2K TE010	101.80	1005.39	8.90

FIG. 51. Here are the calculated calibration coefficients for the RF system during each of the tests performed on the dielectric test cavity.

being 5.94×10^{10} and Q_{ext} of the pick-up probe being 1.17×10^{12}. These values are very close to what was anticipated, for both Q_0 and the two Q_{ext}. The surface resistance measured in the cavity was 965 $n\Omega$.

The temperature of the cavity was reduced to 2K, but yet again the TE_{010} mode could not be found. Measurements were taken of the TM_{010} mode and the TM_{011} mode. The TM_{011} mode was found in the area anticipated, but had a relatively low Q. The RF system was re-calibrated using the same method as described above for this temperature. The Q_0 of the cavity was measured to be 1.29×10^{10} which is a value that is consistent with a standard CEBAF cavity. The surface resistance of the cavity was 21 $n\Omega$. This value was in the neighborhood of most cavities but slightly higher than expected.

The first test of the cavity had mixed results. The measurement of the fundamental mode proved that the cavity was capable of high Q and low surface resistances. However, the TE mode was not found. This could mean that the coupling was so weak that the RF system could not find the signal.

C. Test 2: Sapphire Loaded Cavity

1. Second Bench Test- Empty

A second bench test confirmed the measurements previously taken during the first bench test. At this time the modes found at room temperature and at cryogenic temperatures were compared, see Figure 52. The modes were attempted to be matched up. During this second bench test it became apparent that the tail of the higher order mode near the TE mode artificially increased the coupling to the signal. As the temperature decreases the width of the parasitic mode narrows, removing its contribution to the combined signal measured at room temperature. Hence the signal that

Frequencies Modelled with side port (GHz)		Frequencies found via bench test (GHz)	Frequencies found during cold test (GHz)
1461	TM010	1.46169	1464.64
1853.198	TE111	1.84534	1848.99/1851.606
2038.245	TM110	2.035/2.037	2040.8/2038
2559.069	TE211	2.535678	?
2571.435	TE211	2.56459	?
2638.254	beamtubes	2.647/2.658	2672.3626/2662.8561
2732.730	TM210	2.728496	2733.499
2766.687	TM011	2.760363	2764.3625
2796.879	TE011	2.793835	2788.841/2788.906

FIG. 52. This chart shows the modeled frequencies, the frequencies found during the bench test, and frequencies found during cold testing of the empty cavity.

was sought was unable to be found.

2. Second Bench Test: Sapphire Loaded

Another set of bench measurements were necessary to make sure the signal would be found during the second cold test. A frequency was found at 1.8745 GHz, which is higher than expected from the model. It was noted that the peak was split. The size of the gap between the two grew larger as sapphire was gradually centered along the axis. The TE_{011} mode should not be split or be very sensitive to the position of the sapphire. After examining the lower order frequency peak (low Q), a smaller peak was detected on the front end tail. This peak was small, and not sensitive to the position of the sapphire, but extremely sensitive to the orientation of the hook. The two others modes (splitting modes) are moderately effected by the orientation of the hook. This small peak was identified at 1.85297 GHz, which is 22 MHz closer to the model prediction. Therefore, it is most likely that the TE mode was so small, or rather

NA method	$Q_L = 32{,}202$			
3db method	max frequency	3db frequency	$Q_L = 34{,}975$	
	1.852978926 GHz	1.852952436 GHz		
Phase method	$\Delta\phi$	Δf (kHz)	difference	$Q_L = 35{,}284$
	4.962	3.26		
	10	6.01	2.75	
	15	8.76	2.75	
	17.5	10.26	1.5	X2
	20	11.67	1.4	X2
	25	14.5	2.84	
	30	17.38	2.87	
	35	20.82	3.44	

FIG. 53. This chart shows the data taken to calculate the loaded Q of the TE_{01} mode. All three methods are represented in the chart. The X2 states that the values need to be multiplied by two in order to be compared to the other points. Again for the phase method the point of interest is the 45 degree mark on the curve, or where the difference is linear. The center of the linear region is the location of the -3 dB point.

so narrow (high Q), that during the first cold test the frequency was overlooked.

The Q_L of this newly found peak is $30,283$ compared to the previous mode thought to be the TE mode, which has a loaded Q of 673. This Q_L value fits much better with the TE_{011} mode, as was modeled. In reference to previous data, the TE modes were all off by approximately 20 MHz, and therefore make this frequency a reasonable candidate. After calibrating the network analyzer, measurements were again taken to calculate Q_L more accurately, see Figure 53.

As a last check, the hook antenna was turned 90 degrees so as to be parallel to the

axis. The signal disappeared completely. An extreme sensitivity to hook orientation, high Q, and near the frequency predicted by model are all criteria that this mode needs to be identified as the TE_{011} mode.

The sapphire bench test was completed horizontally, so if the clamps allowed the sapphire to sag or be placed off axis, the frequency and field could be perturbed. Therefore a series of measurements were completed to illustrate the dependence of sapphire's radial position from the axis. As Figure 54 shows, the TE_{011} is quite insensitive to the displacement of the sapphire off axis in regards to frequency. However, the coupling of the mode increased as the sapphire was displaced off center. This made sense, the coupling to the neighboring mode was moderately increased and its tail artificially increased the coupling the TE_{011}. The largest cause for the enormous coupling increase is higher order mode moving drastically towards the TE_{011} mode. It was found that one could overlay the two modes getting a very large signal. Hence the increase in coupling was from the mode overlapping rather than the TE mode itself changing. The higher order modes actually could drop in frequency below the TE_{011} when the sapphire is displaced. Therefore it is crucial to place the sapphire in the center and identify the two higher order modes. These modes are large and are excellent markers to help find the narrower TE mode.

The next effect that needed to be analyzed was cross talk during antenna calibration. Cross talk is where one antenna directly talks to the other without the input signal travelling into the cell and coming back. This phenomenon makes it almost impossible to accurately determine the coupling to an extremely precise level with the setup used for this cavity. The signal contaminated with cross talk versus a clean signal, is given in Figure 55 [33]. Cross talk can artificially increase the loaded Q by narrowing the peak, making the -3 dB point frequency closer to the maximum. If the coupling is strong, the -3 dB point is very close to the peak, whereas a weak signal's

Displacement off axis (inches)	S21 parameter	TE (GHz)	HOM(Peak 1) (GHz)	HOM (Peak 2) (GHz)
0	-72	1.853773	1.870573	1.876753
0.05	-67	1.854753	1.870533	1.884713
0.1	-53	1.855353	1.8266	1.839433

FIG. 54. As the sapphire was shifted off center, the frequency remained relatively unchanged, but the coupling increases by as much as 19 dB at maximum displacement. The increase comes from the neighboring modes shifting in frequency towards the TE_{010} mode.

-3 dB point can be much further way. The three different methods of obtaining the loaded Q was a means of converging on the correct value. Even at lower temperatures the cross talk between the antennas could be seen. In order to minimize cross talk a series of measurements were completed to find the location where the least cross talk occurred.

The copper hook antenna was placed in the side port and another copper hook was placed in the beam pipe. The leg orientation and placement of the hook, with respect to the side port, is described in Figure 56. At location E there appeared to be no cross talk but had very weak coupling, yet maintained a high loaded Q of 24,224. M had similar results, but had some hints of cross talking. Therefore the orientation of both hooks is important to eliminate cross talk. From the measurements it was clear that a clockwise pointed hook reduced cross talk compared to counter-clockwise oriented hook. The reason for this was unknown. Positions A and E were very fuzzy due to weak coupling, but had a strong signal compared against the background. Coupling at positions C and G was extremely high as one would imagine, but as expected, the cross talk was quite prevalent and not pronounced against the background. Comparing the coupling, C's S_{21} parameter was -45.784 dB while E's

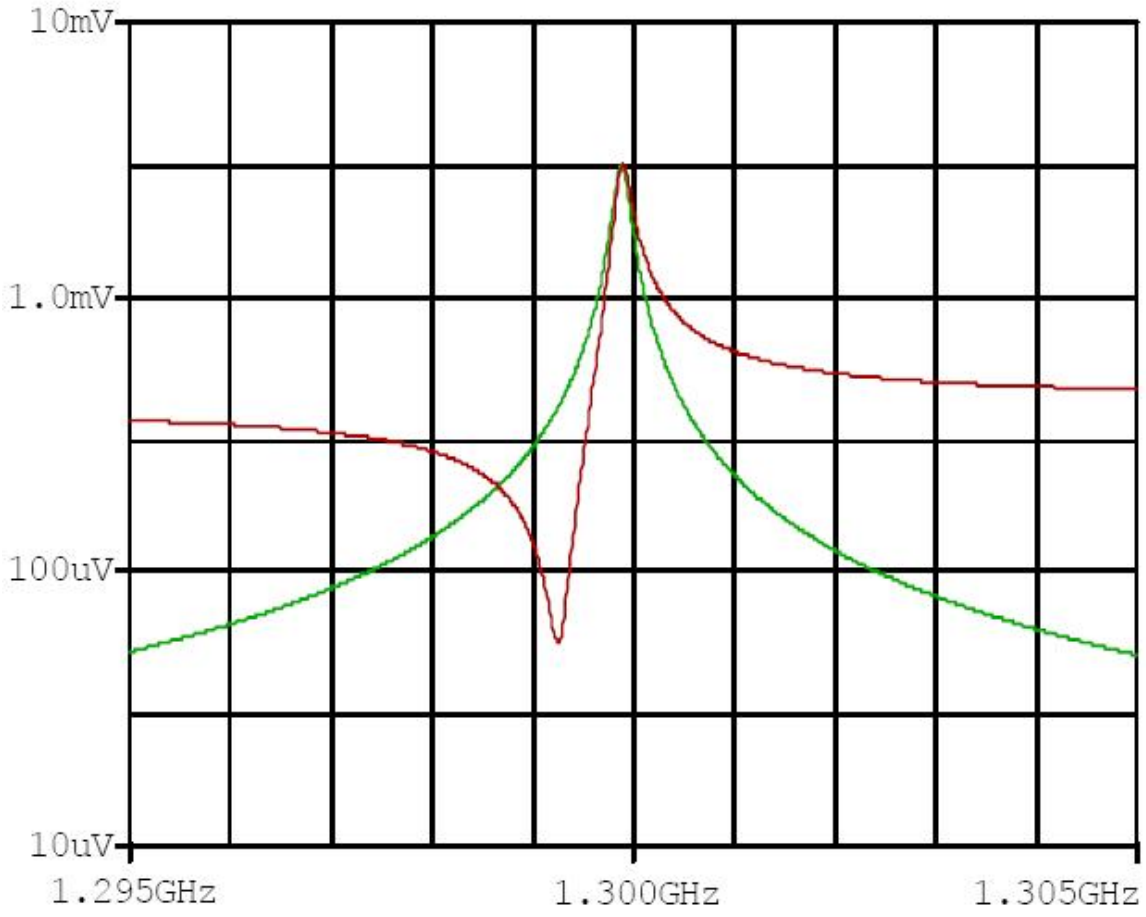

FIG. 55. The green line illustrates the signal if no cross talk exists. The red line shows the same signal with cross talk from another antenna. If the signal is strong, and the -3 dB point is well above the background, cross talk is not a factor. But if the signal is weak and the -3 dB is approaching background the cross talk can severely affect the result [33]. Copyright 2003, IEEE.

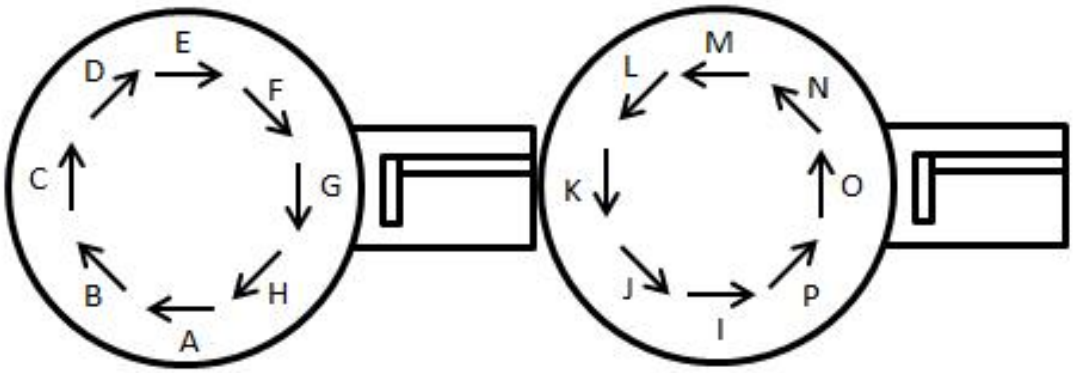

FIG. 56. On the left is a diagram of the hook, pointing clockwise, at various positions around the beam tube relative to the side port hook. The right diagram shows the same locations but with the hook oriented counter clockwise. Location E had the least amount of cross talk compared to all others, where C and G had the most in the clockwise pattern. The counterclockwise oriented positions all had larger cross talk compared to their clockwise positions.

parameter was -84.560 dB. Both positions had loaded Qs of approximately 24,000 for Q_L.

The significant changes in S_{21} based on the antenna geometry was quite disconcerting. It was necessary to verify the conditions for the significant decrease in coupling. A pin was located in the side port and a hook was placed on the end flange. Several values of S_{21} were measured over a range of angles, with minimal cross talk, giving an angular dependence for the coupling as seen in Figure 57. Note that the difference in the S_{21} measurements of the location and angular dependence readings for the same angles was related to the use of two hooks versus a hook and a pin. In both setups, the values directly across from the side port were consistent, and more importantly relatively stable in the area. One interesting item to note is when the angle was less than the 150 degree mark (using the unit circle on the figure), the

signal inverted, becoming a dip. However, at 180 degrees and greater the signal was a peak. The reason for both the significant change in coupling and the flipping of the signal was not understood. Position B was chosen as the location of the hook, to reduce cross talk but have a large signal transmitted. Position E was not chosen for it was uncertain as to the source of the signal inversion.

Another aspect of the orientation is the relative angle of the hook to the azimuth of the beam pipe. The hook is straight and therefore cannot be perfectly parallel to the azimuth. The angle zero was defined as the hook pointing directly down at the 180 degree mark. The hook was then swung out towards the radial direction as seen in Figure 57. As the hook moved radial by 10 degrees the signal coupling had dropped by approximately 8 dB. Therefore it is of the utmost importance to align the hook. For the setup of the antenna great care was taken in positioning the hook both in the beam pipe but also the hook's leg alignment with an azimuthal line.

Once these measurements were completed the length of the hook was set to 3.333 inches protruding from the surface of the vacuum flange, creating a Q_{ext} of 5×10^8. The pin was set to protrude 4.540 inches from the surface of the side port flange. The Q_{ext} of the pin was therefore 7.2×10^8. The purpose behind such strong coupling is to ensure that the TE_{011} signal is located. At room temperature the signal could be seen using the antennas described. The signal was weak but clearly visible at 1.853 GHz. This coupling, hook at the end and pin at the side port, is the opposite configuration from Test 1.

3. Sapphire Cleansing

A standard sapphire cleaning procedure has been established by the NASA Jet propulsion Lab [31]. The procedure involves creating a nitric acid solution comprised of one part pure nitric acid and three parts water in a glass beaker. The sapphire is then

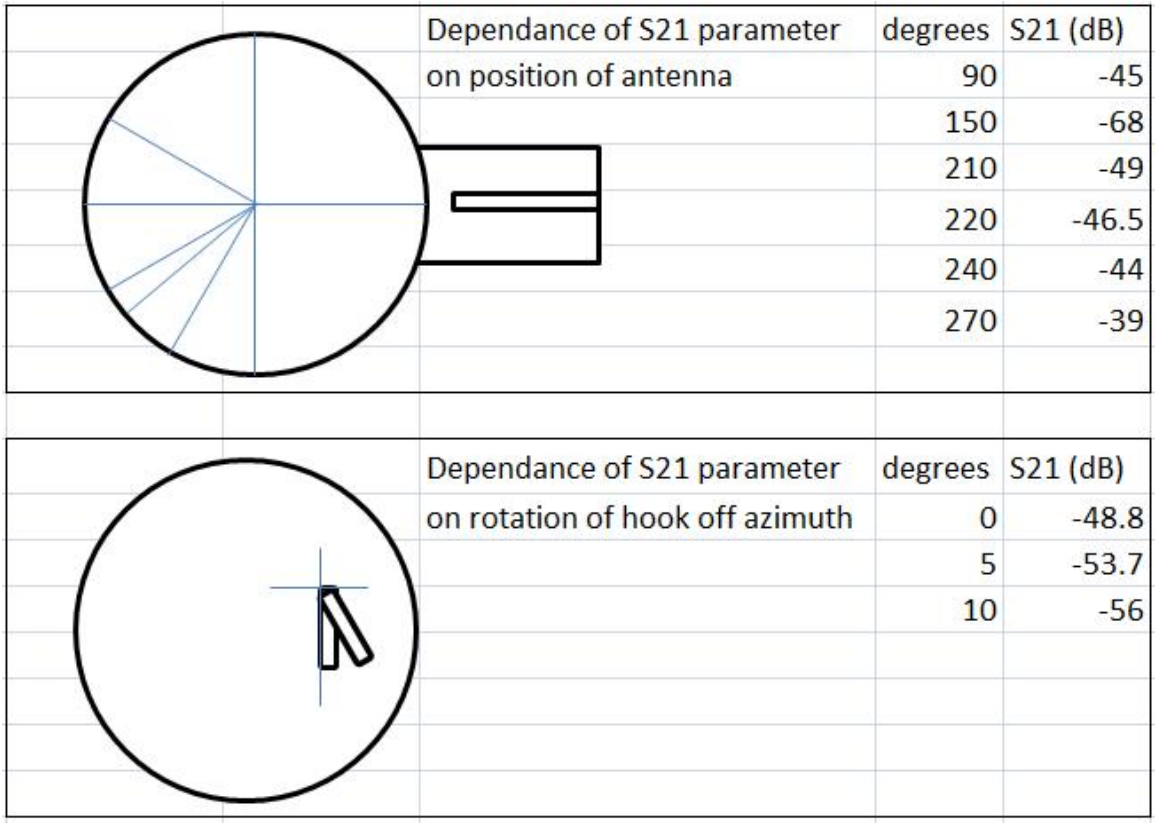

Dependance of S21 parameter on position of antenna	degrees	S21 (dB)
	90	-45
	150	-68
	210	-49
	220	-46.5
	240	-44
	270	-39

Dependance of S21 parameter on rotation of hook off azimuth	degrees	S21 (dB)
	0	-48.8
	5	-53.7
	10	-56

FIG. 57. The upper figure shows the coupling to the cavity with a clockwise oriented hook at various angles around the beam pipe. The angles are defined as in a unit circle. There are two high points, one at 90 degrees and another at 270 degrees. A TE mode should be symmetric and therefore this is somewhat unsettling. The lower figure shows the dependence of the orientation of the leg of the hook to the azimuth of the beam pipe. A decrease of 8 dB is measured with a slight 10 degree angle towards the radial direction.

placed in the solution and inserted into an ultrasonic cleaning device. After 5 minutes, the beaker is removed and heated, bringing the solution to a boil. Once the solution begins to boil, heating is halted and the solution is allowed to cool at room temperature. Twenty minutes is allowed for adequate cooling. The sapphire is then removed from the nitric solution and rinsed with deionized water twice. The sapphire is then placed in another glass container containing acetone and ultrasonically cleaned for five minutes. When the ultrasonication is complete, the sapphire is rinsed with isopropanol and placed in a beaker of isopropanol, and ultrasonicated for another five minute period. The sapphire is then rinsed with 200 proof ethanol, placed in a beaker containing 200 proof ethanol, and ultrasonicated for five minutes. The sapphire is left in the ethanol until assembly.

This procedure was greatly altered due to safety, mechanical, and procedural constraints. The sapphire was inserted into a beaker of the nitric acid solution and ultrasonically agitated. Immediately, it could be seen that the Niobium lines on the sapphire, from a practice fitting in holder, were unaffected. The ultrasonic shaker did not sound particularly powerful, or sound as if it were functioning properly. After five minutes of the ultrasonication, the beaker was moved to a hot plate to boil the nitric acid. The hotplate did not seem to obtain high temperatures even at the highest setting. Once it was clear the heating, or lack thereof, was not working, the sapphire was removed and put through the acetone cycle. The lines of Niobium persisted and at this point detoured from the NASA recipe.

The sapphire was placed in bath of BCP (1:1:1). BCP stand for Buffer Chemical Polishing. This concoction is comprised of equal parts (volume out of the bottle) of three acids: Nitric acid, hydrofluoric acid, and phosphoric acid. The concentrations of these acids in the U.S. in their original containers are typically as follows: Nitric acid (HNO_3) is 69%, Hydroflouric acid (HF) is 49%, and Phosphouric acid (H_3PO_4)

is 85%. The sapphire was inserted into this corrosive and deadly mixture for 15 seconds. The majority of the lines disappeared from the sapphire, but two spots persisted. Other than the niobium being removed, there were no noticeable changes in the crystal.

Once the BCP was complete, the sapphire was rinsed and dried. The sapphire was then transferred to a nitric bath for 10 minutes, rinsed with deionized water, and placed through the acetone, isopropanol, ethanol cycles listed above. The sapphire stayed in the ethanol overnight. The next morning the sapphire was removed and rinsed with 16 MΩ water (important later), dried with dry nitrogen, and placed in a sealed bag in the clean room by the chemistry staff. This last step is the standard procedure for all items going into the clean room.

4. Parts Cleaning

The cavity and other parts were cleaned in the chemical room. The cavity was treated with BCP (1:1:1) to remove 50 microns of the inner surface. The other niobium pieces were only given a light cleaning in BCP and acetone. The flanges were not touched because the NbTi flanges will react differently to the etch. The stainless pieces were cleaned using the standard stainless etch: Nitric acid (30%), Hydroflouric acid (4%), and water (66%) by volume. The copper antennas were also cleaned using a Nitric acid (20%), Phosphoric acid (55%), and Acetic acid (25%) etch.

5. Resistors

Two resistors were obtained to measure the temperature of the internal structure of the cavity. The resistors used were Cernox Silicon Diodes by Lakeshore. The two CX-1050-SD-1.4L model resistors have a calibrated temperature range from 325 K to 1.40 K. The serial number must be kept on the thermometer to identify them.

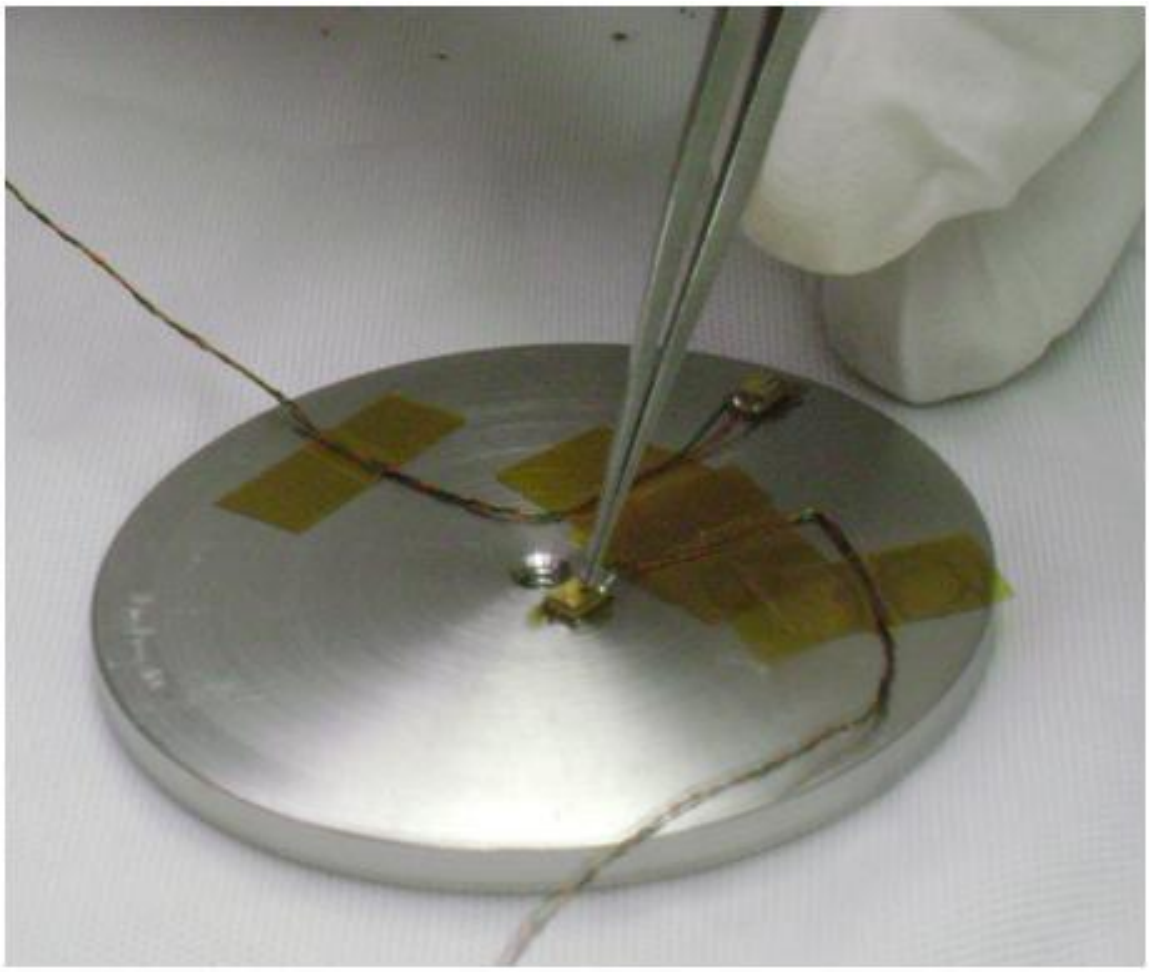

FIG. 58. In this image the resistors are being anchored using a varnish.

Each resistor has its own slightly different calibration curve. The two resistors were placed in different locations on the backing plate. One reistor was near the indium thermal bridge and the other was on the cavity axis, which allows one to see if there is temperature difference or lag in conductivity.

The resistors were cleaned using isopropanol and anchored to the backing plate using GE7031 varnish in the manner illustrated in Figure 58. The GE7031 varnish was used because it should not out-gas. Application of the varnish was done by Steve Dutton, with the supervision of the investigator, under a horizontal flow hood located

in cavity production room.

6. Sapphire Loaded Cold Test

The cavity was assembled, brought under vacuum, placed in the dewar, and thermometers tested, which were operating normally. A network analyzer was attached to the antennas (hook) and transmission (pin) antenna. The TE_{011} signal was identified at 1.85279 GHz at room temperature with a HOM (Higher Order Mode) peak 1 at 1.871065 GHz and another at 1.874945 GHz for HOM peak 2. The TE peak was not extremely strong, but was found, whereas the HOM peaks were very apparent and prevalent.

The temperature was reduced in a semi-controlled manner. Readings were made continuously in attempts to obtain a constant cooling rate. This proved to be most difficult. The rate was difficult to control as well as making sure there were no thermal gradients across the cavity. Referring to Eq. 4.5, Q_0 is related to the loaded Q times 1 plus the coupling coefficients of the antennas. Since the coupling coefficients are very small $Q_L \approx Q_0$. Figure 59 gives the Q of the cavity as a function of temperature.

At 10.5 degrees Kelvin, it appears that a part of the cavity started to become superconducting. There is a temperature gradient on the cavity from the bottom to the top as the dewar fills with helium. The interior thermometers on the backing plate are always read higher than the dewar sensors until the temperature is stabilized because of the time delay of the thermal energy passing through the Niobium holder. At 4 K, the microphonics started to become relevant. The peak was moving several tens of Hertz and the uncertainty in measurements of the network analyzer increased. At these superconducting temperatures, the loss tangent can be approximated by taking one divided by Q_L, as Chapter 2 demonstrated. The Q_L of the cavity, as measured by the network analyzer, at 4.308 K was 4.6628×10^7 giving a loss tangent

Mode	Temperature (K)	Frequency (GHz)	ΔHz	Q_L
TE011	291	1.8530462		
TE011	250	1.8556962		25,000
TE011	200	1.8587637		
TE011	185	1.8599177		
TE011	164	1.8617137		
TE011	136	1.863145		
TE011	96	1.864563		
TE011	70	1.864938		
TE011	52.6	1.865078625		207230
TE011	44	1.865		
TE011	21.143	1.8651375	2700	3.48570E+05
TE011	16.6	1.865133	2300	4.05464E+05
TE011	14	1.865133625	1900	4.90824E+05
TE011	12.5	1.865133625	2000	4.66283E+05
TE011	12.1	1.86513325	2460??	3.79092E+05
TE011	10.5	1.8651365	220	4.23895E+06
TE011	9.25	1.865137	155	6.01657E+06
TE011	9	1.865137063	90	1.03619E+07
TE011	8.5	1.865137196		1.44500E+07
TE011	8	1.865137202		1.55430E+07
TE011	7.5	1.86513736	65	2.70310E+07
TE011	7	1.865137		2.10000E+07
TE011	6.5	1.865137	25	3.73027E+07
TE011	6.175	1.865137415		4.14480E+07
TE011	6	1.865137801	23	4.05465E+07
TE011	5.5	1.865137427	22	4.23895E+07
TE011	5	1.865137491	16.5	5.65193E+07
TE011	4.7	1.865137753	18	5.18094E+07
TE011	4.375	1.865137571	20	4.66284E+07
TE011	4.314	1.865137572	19/22	4.50000E+07
TE011	4.308	1.865137572	16/19	5.32890E+07
TE011	4.308		Loss Tan	1.87656E-08
Peak1	247	1.873255		Very low Q
Peak1	11	1.877248523		Very low Q
Peak1	6	1.877322387		Very low Q
Peak2	247	1.877285		Very low Q
Peak2	11	1.880803523		Very low Q
Peak2	6	1.880827		Very low Q

Frequency of Modes found at 4.309 Kelvin (GHz)				
0.903	1.50887	1.69805	1.87732	2.10459
1.1548	1.55556	1.81832	1.88084	2.16706
1.41218	1.55713	1.82119	2.00286	2.16735
1.4135	1.68494	1.86512	2.09313	

FIG. 59. This chart shows the frequency and the quality factor dependence as a function of temperature. The superconducting transition can be seen starting around 11 K. Note the temperatures read are from the resistors on the backing plate, which should tell us the temperature of the sapphire. The reason for the broad superconducting transition (low to high Q) is the lower part of the cavity has been cooled to a superconducting state and the upper part is still normal, hence no sharp transition because of the temperature gradient.

of the sapphire in the TE_{011} mode a value of 2.14463×10^{-8}.

Once the coupling constants were calculated, the measurement of Q_0 was performed using the decay time method. The Q_0 for the loaded cavity was 1.13×10^8 at 4.2 K. Comparing this measurement to the empty cavity, there is only a factor of 2.5 difference. This was an encouraging sign. Therefore, the temperature was dropped to 2 K and tested again. During the test an unusual signal appeared. The transmitted power became unstable. There were short bursts of reduced power indicating the cavity was multipactoring, or an avalanche of electrons is causing the cavity to quench.

The reason for multipactoring was guessed to be the antennas since they protruded inside the cavity in a non-trivial manner. However, this was met with a large amount of skepticism. A series of trials were performed until an almost completely clean signal was obtained. There was a slight drop in the transmitted power when the power was turned off, most likely from multipactoring, but was the least significant drop recorded. This may or may not have been from the erratic signal itself. The Q_0 measured was 2.17×10^8. The drive port Q_{ext} increased to 7.05×10^6, which is an order of magnitude decrease, which clearly shows the cavity is overcoupled. On the other hand there was an order of magnitude increase in Q_{ext} for the probe antenna to 2.08×10^9. These values were somewhat disappointing. The Q appeared to be limited by a hard boundary of multipactoring.

Upon removal of the hook (drive) antenna in the clean room, a dark discoloration was noticed on the drive antenna as shown in Figure 60. From this observation, it was decided to keep the cavity intact and just replace the hook antenna with a shorter one.

FIG. 60. Dark discoloration on copper may be proof that multipactoring was occurring on drive port antenna.

D. Test 3: Eliminate Multipactoring

The drive port coupler was reduced to protrude only 2.575 inches. This was approximately a $\frac{3}{4}$ inch reduction. The cavity was resealed and placed back in the dewar for cooling over a span of two days. The dewar was pumped directly down to 2 K. The signal was 'fuzzy', in that the transmitted power had very slight fluctuations. These fluctuations were periodic, not similar to the multipactoring signal. Clearly the antennas were the source of multipactoring. The results of the third test were worse than the previous set. The Q_0 was 8.04×10^7, which is slightly lower than before. The Q_{ext} of the drive port is 5.72×10^8 with the Q_{ext} of the probe being 6.34×10^{10}. The drive antenna moved the correct direction, however the probe antenna's coupling should have been unchanged, but the signal increased by 32.8 times the previous test. The only plausible explanation is that by having the drive port recessed more the fields penetrated the side port more, increasing the transmitted power seen by the probe.

The fact the Q was diminished opens many questions. One reason may be the contamination. Since cavity had the bottom flange removed in the assembly and not in the class 10, there could have been dust or other small particulates causing lower Q. This perhaps caused the 'fuzzy' signal. The pressure in the cavity was elevated above previous test levels. Generally in the previous tests, the pressure has been in the 5×10^{-9} mbar region. In this test the pressure was at the 6.4×10^{-8} mbar level. This lead to thoughts that the varnish, or perhaps residue from the tape, had out gassed during the thermal cycling. Since the vacuum port is located at the bottom, the gas would have to travel through the entire cavity and the past the surface of the sapphire. However, from the information received from Jefferson Lab scientists and staff, along with a technician from the thermometer manufacturer, no out gassing

should have occurred.

E. Test 4: Eliminate Possible Sources of Low Q

The cavity was disassembled and tested on the bench once more. The bench test did not match the results returned from the RF system. In efforts to attain consistent measurements, the pin was placed in the beam pipe and the hook in the side port. The measurements for the pin are as follows: 2.034 inches protruding into the cavity produced an S_{21} parameter of -45.637 dB, and .595 inches of pin protrusion was lead to -74.62 dB as an S_{21} parameter. The actual length of the pin from tip to tail was 2.422 inches long. Therefore the length was cut to 2.350 to get the Q_{ext} of 5×10^{11}.

After a cool down to 2 K, there were two frequencies found. One frequency was located at 1.8650815 GHz and another at 1.8650816 GHz. There could be a slight asymmetry that caused the splitting. The signal was very weak, but using the network analyzer, the width was measured to be 5 Hz. This was visually confirmed by Charlie Reece. The network analyzer gave a value of Q_L of 3.4×10^8. This would give a loss tangent of approximately 2.9×10^{-9}. However as stated earlier, due to the sensitivity of the network analyzer, a reliable measurement cannot be made past a Q_L of 1.8650×10^8. Sadly the signal was extremely weak and the RF system was unable to lock onto the signal. RF system was also unable to lock on the signal for the stronger, higher order mode. Therefore the cavity was warmed up and taken out of the dewar.

F. Test 5: Establish Good Coupling

For the fifth test the coupling was replaced. It is clear from evidence in Test 1 and 4 that the coupling strategy of the hook in the side port and the pin in the beam pipe

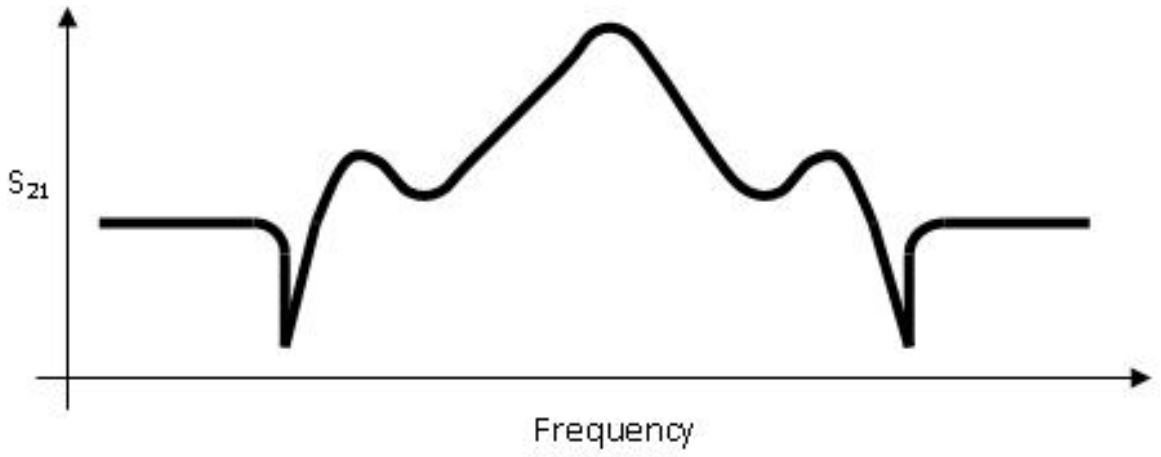

FIG. 61. The TE_{011} signal over a 1 kHz span from the network analyzer.

does not work. Therefore the only working strategy is to use the hook at the vacuum beam pipe flange, as long as it is kept short to bypass multipactoring, and the pin in the side port.

For the fifth test, the length of the pin was set at 4 inches long. The length of the hook was set at 2.5 inches and could be reduced if necessary. The cavity was cooled down in a timely manner, in that it did not sit for more than a day. The cavity at 4 K produced a signal that is similar to Figure 61. The cause for this irregular, yet symmetric, signal is not known. The signal was strong and a measurement of the Q could be made with the RF system. No measurement was made at 4 K since good coupling was established by network analyzer.

Once cooled to 2 K, the RF system was turned on. During the first measurement and interesting phenomenon occurred as seen on Figure 62. The sapphire was heating. To what extent this heating occurred is not known since the resistors were not attached to the niobium backing plate for this experiment to see if they were impacting performance. Several measurements were made at this time. In the continuous wave mode, the effect could not be seen. After a sufficiently long time the heating

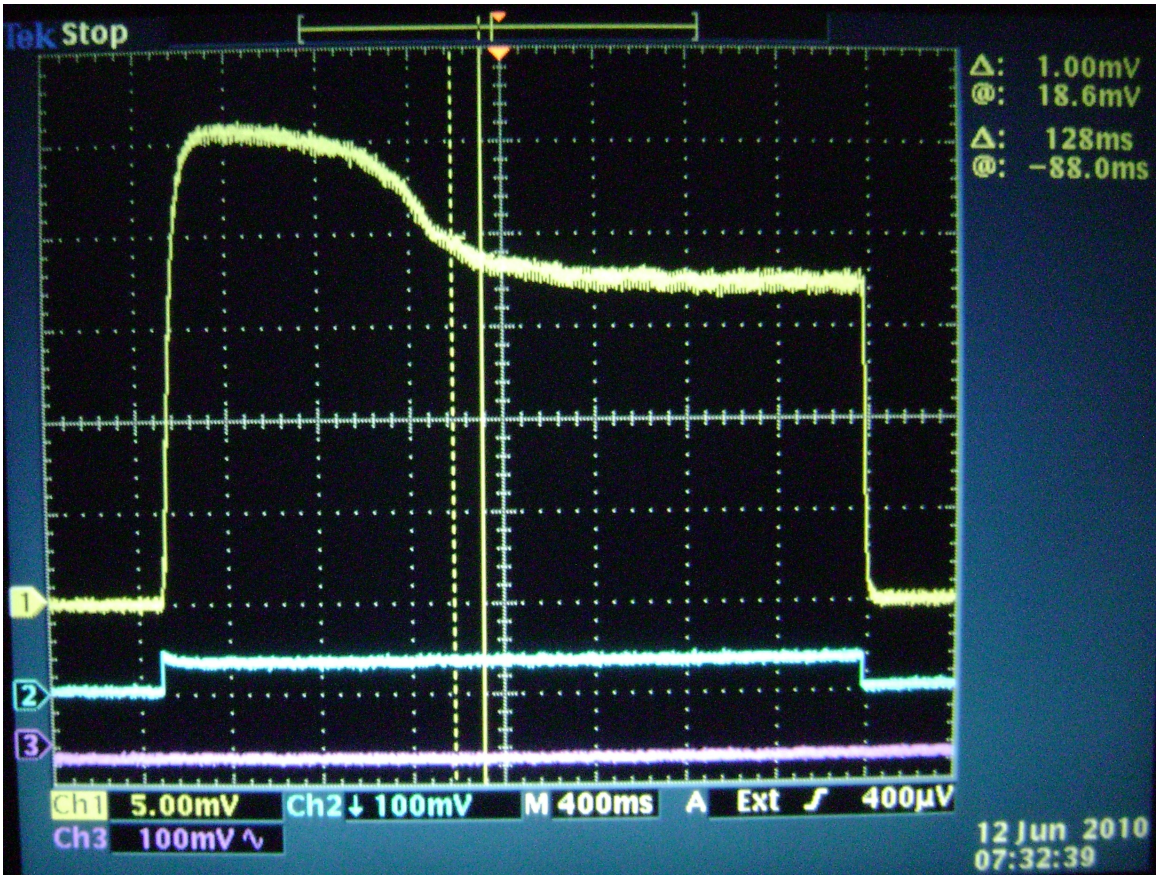

FIG. 62. This signal shows the sapphire is heating in the cavity. As the time progresses the voltage decreased, meaning the transmitted power decreased, which implies the Q has been diminished.

reached a state of equilibrium between dissipated power and cooling power by the bath via the holder. Only in the pulsed mode, or directly after a decay measurement, was the heating effect seen. For this input power level, the cavity was filled and the transmitted power started to decrease at approximately 400 ms, then leveled off after 1.2 seconds. Several measurements were taken at varying powers. On average, the Q_0 was 1.1×10^8. As the power was gradually increased, the Q gradually decreased as one would expect as did the time required to see the heating phenomenon. It was quite difficult to obtain a decay measurement before the sapphire was able to heat. To quantify this effect, the voltage squared, which is proportional to Q, was measured to be 25 mV for the continuous wave mode. After turning off the power for a few seconds and re-measuring, the voltage increased to 34 mV. Hence there was a substantial difference in the quality factor as the sapphire heats up. It was quite difficult to turn off the power, letting the sapphire cool, then quickly lock on the signal, and take a decay measurement before any significant heating occurred. In actuality the equipment necessary for the measurement was available but the author did not have sufficient knowledge and experience with the RF system to recognize the instrumentation was available.

A key success for Test 5 was that the coupling strategy worked well. The RF system was able to achieve lock and the coupling (Q_{ext}) for the antennas was quite good; 2×10^9 for the hook, and 3×10^8 for the hook. It is evident that an absolute minimum S_{21} parameter of -65 dB, read from the network analyzer, is needed to see the signal using the RF system.

G. Test 6: Quantify Heating Effect

The sixth test was set up to be the final test, and to fully understand the loss tangent as a function of temperature. The sapphire was put in a BCP 1:1:1 bath for 30 seconds, and afterwards no indium or niobium could be noticed on the surface. Because of the timing, the sapphire was not given the usual rinsing of isopropanol or ethanol with their respective ultrasonic agitation. The cavity was given a BCP etch of 10 microns as well as the niobium holder. This was followed by the cavity receiving a high pressure rinse on the R&D HPR system. After the high pressure rinse, the cavity was set out for drying in the class 10 room and assembled in the same day. The end flange with the hook coupler was rotated by about 60 degrees from its previous location as in Test 5, still placing it on the far side from the side port. It was just reflected over the symmetry plane created by the side port. The decision for this alteration came from the prospect to decrease the possible cross talk which might have caused unusual signal in Test 5, Figure 61. However, retrospectively this caused the coupling to decrease as shown in Figure 57. In this case the S_{21} parameter went from -65 dB (Test 5 with same antennas) to -87 dB. Thermometers were attached to the backing plate, but rather than using the GE 7031 varnish, mechanical clamps were installed to eliminate possible out gassing.

The sixth experiment was a ““shit can,” and that is a technical term.” Using the network analyzer alone it was clear the Q was below 5×10^6 at 4 and at 2 K. No measurement was made with the RF system, since it would not have located the signal at the -87 dB level. If the RF system had been able to lock onto the signal, the measurement could not have been far off from the network analyzer.

During thoughts regarding the explanation as to why this occurred revealed that several steps omitted were extremely pertinent, as well as illuminated other

precautions that needed to be taken. First, the sapphire is extremely sensitive to water as Rabi Wang stated [31]. Therefore the lack of drying time between the HPR and the assembly could have attributed a significant amount to the problem, as well as rinsing the sapphire with 16 MΩ water once it was removed from the ethanol bath. The water can attack the sapphire surface forming aluminum hydride compounds. This only occurs at the surface where the crystal edges are exposed. The sapphire was ground and therefore had a lot of surface area with exposed edges. Most of the losses should come from this phenomenon. Also the lack of using the isopropanol and ethanol most likely contributed to the poor performance. The sapphire should sit in the ethanol container until just before it is necessary to seal and pump down the cavity. By polishing the crystal to an optical finish and taking the other precaution described, there could be a drop in loss tangent by as much a factor of 4. Therefore a polish and a bake, to remove lattice defects were performed by Crystal Systems and their subcontractors.

H. Test 7: Polished Sapphire - Quantify Heating Effect.

The sapphire was sent to Crystal Systems where a bake and polish were performed. The crystal was annealed at 1450 degrees Celsius in an environment of air for 48 hours. Once the bake was completed, the sapphire was allowed to cool and then given and optical finish. The sapphire was then washed by hand with Joy soap and water. The sapphire was then air dried and placed in a plastic bag.

The cavity was degreased and high pressure rinsed. The sapphire was cleaned according to the altered NASA recipe. Once the ethanol agitation was completed the sapphire was stored in the beaker. The beaker containing the sapphire, still filled with 200 proof ethanol, was taken into the class 10 clean room and awaited cavity

assembly. The sapphire was inserted after all other components were attached. Once the sapphire was inserted, the last flange was tightened and put on the stand for vacuum pumping. It was continuously pumped for 5 days at room temperature then cooled. After assembly, it was found that one resistor was malfunctioning, a wire had broken free.

The frequency of the TE_{01} was found at 1.866313171 GHz which was .07% higher than frequency of the previous test. It was therefore clear that only a small portion of the sapphire was removed during the optical polishing process. Performing a quick calculation estimates that the polish removed approximately 17 microns from the surface or .0007 inches. The frequency had the same unusual shape that has been seen several times before, but this time was asymmetric. An image of the signal is shown in Figure 63. The signal was shown to several individuals and none could explain the strange shape. The strong center point was able to be locked on since it was orders of magnitude higher than the other peripheral peaks and plateaus shown. During testing at 4.31 K, the temperature thermometer indicated a range of temperatures, from 4.5 Kelvin to 4.7 Kelvin, when power was sent to the cavity. Turning the power off, the thermometer read 4.435 K, which was reduced by approximately .12 degrees. This is very little fluctuation therefore at this temperature the heat generated from the sapphire is sufficiently pulled out of the system through heat transportation via the NbTi holder.

In the non-energized state, a discrepancy existed between the thermometer on the backing plate and the sensor in dewar. This was assumed to be attributed to the mechanical clamping process. The pressure of the clamp might have slightly altered the calibration curve of the thermometer through a capacitive effect. The Cernox resistors are a thin film thermometer and therefore any change in capacitance would affect the temperature measurement. Lakeshore, upon retrospect, does sell

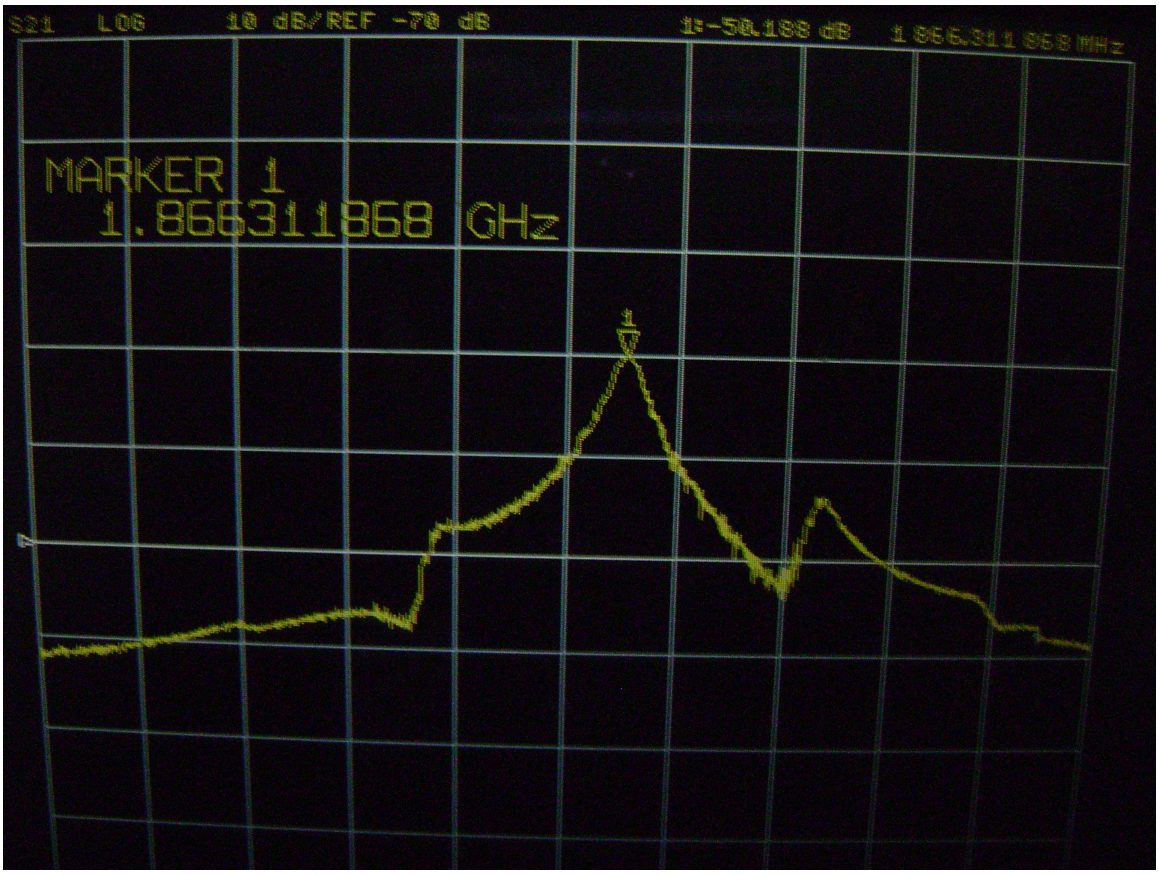

FIG. 63. Oddly shaped signal produced on the network analyzer by the sapphire test cavity.

custom made clamps which apply the appropriate, or correct, pressure for the Cernox resistor at a premium price and with a lengthy processing time. It was a pity the second resistor was not working which would have allowed for a back up verification of the temperature.

Using the network analyzer, the -3 dB half width was 7 Hz corresponding to a Q_L of 1.3328×10^8. However once again the analyzer is only good to 10 Hz, which corresponds to a limit of a Q_L of 9.33×10^7. A time decay measurement was made. The decay time was 8.2 ms, which corresponds to a Q_0 of 9.05×10^7. The temperature appeared to be stable during the measurement and consistently varied between 4.5

and 4.7 Kelvin. This experiment was performed with Gigi Ciovati.

The dewar was then cooled to 2.07 Kelvin. The reading on the interior Cernox thermometer was 2.48 K instead of 2.07 K. Therefore everything was renormalized to this value by this difference.

The frequency found by the RF system was 1.8662942 GHz with slight fluctuations due to microphonics. When the system sent power to the cavity, it could be seen that the sapphire would rapidly heat in a fraction of a second. The temperature of the sapphire and backing plate steadily rose until it equilibrated to about 3.41 K; note the input power was set at 1.75 mW. Once the temperature was steady, the power was turned off and as the temperature decayed, a series of measurements of the temperature were taken. This temperature decay is shown in Figure 64. It took around 15 minutes to cool back down to 2 K, or as read on the meter, 2.48 K.

In addition, time measurements were made at a variety of different points during the temperature rise due to heating. Because of the long time needed for the cavity to cool down to 2 K, the starting temperature was 2.7 K, as read off the meter. Rescaling as mentioned before, the temperature was really 2.29 K. The method for making the time decay measurements was somewhat make-shift. An internal pulse generator was used to turn the power on and off. Then using a kill switch, the power could be turn off immediately during any part of the pulse, which also paused the clock for the internal generator. After each measurement the power was killed until the temperature of the cavity reached 2.3 degrees.

Once the starting temperature was reached, the power was turned on. The kill switch was then hit when the energy in the cavity began to rise. The timing was quite difficult in that the kill switch had to be pushed, while attempting to capture the signal on the oscilloscope with only the decay curve on the screen. An image of a rise and decay of the cavity's stored energy is shown in Figure 65. The image shown

Cool down Time*		
3.41 to 2.9 K takes	2	sec
3.41 to 2.8 K takes	6	sec
3.41 to 2.7 K takes	15	sec
3.41 to 2.6K takes	48	sec
3.41 to 2.4K takes	several minutes	

*All temepratures must be subtracted by .41 degrees Kelvin for true temperatures.

Time to heat to Temperature*		
160	ms	2.9 K
120	ms	2.75 K
70	ms	2.7 K

Time of power on vs time decay measurement			
320	ms	9.5	ms
200	ms	9.7	ms
70	ms	10.5	ms

Time decay measurements

f	P	T	pi [W]	pr [W]	pt [W]	t [ms]	Beta inc.	Q0	Qext1	Qext2
1866.31	835	4.31021	0.00175	0.00013	5.6E-07	8.2	0.03379	90502253	2.68E+09	4.15E+11
1866.29	24	2.00284	0.00176	0.00014	1E-06	9.4	0.029642	1.03E+08	3.49E+09	2.36E+11
1866.29	24	2.00284	0.00176	0.00014	1E-06	9.5	0.029642	1.04E+08	3.52E+09	2.39E+11
1866.29	24	2.00284	0.00176	0.00014	1E-06	9.7	0.029642	1.07E+08	3.6E+09	2.44E+11
1866.29	24	2.00284	0.00176	0.00014	1E-06	10.5	0.029642	1.15E+08	3.89E+09	2.64E+11

FIG. 64. Upper Left: Decay time needed to cool from the equilibrium point (where the system is in equilibrium between cooling power versus power losses in heating of the sapphire) to the specified temperature. This equilibrium temperature is 3.41 K, as read off the internal thermometers. In reality this point is renormalized to 3 K because of the capacitive disruption in the thermometer. In this figure, the values given are the data recorded, and therefore the decay time is from 3.41 K (3 K real value) to 2.4 K (2 K real value) with specified temperature measured. Upper Right: (top) The amount of time it takes to heat from 2.4 to specified temperature with 1.75 mW input power. Note values need to be normalized. (bottom) This shows how the amount of time the power is on ,or sapphire heating, affects the decay constant of the cavity. It can be seen that the longer the time, the shorter the decay time, or the lower the Q. Lower Half: The raw data taken by the RF system. showing that as the investigator was able to lock in on shorter and shorter pulses the decay time increased as well as Q.

FIG. 65. The image shows the cavity powering up, then the power is turned off and the cavity decays. An important note regarding this picture is that the temperature was not 2.3 during the capturing of this image on the scope.

allows you to visually calculate the decay time as well as know the time the cavity is heating. However the capture program (Lab View Simplicity Solutions 830 Decay with Scope) used to statistically calculate the decay time will not be able to use this image. The only images that the program is able to use is where the apex of the curve is on the left edge and the decay curve is the only line with slope on the screen, as Figure 66 shows.

Taking these measurements was quite difficult to do with such small time scales. Several measurements were taken at a variety of times in an attempt to quantifying the heat generation vs. time. The meager amount of data acquired took hours to produce, but nonetheless showed that the sapphire heated quickly and was not extremely sensitive to the temperature at this level. The data is given in Figure 64.

The best Q measurement made was with the shortest rise time captured, 70 ms, and at the starting temperature of 2.3 degrees Kelvin. The decay time was 10.5 ms, giving a Q_0 of 1.15×10^8. This is sadly similar to the previous measurements, and therefore the heat treatment and polishing did not have a major effect on the loss tangent. However, significant heating could be seen in a short time. Therefore another test was set up where the entire cavity was filled with superfluid helium.

I. Test 8: Cavity is Filled with Helium.

The last test performed was to fill the cavity with superfluid helium. This was done by putting micron filters on all ports to allow helium in but keep floating debris out of the interior of the cavity that might cause poor performance. The cavity interior was exposed to air, via the filter, during transit from the clean room to the dewar. The cavity was cooled down to 2 K directly. During cool down the TE_{01} mode was found. However, as the cool down progressed several modes were generated. As many

FIG. 66. The apex of the stored energy is captured during this measurement the left. Only the decay curve, the only slope changing line, was captured allowing the Lab View program to statistically calculate the decay time.

as 10 were at one point seen, however when the temperature stabilized all of these modes disappeared.

At 2 K, after the cavity stabilized, the signal seen by the RF system was somewhat fuzzy (Figure 67). Using the network analyzer, the width was 15 Hz at the 3dB point. This corresponds to a Q of 6.2012×10^7, this is almost a factor of two lower than what was seen in the previous test. The frequency stabilized at 1.86038 GHz. This mode was only found after attaching a larger external amplifier. The transmitted signal was greatly reduced compared to the previous experiment. Once the external amplifier was attached, the power was increased substantially compared to the previous experiment's transmitted power, therefore the antennas' coupling to the cavity must be much smaller, or Q_{ext} is much higher.

The frequency had shifted slightly lower (6 MHz) which was anticipated because the helium. The measured dielectric constant is 1.0575 [34]. When this constant is entered into the model, it gives a frequency change of 6 MHz. Therefore the helium is changing the fields as predicted by the model, and therefore should be able to calculate the loss tangent for this experiment in the same manner as the empty cavity with the slight variation of adding the losses from the sapphire's and the helium's loss tangent. Helium's loss tangent has been measured to be at most 3.33×10^{-10} at 2 K [34]. Figures 68 and 69 show helium's dielectric constant and loss tangent as a function of temperature.

A measurement was taken using the RF system and indeed confirmed the network analyzer. The Q_0 was 5.77×10^7. Error in this measurement should be extremely small because

$$Q_0 \approx (1 + \beta) 2\pi f \tau. \tag{4.11}$$

So only in the case where β is near or greater than one will the error be a major

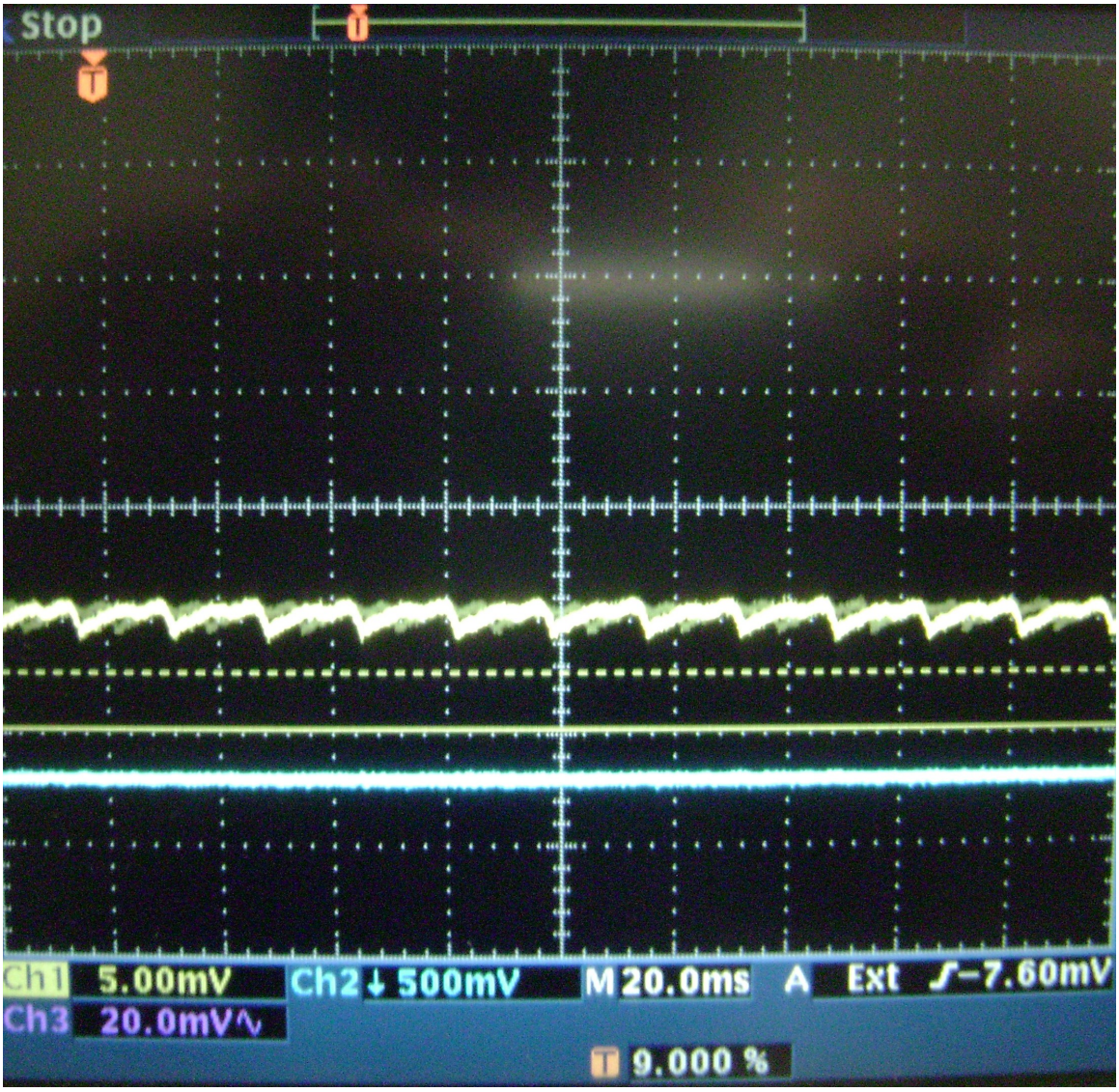

FIG. 67. A captured sweep of the power from the oscilloscope. The signal has a periodic signal that is irregularly shape.

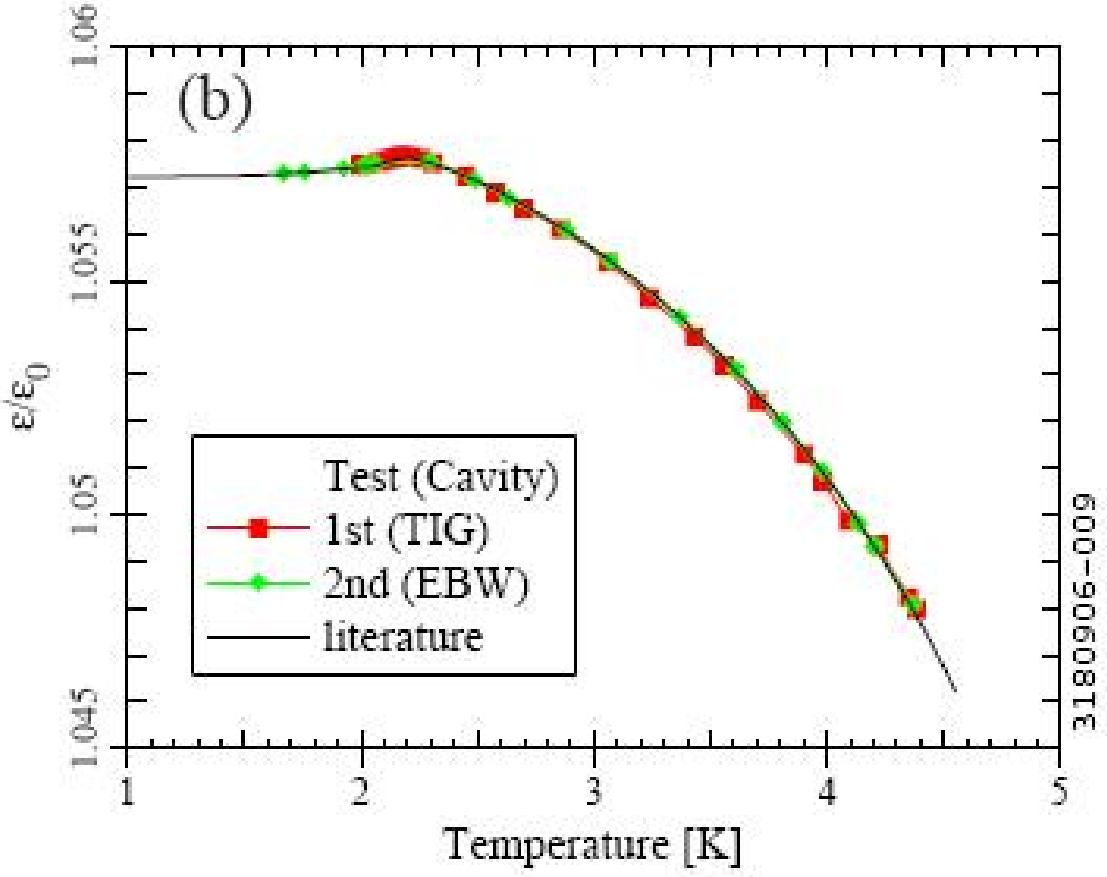

FIG. 68. The dielectric constant of helium as a function of temperature [34].

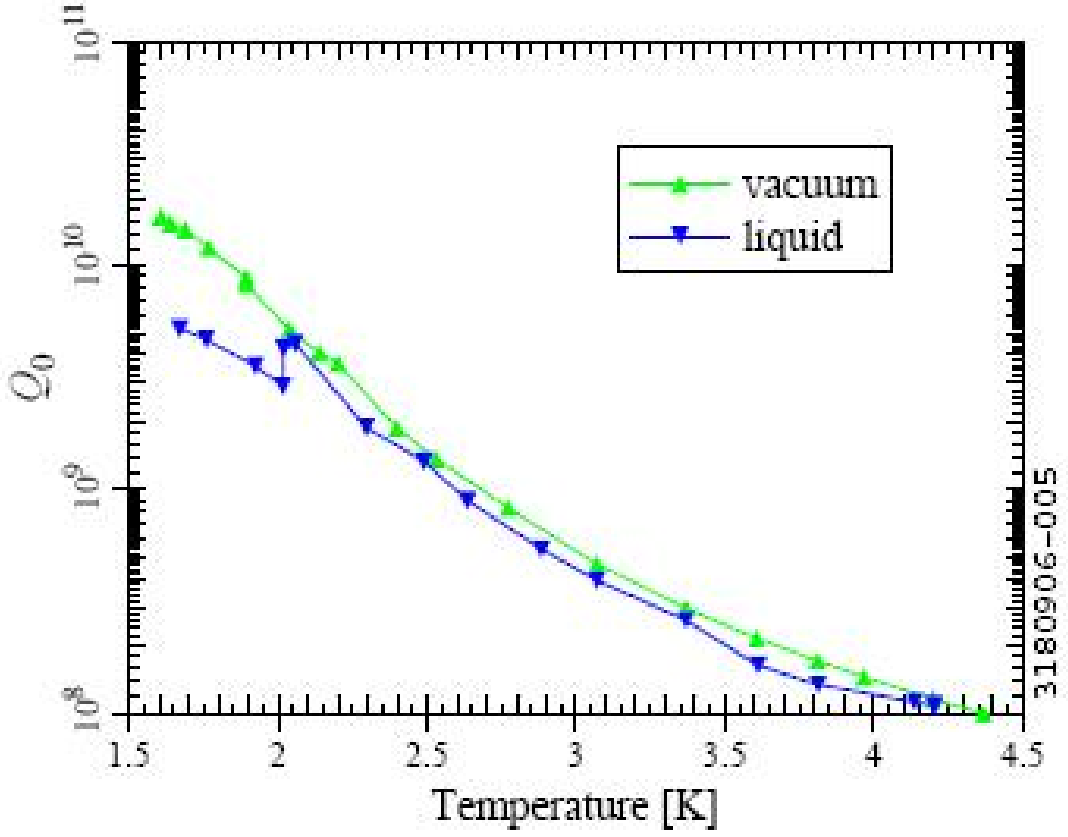

FIG. 69. Comparison of the Q_0 of an empty cavity compared to the Q_0 of a cavity filled with helium [34].

factor. Therefore logically the helium was contaminated with other material and reduced the Q of the cavity. It also changed the frequency by a few MHz, as well as the coupling reduced by a factor of 22. Directly cooling the sapphire and the Nb holder did not increase the Q of the cavity. Further analysis is necessary to determine the exact loss tangent of the sapphire from the performance of the cavity. Up until now an approximation has been used, but more accurate numbers will be calculated for all tests.

During this series of experiments a variety of methods, techniques, and processes were performed to establish the value for the sapphire's loss tangent. From these measurements, the cavity had a highest Q value of 2.17×10^8 measured by the RF system at 2 K. The average was around 1×10^8.

CHAPTER V

ANALYSIS AND CONCLUSIONS

Several Q values have been measured and the loss tangents correlating to them as well as any procedural alterations needed for future use. This analysis will provide the parameters for operating the Wafer Test Cavity with current materials. These parameters will determine whether or not there is sufficient evidence to continue onto construction.

A. Experimental Measurement Analysis

The first experiment performed was on the empty test cavity. The coupling was excellent for the TM_{010} mode but the TE_{011} mode could not be found. There were several important results from this experiment. It confirmed that the cavity was operating properly within the realm of normal CEBAF cavities. The cavity operated to a level of 2.38×10^8 at 4.2 K and 1.29×10^{10} at 2 K. Therefore the cavity indeed performs as expected at the appropriate frequency. From these results the surface resistance of the niobium cavity could be acquired. At 4.2 K, the resistance of the niobium cavity surface was $965n\Omega$. Only a 3% error in the measurement is assumed and will be explained momentarily. Dropping the temperature to 2 K drastically dropped the cavities resistance to 21.1 $n\Omega$. These two values can be used as the resistance of niobium in the following analytical computations for each experiment.

The first and fourth tests, described in Chapter 4, should have produced the anticipated coupling for the TE mode; however it did not. The coupling strategy of the hook in the side port and the pin in the beam tube did not produce a visible signal by the RF system. That is why in the second test (sapphire loaded) the antennas were switched and intentionally given extra length for enhanced coupling. The signal

in the second test was found rapidly well above 250 K, meaning that coupling was indeed better and much stronger.

The coupling was so intense the cavity began multipactoring, which was detected by the RF system. The source of the multipactoring was the antenna itself. This conclusion was drawn from the speckled copper antenna. For the 4.2 K measurement, the Q_0 value was 1.13×10^8 and at 2 K the value was 2.17×10^8. Using Eq. 2.4, the loss tangent can be calculated. Inserting the new values for the Niobium surface resistance, the loss tangent is calculated to be 9.58×10^{-9} at 4.2 K, which is higher than anticipated. The 2 K measurement gives a loss tangent value of 5.54×10^{-9}. These values are quite close and are on the same order of separation as described by Rabi Wang about his sapphire (half the size of this crystal).

The certainty of these values is questionable for several reasons. The largest source of error in the measurement comes from the coupling constant. In Eq. 4.11, it is clear why such large errors can come from the coupling. In the case of an undercoupled cavity (i.e. $\beta < 1$) the errors are less than 3%. Figure 70 shows, as long as a cavity is undercoupled, a time decay measurement of Q has an error less than 3%. If the cavity is overcoupled, as in this case, the error in the time decay could be quite large. The reasons for such large error will not be expounded here, please refer to Tom Powers' paper [35]. Extrapolating, the errors in the second experiment are less than 3% for the 4.2 K measurement, and 45% for the 2K measurement. The 2 K measurement is the best measurement of the loss tangent for all experiments using the RF system but has a large error. However, this does not mean it is a higher loss tangent, it could also be lower.

Other uncertainty can come from the coupling geometry in the cavity itself, for it is not optimum for taking Q measurements. The reason why is that the transmitted power seen by the probe could have a component of the power emitted from the input

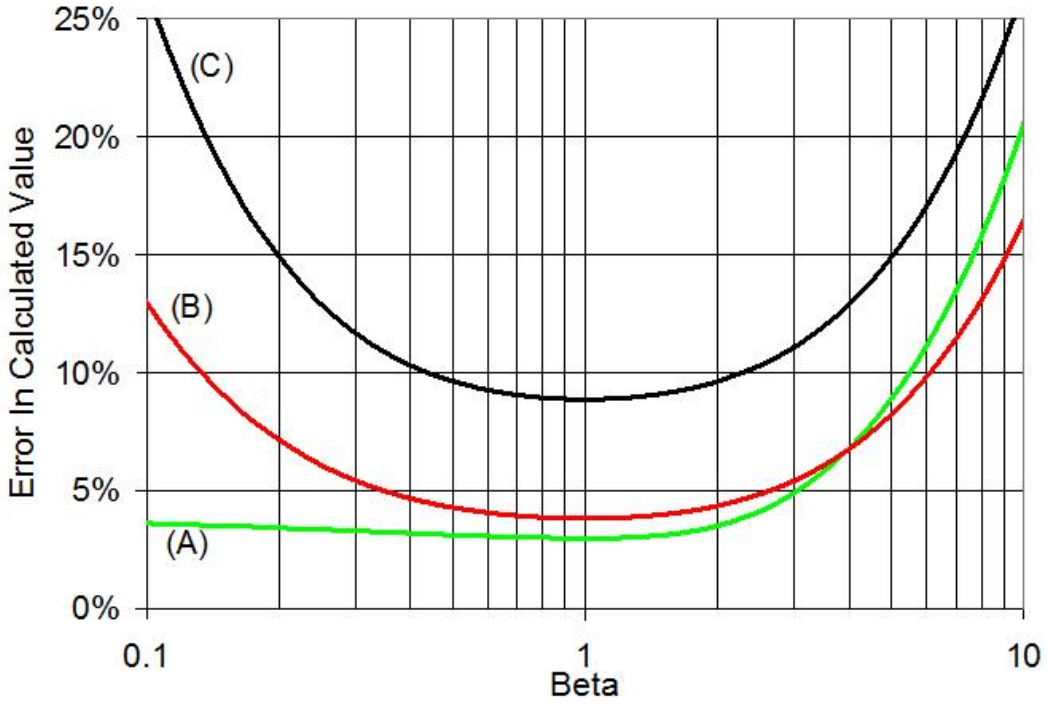

FIG. 70. Figure of the error of measurement as a function of β.(A) This green line represents the error in the value of Q_0 as quantified by a decay measurement.(B) The error in the stored energy quantified by a decay measurement.(C) Q_0's error as measured using a CW measurement as a function of β.

antenna. The decay time could be altered by the overlapping fields from the input antenna to the probe, which bypasses the sapphire loaded cell. If the fields bypass the loaded cell, the fields that leak out to the probe are not necessarily circulating TE modes. Therefore, the decay time might be reduced. The reason is the way the decay measurement is made. The highest point is measured, and when the value reaches 1/e, that is the decay time. If the transmitted power is artificially enhanced by the power traveling directly from the input to the probe, the time for the parasitic mode to reach the probe is almost immediate for it bypasses the loaded cell. When the power is dissipated rapidly, this artificially reduces the stored energy and consequently diminished the decay time, therefore Q decreases.

Similarly, multipactoring could have an effect. This second test at 2 K is the only test where multipactoring occurred. This might have had an effect on the value of the time decay, but to what degree is unknown; though it might have hindered the Q value as explained earlier.

In addition, the sapphire was operating under continuous wave. At this time there was no heating effect seen. Perhaps the loss tangent was low enough that significant heating did not occur, which may put the dielectric loss tangent much lower than measured. In this measurement the Q could have been degraded by the antennas, but this was found to be untrue. The model that was used ignored the copper antennas, but the external Q for the input coupler was 8.01×10^7 at 4.2 K and 7.05×10^6 at 2 K. A new model was created adding the hook and pin. Adding in the losses of the copper antenna, there were only slight losses. Comparing the model with antennas (Figure 71), and one without, the difference is approximately 2%. The loss tangent produced is 9.10×10^{-9} for 4 K and 5.42×10^{-9} at 2 K. If the loss tangent had been a factor of 5 to 10 times better, the cavity would have been unable to be used as a measurement instrument. The comparable losses in the cavity would have

been equivalent or greater to the losses in the sapphire, refer to Figure 72.

During this measurement it was noted that there was no heating involved even at 2 K. If no heating was seen at a higher Q, then one makes the logical leap in that the loss tangent could have been low enough not to dissipate heat within. The lack of heating makes one think the loss tangent is lower than in latter measurements, which is consistent with the experimental data. This does pose an interesting question, whether the sapphire was damaged during the BCP etch. During polishing, approximately .007 inches of material was removed. This did not increase the cavity's performance but rather slightly degraded it. Perhaps some damage was done, but any damage should have been constrained to the surface layer. No evidence suggests migration of etchants into the bulk.

For the third test the hook was shortened by $\frac{3}{4}$ inch and had a worse Q. At both 4.2 K and 2 K the Q was approximately 8×10^7. This corresponds to a loss tangent of 1.4 or 1.5×10^{-8}. The contamination must have come from the opening the cavity. As to whether or not the varnish off gassed during the cycling of warm to cold, then warm to cold again, is at this point irrelevant. The varnish will never be used again in the cavity and all evidence as to whether the cavity contaminated was clean away for the fourth test.

The fourth test proved that the coupling in test one was the reason for the failure to find the TE mode. It appears that the hook in the side port does not couple well at all. Therefore the hook must be placed in the beam pipe in order to get a strong signal. Therefore no measurement was made with the RF system. A measurement was made using the Network Analyzer with low sweep rates where the error is quite large. Reducing the bandwidth to 10 Hz, the best error-free measurement possible for Q using the network analyzer was 1.8×10^8, or loss tangent of 6.66×10^{-9}.

The actual width of the peak measured was less than 5 Hz. This approximately 5

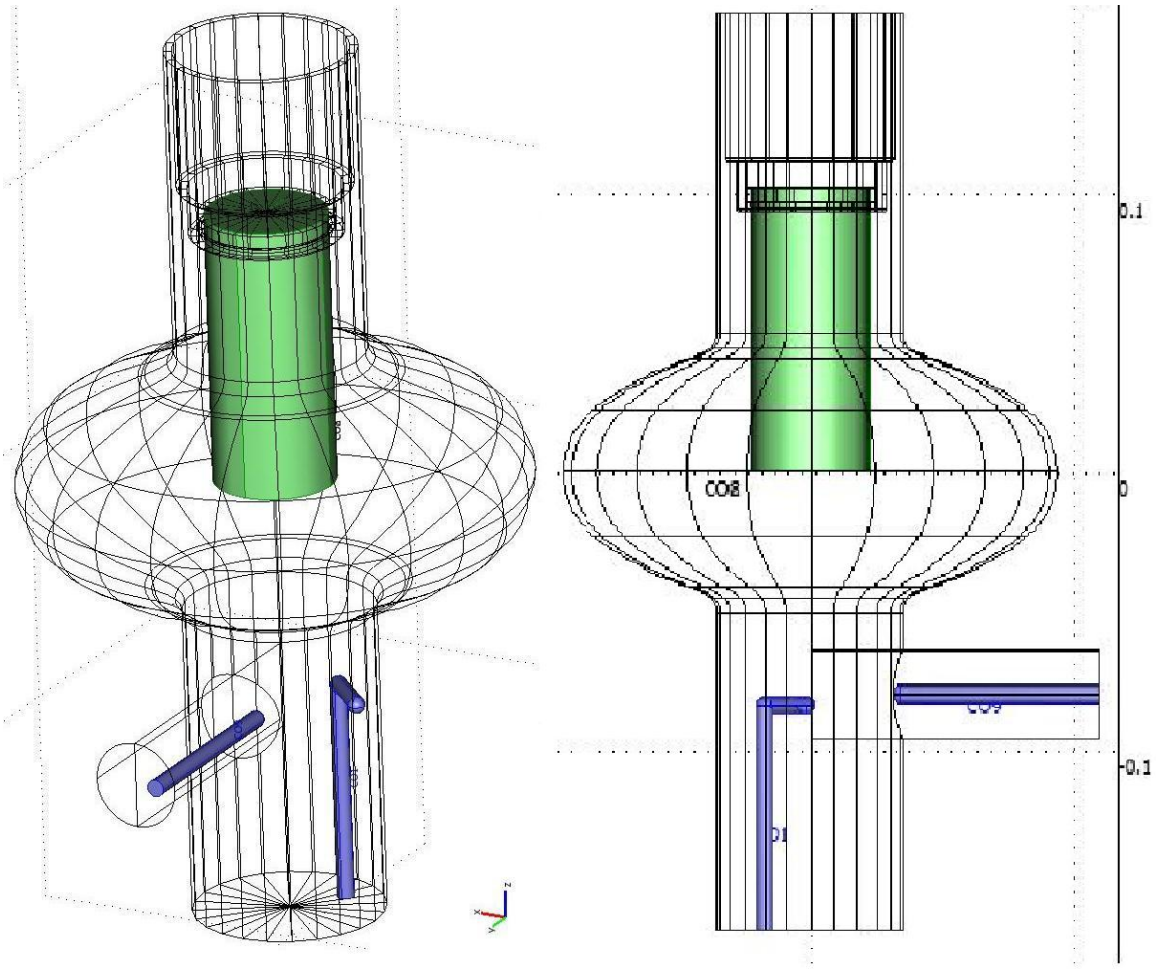

FIG. 71. Two images of the cavity with the antennas used in Experiment 2. This setup lead to the best measurement of loss tangent, but with the greatest source of error. Notice that the antennas are directly above one another, leading to the opportunity of cross talking generated from line of sight to each other.

Q of the cavity with varying loss tangents

loss tan	1.00E-08	5.00E-09	1.00E-09	5.00E-10	1.00E-10
Q at 4K	1.05E+08	1.85E+08	4.81E+08	6.02E+08	7.52E+08
Q at 2K	1.19E+08	2.34E+08	1.06E+09	1.90E+09	5.16E+09

Losses in sapphire compared to total losses in entire cavity

loss tan	1.00E-08	5.00E-09	1.00E-09	5.00E-10	1.00E-10
Sapphire loss 4K	89.84%	81.55%	46.92%	30.65%	8.12%
Sapphire loss 2K	98.82%	97.67%	89.34%	80.74%	45.60%

FIG. 72. This is the model parameters that are produced with the antennas compared to the parameters shown in Chapter 2. There was not a significant change in higher loss tangents, but beyond 5×10^{-9} the Qs and percentage of stored energy changes by as much as a factor of two. Beyond this threshold, the losses in the cavity (includes holder, antenna, indium, etc) would exceed the losses in the sapphire.

Hz peak width was visually confirmed by Charlie Reece over several sweeps. This was the smallest width measured with the network analyzer for all experiments. In test 2 the analyzer has matched previous measurements within a factor of 10%. Looking the data from Tests 7 and 8, this trend of close measurements continues to the same level. Therefore it is not an unreasonable to say that the loss tangent measurement made in Test 4 by the network analyzer, 3.52×10^{-9}, or a Q of 3.4×10^{8}, is somewhat accurate. This loss tangent value is calculated using the models with and without the antennas. The difference is less than 3%. It would have been nice if this value could have been confirmed by the RF system. However, there was not significant coupling to get a signal through. Using the network analyzer as a method of measurement insures that the sapphire is not significantly heating. Therefore this could be a very accurate measurement of the loss tangent at 2 K, since the power inserted is not large enough to heat the sapphire.

Skipping test 5 momentarily, in Test 6 the coupling was mirrored across the symmetry axis of the cavity in attempts to clean the signal. The hook was rotated by at most 45 degrees to clean up the signal. The result was a drop in signal by 23 dB, but a clearer signal was produced. Investigation was necessary as to why there was such a persistent problem with coupling. Using a more refined model of the cavity (i.e. model cavity with side port), the culprit was found. The side port added a significant asymmetry larger than what was anticipated. The TE structure is altered as the fields pass the opening as Figure 73 shows.

The field profile as you travel down the beam tube is greatly perturbed. The asymmetry is symmetric around the vertical axis or symmetry plane. As seen in Figure 57, the profile seen during the bench test confirms the models magnetic and electric fields' topology. This explains the difficulty in the coupling using the pin located in the beam tube versus the hook which is able to couple to the fringe fields,

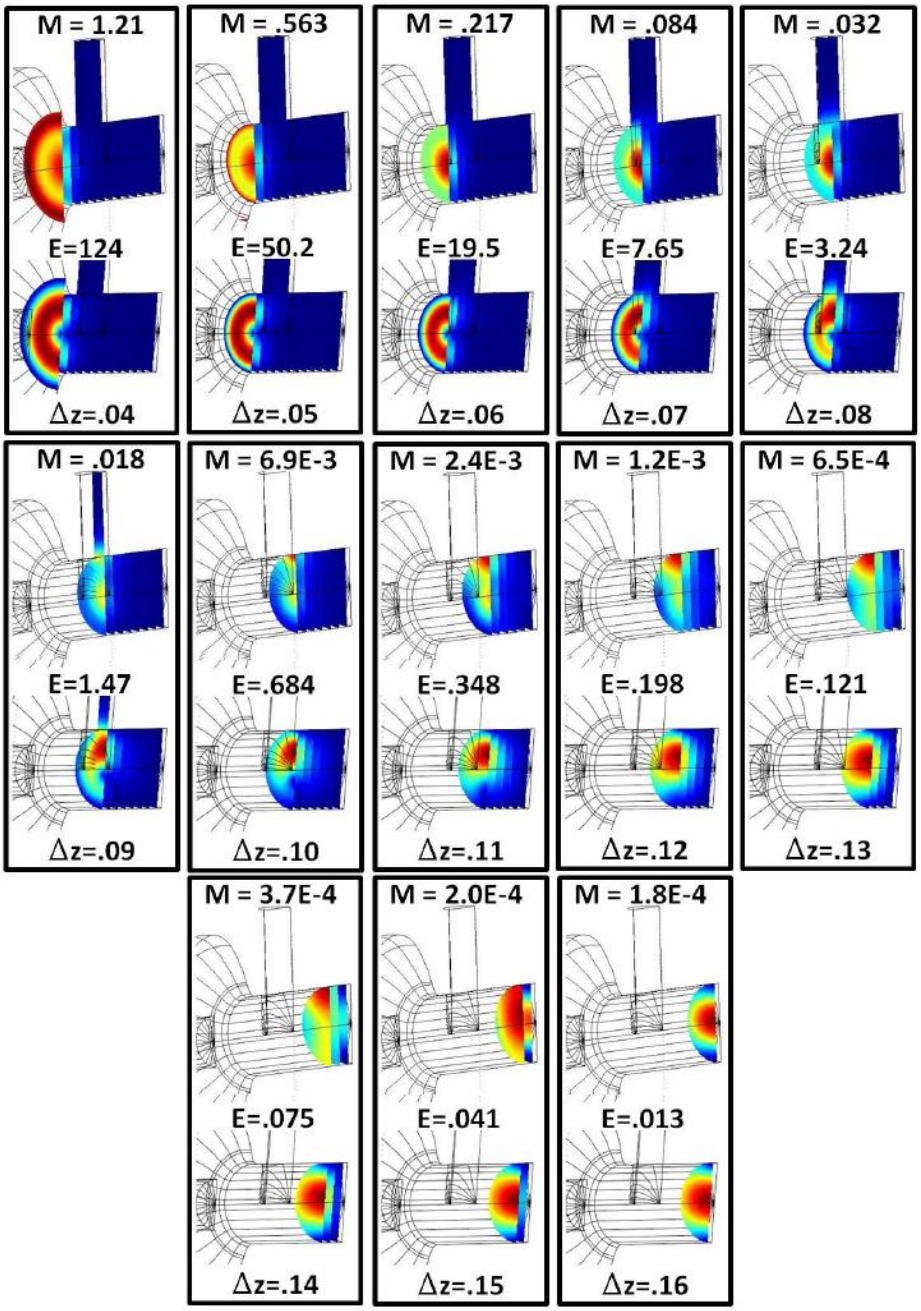

FIG. 73. This set of images shows progressive cuts down the beam tube. It illustrates the asymmetry generated by the side port. The maximum magnetic field is 40.71 units and the maximum electric field is 2887 units in the cavity. This is for comparison to the maximum field on the slices shown.

refer to Figure 71. Therefore in future tests, possibly in testing of other dielectrics, the coupling must be held in the same position as in Test 2, 5, 7, and 8.

In Test 5 a new phenomenon was seen, heating. This was somewhat expected but had not previously been seen in other tests. As mentioned above, perhaps the sapphire changed due to etching, thereby increasing the loss tangent and making the heating visible for the first time. It could also be that the earlier measurement were not precise enough, or had incorrect coupling to the degree that the heating could not be seen. In either case, heating is now an issue. A temperature vs. loss tangent graph was made using data shown in Figure 59, but the resistance of the niobium cavity over the whole variety of temperature ranges is not known. Using resistivity data from the Cryogenic Handbook [26] and the Q measurements made as a function of temperature, the loss tangent could be extrapolated, but with some error. An important note is that for the points at 6 and 8 degrees K, the equation for normal conductivity was used. This choice was made because the BCS resistance equation is only valid within the range of $T_c/2$, where T_c of Niobium is 9.25 K.

An extrapolation is shown in Figure 74. Note that the point at 16.6 degrees Kelvin is an outlier. When calculating the loss tangent for a variety of temperatures, the calculation returned negative numbers. This is because all but one value, Q, is model dependent. Therefore those that gave real numbers are shown in Figure 74. There are striking similarities between this graph and the data taken by the NASA JPL, Figure 28. The lowest measured loss tangents in these experiments are much higher than the lowest value recorded 2×10^{-10}, by Buckley [29]. Buckley's measurement is the only measurement though that uses calorimetry, not a resonator.

In comparison, to other previous work, the measurement of 9.10×10^{-9} at 4.2K by resonator is better than most measurements. The following are measurements made at 4.2K: Braginsky 1.6×10^{-8} at 8-10 GHz by resonator [36], Braginsky 6.5×10^{-9}

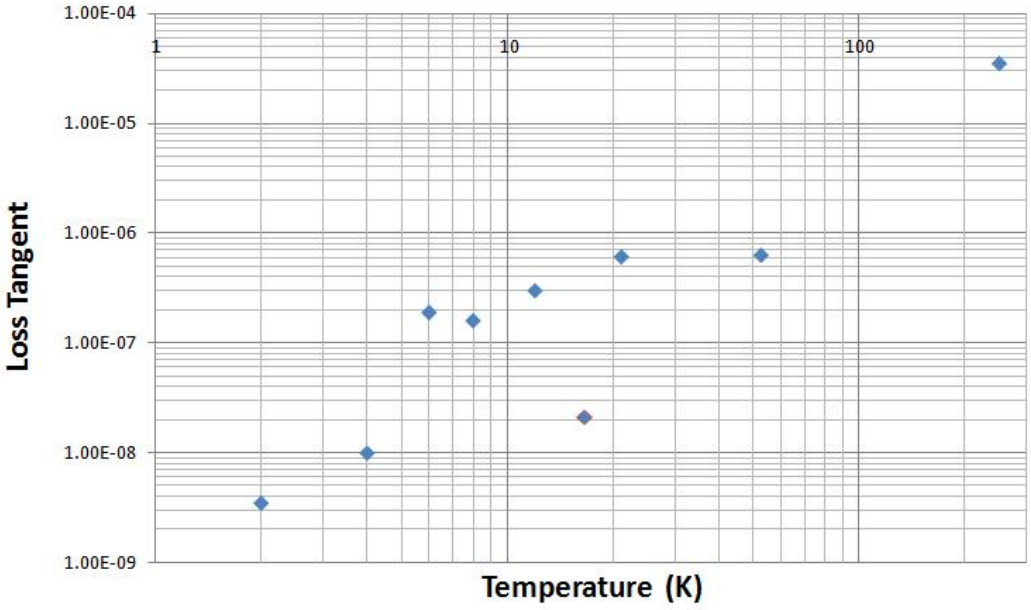

FIG. 74. A graph of the extrapolated loss tangent as a function of temperature. This data is comprised of the results of all the tests that were made in this study as well as the models used to ascertain the loss tangent of the sapphire.

at 9 GHz by resonator [30], Thakoor 1.1×10^{-8} at 2.69 GHz by resonator [37], Blair 3×10^{-8} at 9 GHz by resonator [38], and Buckley 2×10^{-10} at 2.45 GHz by calorimetry [29].

The 7th test was an attempt to measure the amount of energy necessary to heat the sapphire. From the data taken it is possible to calculate the stored energy in the cavity and therefore the amount of heat dissipated in the sapphire.

$$P_{loss} = \frac{\omega U}{Q}. \tag{5.1}$$

Looking at the rate of change the energy

$$\frac{dE}{dt} = \frac{-\omega E}{Q} + P_0, \tag{5.2}$$

where

$$E(t) = E_H + E_P, \tag{5.3}$$

the homogeneous and particular solutions. These are defined as

$$E_H = E_0 e^{\frac{-\omega t}{Q}}, E_0 = P_0 \frac{Q}{\omega} \tag{5.4}$$

and

$$E_P = P_0 \frac{Q}{\omega}. \tag{5.5}$$

Therefore

$$E(t) = P_0 \frac{Q}{\omega} \left(1 - e^{\frac{-\omega t}{Q}}\right) \tag{5.6}$$

tells you the stored energy in the cavity. $P_0 t$ is the energy put into the system, or the input energy minus the reflected energy and transmitted energy. The difference between the total energy put into the system and the energy that the cavity stores is the dissipated energy. Hence the dissipated energy is

$$E(diss) = P_0 t - P_0 \frac{Q}{\omega} \left(1 - e^{\frac{-\omega t}{Q}}\right) \tag{5.7}$$

Using a single data point from Test 7 as an example, the time with the power on was .070 seconds and the temperature increased to 2.29 K with a input power of .001619 W, states that the total energy lost in the system was $9.935 \times 10^{-5} J$. Since it is expected from our model that about 98% of the energy is located within the sapphire this value for the stored energy will not change much. Using heat capacity data known for sapphire [39], it is possible to find the extrapolated temperature. Using the curved relation given by Fugate (note that the authors of this paper limit the fit to above 13 K) [39], the temperature to match our total energy is approximately 1.7 K, which is clearly not correct since the bath temperature of the test was 2.07 K. Therefore a discrepancy in the heat capacity of sapphire exists at 2.3 K. Using

the energy dissipation data that was collected over the series of experiments, it is possible to find the enthalpy with a T^4 dependence, and differentiate to obtain the heat capacity. Next, one would compare the measured data against previously gather data.

Using the data acquired from Test 7 plotted in Figure 75, it is readily apparent that after .200 seconds the cavity (thermal bridge) is actively cooling the sapphire. At .320 seconds the cavity has almost reached its equilibrium point of 3.03 K, thereby creating an asymptote at the 3 degree mark. In Figure 75 only the data below this point was used.

From this best fit curve, the heat capacity can be directly computed. Taking the derivative of the equation produces

$$C_s = 0.00342479 - 0.00017342T^3. \tag{5.8}$$

This is the best fit relation of the heat capacity for the data taken in Test 7.

Sadly these results cannot be check with any real data that has been found by the author. The minimum value found was 3 K by Fugate, other values have been found but have been curve fits to data above 3 K extrapolated to 1.8 K. Therefore a curve fit was created to combine the data collected in experiment 7 with previously published data into one smooth curve up to 10 degrees K, Figure 76.

This shows that indeed the fit is good over the entire temperature space that the Dielectric Test cavity was tested under and the space where the Wafer Test cavity will be tested. The heat capacity is then calculated from the derivative of the trend line specified in Figure 76.

$$C_{s_{data}} = 0.0000883894T^3 \tag{5.9}$$

This equation can be checked against other trend lines that are available and

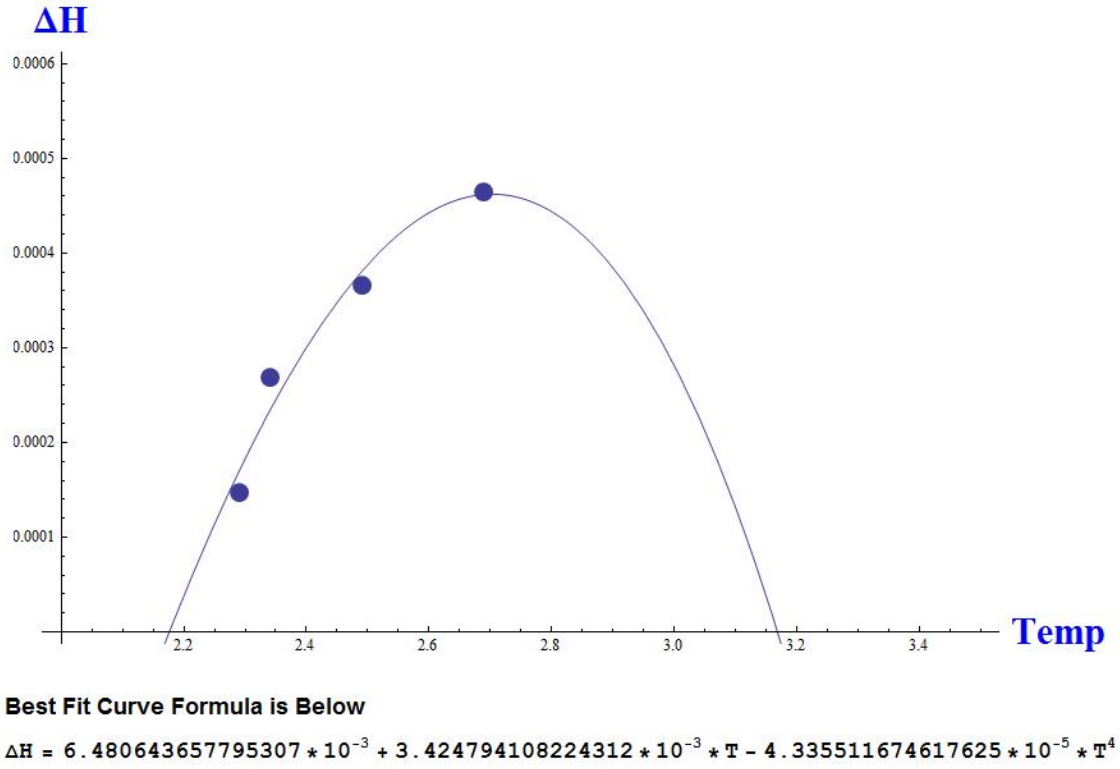

FIG. 75. This is plot of the data taken in Test 7 in regards to the total enthalpy change and the corresponding change in temperature. There is a gradual decay in the rate, which means that the cavity is actively cooling the sapphire as the temperature increases. As the temperature rises, the thermal gradient increases accelerating the cooling effect.

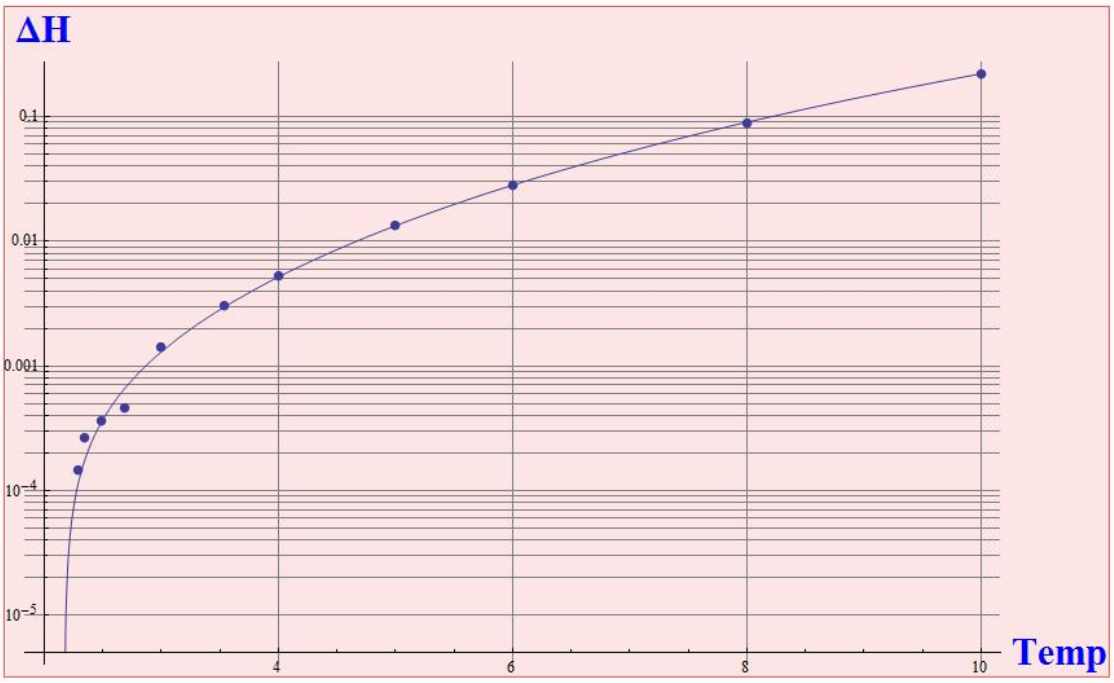

- **Best Fit Curve Formula is Below**
- $\Delta H = -0.000495191 + 0.0000220973 * T^4$

FIG. 76. Logarithmic plot of the entire data set below 10 K. This is plot of the data taken in Test 7 combined with data taken from Fugate [39]. A T^4 dependence is achieved, which is similar to many materials.

the data given by Fugate. In Figure 77, the heat capacities, generated by Eq. 5.9, are evaluated for specific values. These values are compared to data available and trend lines evaluated for these specific temperatures. Cryocomp is software used by National High Magnetic Field Laboratory [40] and the values generated by Cryocomp for sapphire were relayed to Texas A&M from NHMFL [41].

This set has provided four experimental data points of heat capacity below 3 K. It has also shown that the measurements are within the same realm as previous measurements and allowed us to understand how the sapphire is heating. Among the many assumptions made above, it is imperative to assume that the sapphire is heating uniformly.

From modeling, the highest field energy density is located in the front end of the sapphire. The heat deposited is done so in that particular location. It is assumed during heating the sapphire can be treated as if the whole mass (653 g) is sharing the dissipated energy. This assumption is true as long at the thermal relaxation time is short compared to the measurement time.

Using a simple heat equation it is possible to calculate the time it takes for the entire sapphire to come to equilibrium, to a good approximation. Assume at $x = 0$ is the location of the heating during RF operation, producing a temperature T_H. The other end of the sapphire, $x = L$, the temperature is held at the bath temperature T_C. The temperature of the sapphire is then a function of the position of the heating and the time of the heating.

$$T(t, x) = Y(t)R(x) \tag{5.10}$$

Inserting this dependence into the heat equation

$$\frac{\partial}{\partial x}\left(\kappa(T)\left(\frac{\partial Y(t)R(x)}{\partial x}\right)\right) = \frac{\partial}{\partial t}\left(C(T)Y(t)R(x)\right), \tag{5.11}$$

Heat Capacity (J/(kg*K)) as a function of Temp.			
Temp (K)	Model Fit	Fugate	Cryocomp
2.29	1.06E-03		2.25E-04
2.35	1.15E-03		2.55E-04
2.49	1.36E-03		3.76E-04
2.69	1.72E-03		5.72E-04
3	2.39E-03	2.34E-03	9.62E-04
3.54	3.92E-03	3.87E-03	1.91E-03
3.75	4.66E-03		2.50E-03
4	5.66E-03	5.61E-03	3.30E-03
4.2	6.55E-03	6.49E-03	4.00E-04
5	1.10E-02	1.10E-02	7.96E-03
5.5	1.47E-02	1.46E-02	1.14E-02
6	1.91E-02	1.89E-02	1.54E-02
8	4.53E-02	4.49E-02	4.06E-02
10	8.84E-02	8.83E-04	8.30E-02

FIG. 77. This show the model fit trend line evaluated at a variety of temperatures. At these temperatures the model value, the Cryocomp value, and the experimental Fugate data are compared. The Cryocomp values are always lower than the model and Fugate data. However the Cryocomp is always within a factor of 5 of the model and Fugate data points. The highlighted cells are the Test 7 data points.

where $\kappa(T)$ is the thermal conductivity and $C(T)$ is the specific heat. Simplifying,

$$\kappa(T)Y(t)R''(x) = C(T)\dot{Y}(t)R(x) \tag{5.12}$$

Now assume solutions for both $Y(t)$ and $R(x)$.

$$Y(t) = e^{-\alpha t}$$

$$\dot{Y}(t) = -\alpha e^{-\alpha t}$$

$$\frac{\dot{Y}(t)}{Y(t)} = -\alpha \tag{5.13}$$

$$R(x) = R_o \cos(mx - \delta)$$

$$R'(x) = -mR_o \sin(mx - \delta)$$

$$R''(x) = -m^2 R_o \cos(mx - \delta)$$

$$\frac{R''(x)}{R(x)} = -m^2 = -\frac{\alpha C(T)}{\kappa(T)} \tag{5.14}$$

An assumption necessary, which makes physical sense, is that no flux occurs at the boundaries.

$$\left.\frac{\partial T}{\partial x}\right|_{x=0} = 0 = \left.\frac{\partial T}{\partial x}\right|_{x=L}. \tag{5.15}$$

This statement tells us that δ must be zero. So the temperature can be written concisely as

$$T - T_f = R_o e^{-\alpha t} \cos\left(\sqrt{\frac{\alpha C(T)}{\kappa(T)}}x\right), \tag{5.16}$$

where T_f is the final temperature, or equilibrium temperature. In the limit as time goes to infinity, the equation goes to zero as needed. Therefore, evaluating at the boundaries,

$$T_H - T_f = R_o, \text{ at } t = 0, x = 0$$

$$T_C - T_f = R_o \cos \sqrt{\frac{\alpha C(T)}{\kappa(T)}} L, \text{ at } t = 0, x = L$$

Therefore

$$T_C - T_f = (T_H - T_f) \cos \sqrt{\frac{\alpha C(T)}{\kappa(T)}} L. \tag{5.17}$$

The path of energy will travel from high temperatures to low temperatures and reach an equilibrium point. Using this logic, eventually

$$\frac{T_H + T_C}{2} = T_f.$$

This occurs when the argument of the cosine is -1. Hence

$$\alpha = \frac{\kappa(T)\pi^2}{C(T)L^2}. \tag{5.18}$$

The relaxation time, or decay constant, is when

$$t = \frac{1}{\alpha} = \tau$$

and therefore

$$\tau = \frac{C(T)L^2}{\kappa(T)\pi^2}. \tag{5.19}$$

One might point out that the thermal conductivity and the specific heat are functions of temperature themselves. Both are assumed to have a T^3 dependence, thereby canceling out. Indeed the ratio does vary, but only mildly over a large range of temperatures and therefore can be treated as constant in this approximation. The heat capacity was used for these calculations and therefore the density of the sapphire ($3890\ kg/m^3$) was multiplied to convert from specific heat. The length of the sapphire was 10.2 cm and will be used as L. The location of the energy density is closer but this approximation is looking for the worst case scenario. At a bath temperature of 1.9 K, Figure 78 shows the relaxation time for a variety of temperatures. These times

are less than the smallest measurement made during Test 7, .070 ms. Therefore the sapphire can be treated as an isotherm for all calculations.

In test 8, the entire cavity was filled with superfluid helium to directly cool the sapphire but had degraded performance. Clearly contamination occurred inside the cavity. The helium itself has a loss tangent as well as a dielectric constant. These two factors could have an effect. Therefore a model was created to see if the field where altered significantly. The dielectric constant of helium at 2.07 K is 1.0577 according to the Cryogenic Handbook[26] and Hartung[34]. The frequency shift in the model due to the dielectric is 5.88 MHz as compared to the real cavity which shifted by 5.91 MHz. The loss tangent of the helium is debatable. The loss tangent is heavily dependent on the purity of the helium. The helium used for the experiment is from the central cryogenics facility at Jefferson Lab and should be relatively clean. The dewar is most likely the source of most of the contamination in that it is exposed to the outside world on a regular basis. Therefore the value used for the loss tangent of superfluid helium is 2×10^{-10}[34]. Using these values, and the model filled with helium, the Q value is expected to be the same as the cavity under vacuum because the losses are completely negligible. The Q of the filled cavity actually dropped to 5.77×10^{8}, meaning that contamination was introduced. The level of contamination is not known or the distribution, but the loss tangent of the helium volume, treated uniformly, would have to possess a loss tangent of 5×10^{-8} in order to produce that low Q value. This is much higher than previously measured values of the loss tangent of helium. Therefore other materials must have penetrated the mesh screen.

In Figure 79, the cavity parts are shown in the final state after the eighth test. Visually there appeared to be no contamination of any kind on the niobium surface or on the sapphire surface. A few marks on the sapphire were noticed but they are minimal. Sadly this test could have told us the lower loss tangent at 2 K, by direct

Temp	C(T)	κ(T)	τ
K	J/kg-K	W/m-K	s
2	7.40E-05	17.2	1.76E-05
3	9.62E-04	53.3	7.40E-05
4	3.30E-03	111	1.22E-04
5	7.96E-03	192	1.70E-04
6	1.54E-02	294	2.15E-04
7	2.62E-02	417	2.58E-04
8	4.06E-02	560	2.97E-04
9	5.94E-02	721	3.38E-04
10	8.30E-02	900	3.78E-04

FIG. 78. Here are the time constants showing the sapphire essentially becomes an isotherm. These values are calculated using data from Cryocomp[40] as a function of temperature.

FIG. 79. Final state of dielectric test cavity. Upper left: interior parts of cavity laid out, note the dielectric feed through is not in the port because it was replaced with mesh on the last test allowing it to freely hanging inside the cavity. Upper Right: sapphire assembled with pusher plate slightly inserted into the holder. Lower Left: Assembly view. Middle: interior of the Niobium cavity. The side port is directly up and the hook antenna can be seen at the far end, pointing azimuthally as modeled. Lower Middle: Backing plate attached to the sapphire. Here Niobium marks can be seen on the crystal surface. Also looking at the resistor leads it can be seen that the gold lead is broken. Lower Right: Good thermal contact between the sapphire and backing plate is shown, the resistors are firmly mounted, and the surface of the sapphire is still extraordinarily clean. The streaks seen are the holes in the class 100 towels used as a clean barrier on the table below the sapphire.

cooling, but rather the contamination thwarted that effort creating a lower Q.

B. Future of the Wafer Test Cavity

In the previous section several conclusions were made about the results of the eight tests performed at Thomas Jefferson National Lab. The results of test are of particular interest and necessity to determine the operational parameters of the Wafer Test Cavity. First, the dielectric constant was verified, meaning that the models produced are creating the correct field distribution and frequency. Even during the removal of material from the polish, and the addition of helium in the final experiment, all were shifted correctly in the model as they were in the measurement.

The most important aspect of this experiment is to determine the upper limit of Q for the Wafer Test cavity using the values measured in these experiments. The Q as a function of T is a critical relation to know in order to make high Q and surface resistance measurements in the wafer test cavity. The Q is of course a function of the loss tangent, that is a function of T. To push the surface field on the sample to the BCS limit it is necessary to know the highest Q that can be achieved at a high field level and the power needed to effectively fill the cavity and keep the temperature to a minimum.

This analysis was derived by Akydior Sattarov in his paper, "Direct Cooling (analytical model)"[42], and the associated code. Making the assumption that the connecting rod to the helium bath is small in mass compared to the hemisphere, it is possible to calculate the amount of heat transferred away from the sapphire hemisphere through the sapphire rod. The rod has a cross sectional area of A, and a length L. The hemisphere is a point source like object that is attached to the base of the rod. This is a very good approximation even with these general assumptions.

The amount of energy that will be transferred is

$$\dot{E}_{Therm}(T) = -\frac{A}{L}\int_{T_B}^{T} \kappa(T)dT. \tag{5.20}$$

Here T_B is the temperature of the bath and $\kappa(T)$ is the thermal conductivity that is defined as

$$\kappa(T) = k_o T^3 \tag{5.21}$$

The energy stored in the sapphire can be defined as

$$E_{Therm}(T) = m_s \int_{T_B}^{T} C(T)dT \tag{5.22}$$

where $C(T)$ is

$$C(T) = c_o T^3 \tag{5.23}$$

and m_s is the mass of the sapphire.

Dividing Eq. 5.22 by Eq. 5.20, $E_{Therm}/\dot{E}_{Therm}$, produces the cooling time constant in seconds.

$$\tau_c = \frac{L m_s c_o}{A k_o} \tag{5.24}$$

Now insert an input power, P_0, into the mushroom cavity. The electromagnetic fields are dissipated in the sapphire causing heat created by the loss tangent, δ. The change in the sapphire's temperature will be the dissipated heat generated by E_{die}, which is the fraction of the total energy (E_{total}) within the cavity that is encompassed by the sapphire, minus the amount of heat pulled out of the sapphire by the helium bath via the rod.

$$\dot{E}_{Therm} = 2\pi f E_{die}(T)\delta - \frac{A}{L}\int_{T_B}^{T} \kappa(T)dT. \tag{5.25}$$

In a similar fashion, the amount of energy stored in the cavity can be calculated,

as was done in Eqs. 5.2-5.6. Using this same technique, a solution to

$$\dot{E}_{Therm} + \frac{E_{Therm}}{\tau_c} = E_{die}\delta Q P_0 \begin{cases} 1 - e^{-\frac{\omega t}{Q}} & t \leq t_0 \\ e^{-\frac{(t-t_0)\omega}{Q}} - e^{-\frac{\omega t}{Q}} & t > t_0 \end{cases} \tag{5.26}$$

can be found,

$$E_{Therm} = E_{die}\delta Q P_0 \tau_c \begin{cases} A(t) & t \leq t_0 \\ B(t) & t > t_0 \end{cases}, \tag{5.27}$$

where

$$A(t) = \frac{Qe^{-\frac{\omega t}{Q}}}{\omega(\tau_c - \frac{Q}{\omega})} - \frac{\tau_c e^{-\frac{t}{\tau_c}}}{\tau_c - \frac{Q}{\omega}} + 1 \tag{5.28}$$

and

$$B(t) = -\frac{Qe^{-\frac{\omega(t-t_0)}{Q}}(1 - e^{-\frac{\omega t}{Q}})}{\omega(\tau_c - \frac{Q}{\omega})} + \frac{\tau_c e^{-\frac{(t-t_0)}{\tau_c}}(1 - e^{-\frac{t_0}{\tau_c}})}{\tau_c - \frac{Q}{\omega}} + 1. \tag{5.29}$$

Using these equations, the model is compared to the computational program ALGOR. Figure 80 shows the comparison of this analytical model versus a 3d FEA ALGOR model for the case of a 20 ms 400 Watt pulse on a Niobium sample, which would bring the field to the superconducting critical field. In both models a loss tangent of 1×10^{-10} was used for the sapphire. Three sets of data are located on this graph. The first is the ALGOR model and analytical model while cooled by a 1.8 K bath, and lastly the case where the hemisphere is not cooled at all.

The two models are extremely close even at such a low loss tangent, therefore the analytical model can be used for further calculations. This is needed because ALGOR does not easily allow the user to incorporate the loss tangent's temperature dependence. However since the two models are extremely close, the equation given above were solved numerically using a 4^{th} order Runge-Kutta method. This method is a numerical integration of ordinary differential equations where a trial interval is tested. Within that interval small steps taken and the function is evaluated. A weighted average is compiled from the sub-interval to give a value for the interval.

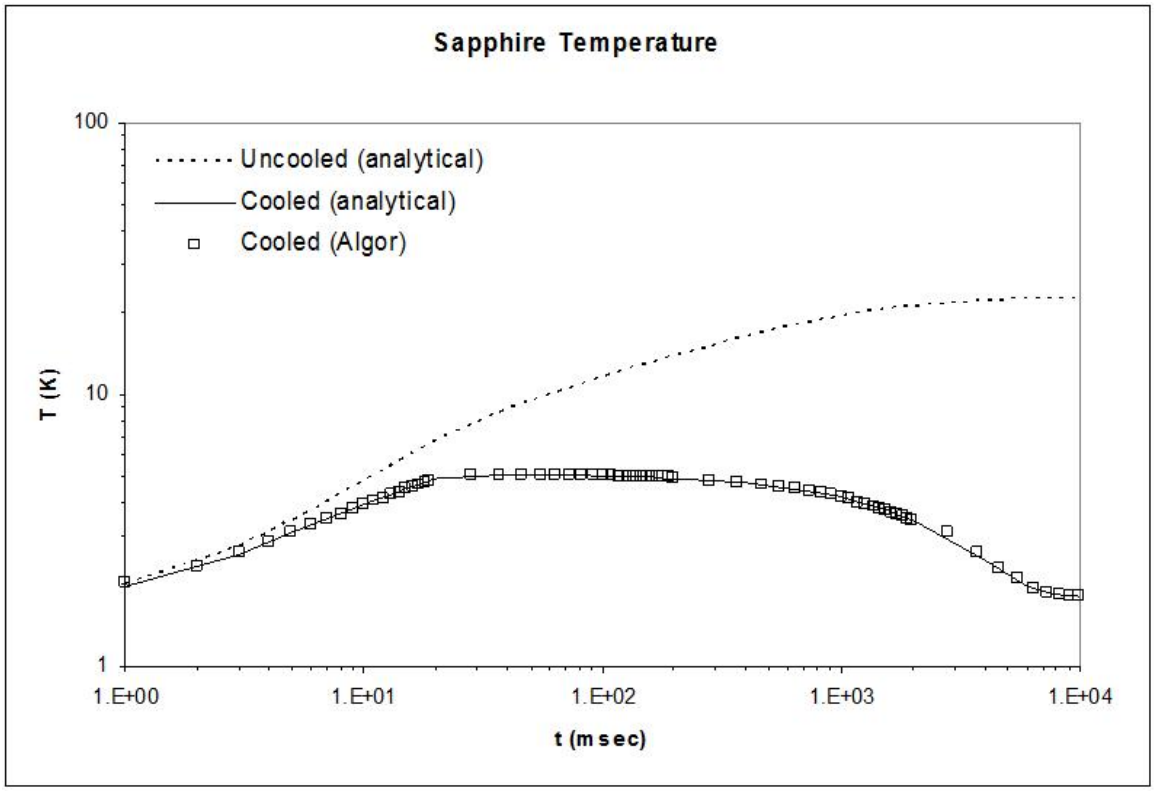

FIG. 80. Comparison of the ALGOR model to the analytical model. The hemisphere was modeled with and without cooling. The cooled version of the analytical model is compared to a computational ALGOR model and they match quite well even for a low loss tangent.

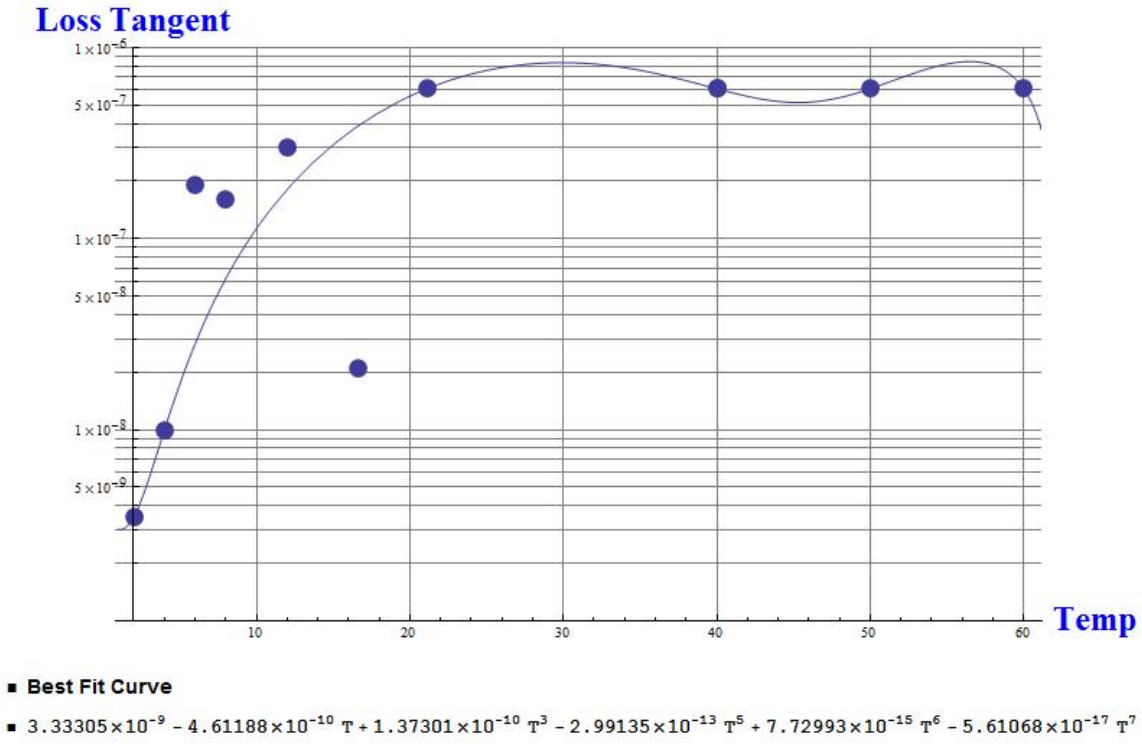

FIG. 81. A 7th order polynomial fit of the loss tangent data as a function of temperature. The points include 1×10^{-8} at 4K and 3.52×10^{-9} at 2K and data taken from the measurements made at higher temperature in Test 2. Beyond 40 K the loss tangent is assumed to level out as was seen in Figure 28.

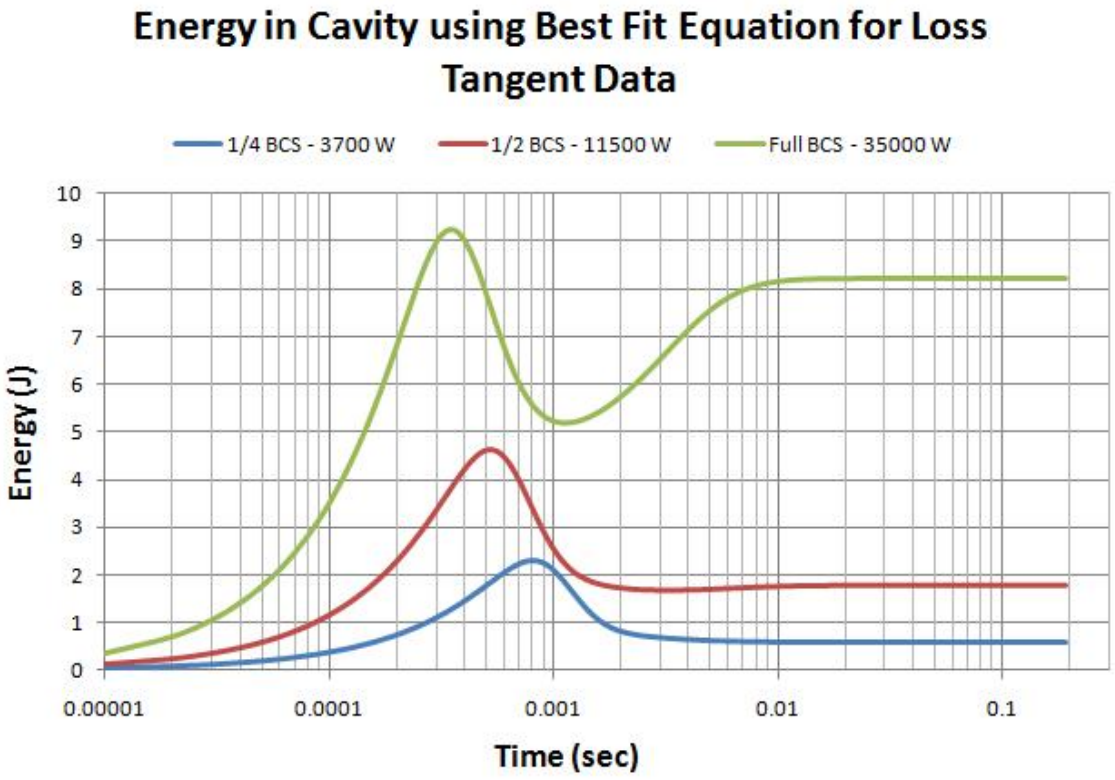

FIG. 82. The stored energy inside the cavity as a function of time and the ultimate magnetic field on the sample surface. These curves are generated by the best fit of the data presented in Figure 81

.

Utilizing this method several important trends can be shown. Using data that was collected in Test 1-8, a best fit curve was made for the loss tangent as a function of temperature, Figure 81. Using this seventh order polynomial "Fit", the cavity's stored energy (Figures 82, 83), sapphire's heating (Figure 84) and the Q of the cavity (Figure 85) were computed. The best loss tangent points for each temperature were used as references and indicate the best case scenario, that is if the loss tangent was not temperature dependent.

In Figures 82, 83, 84, and 85, the power needed to attain these fields is stated.

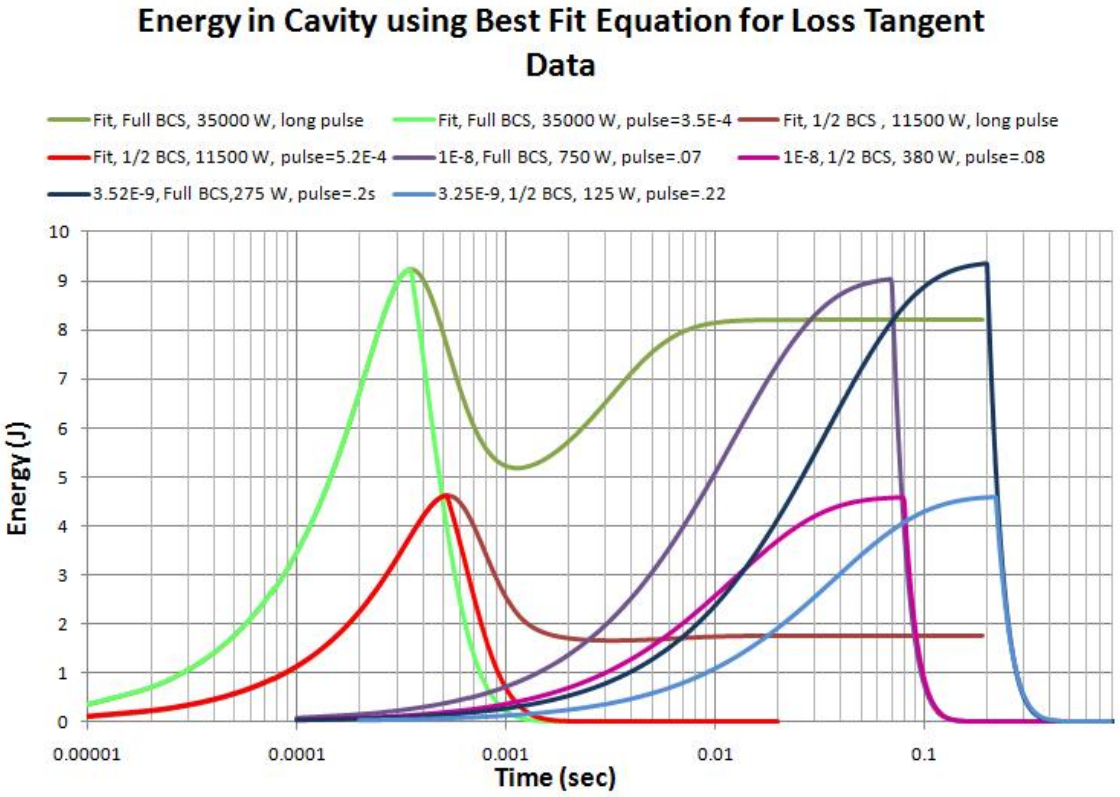

FIG. 83. Stored energy as a function of time, loss tangent, and pulse length. Each loss tangent dependency was put at the full BCS limit (230 mT) and half the BCS limit. Then when each peak reaches its apex the power is turned off, showing the decay of the stored energy inside the cavity. The "Fit" referred to is the loss tangent as a function of time created by the best fit curve in Figure 81. The other two are held at constant value for reference.

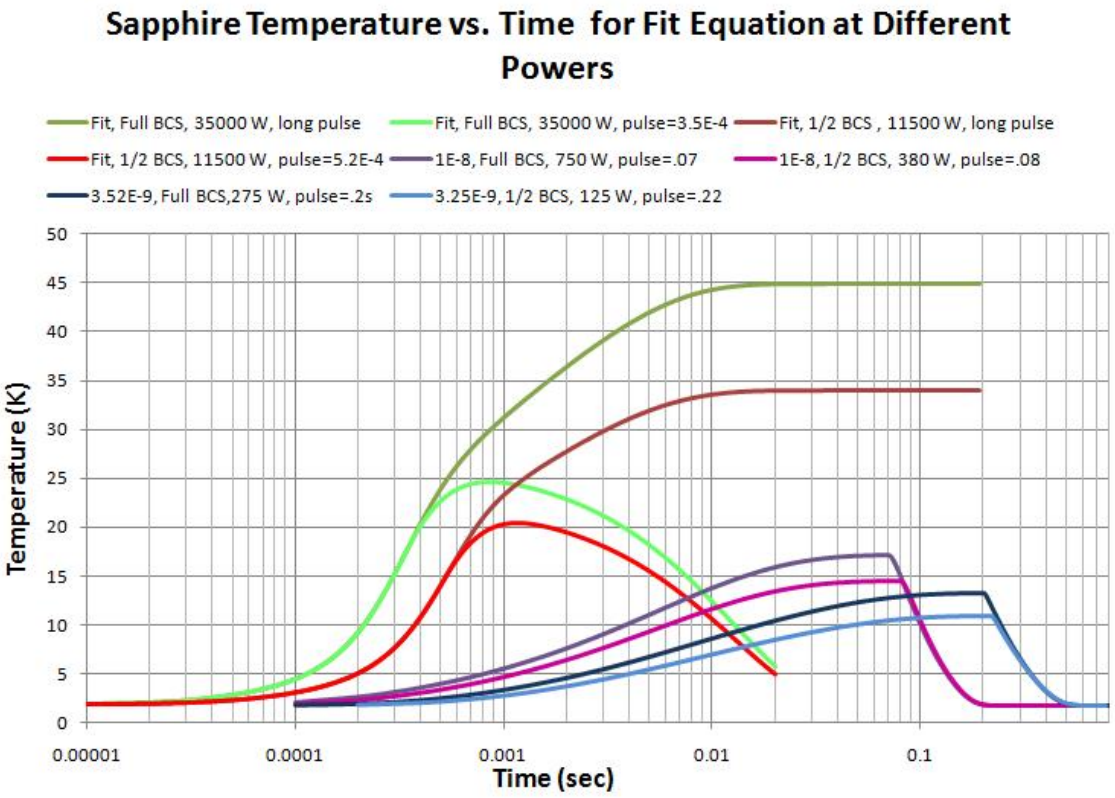

FIG. 84. Sapphire temperature rise with pulse time, input power, and stored energy level required.

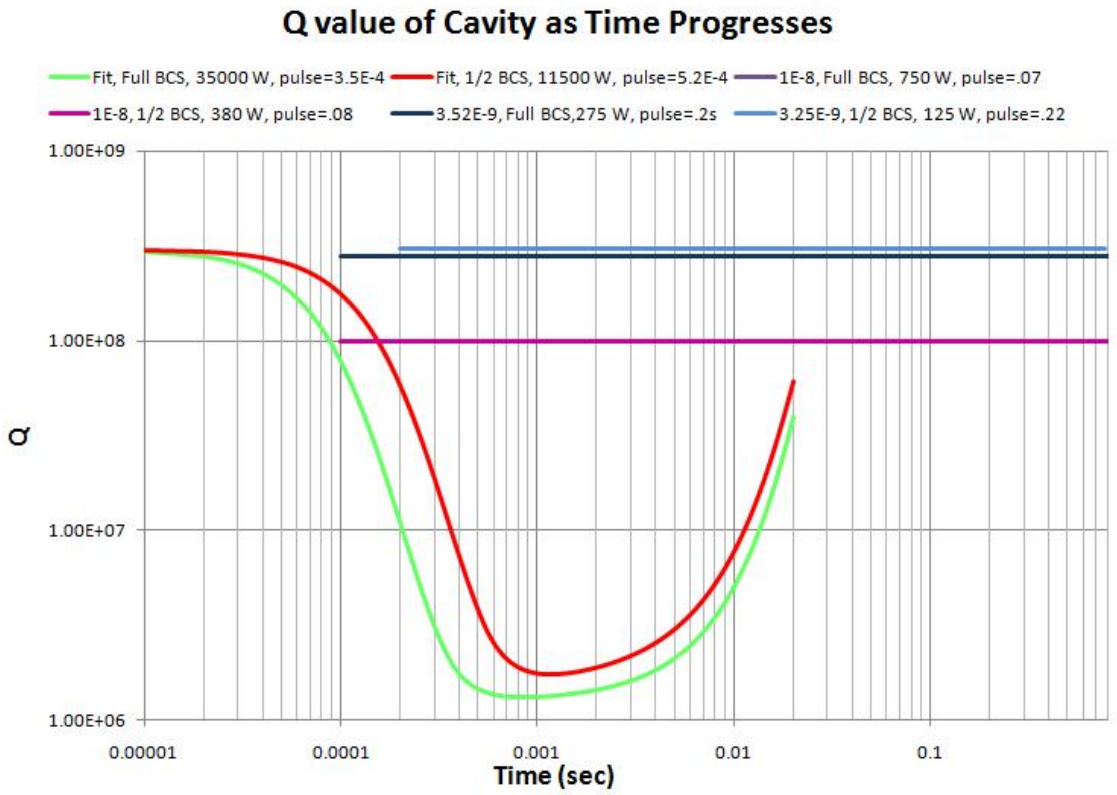

FIG. 85. Q-value of the cavity as time progresses. As should be clear, the only varying model is the Fit model. It shows that the Q drops significantly to around 1×10^6 then as the sapphire cools the Q increase once again. The time indicated is how many seconds of drive power is necessary to produce the required magnetic field.

In all cases, the shortest pulse length needed to reach the desired field is given as well. The shorter pulse produces less of a temperature rise and a higher Q. In the fitted case, a CW pulse is added to show how the sapphire reacts for long periods of time under high loss tangent conditions. Near the BCS limit there is an unusual dip followed by a rise to an equilibrium point. The dip occurring at .001 seconds is caused by the depression in the 'Fit' curve for the loss tangent, starting at 35 K. This is an artifact of the bad fit. The focus on this line should be the peak energy and location in time and the amount of power. If the cavity reaches 35 K, then this dip occurs, but the cavity is not longer useful. The figures are color coordinated for ease of comparison; the blues are the same model, as are the purples, etc.

This effectively shows that the current measured values of the sapphire loss tangent will not produce the desired effects needed for high Q operations in the Wafer Test Cavity. The field can be reached, however it requires a high power, a short RF burst source on the order of a half a millisecond, with a decay time around .15 ms. The power can be dropped quite a bit if the only a quarter of the BCS limit is needed, even then, this will be most challenging. Second, the Q is around three orders of magnitude lower than the minimum needed to effectively measure the surface resistance at the BCS limit. Third, with such power being dissipated, the amount of energy the superfluid helium can absorb is dictated by the cross section of the rod. In general, the amount of heat that can be pulled off the sapphire is .8 W/cm^2. Therefore dumping such a massive load could break down the superfluid near the surface of the exposed sapphire, causing bubbling, at which point the thermal conductivity is drastically reduced.

With the current measurements of the loss tangent over a variety of temperatures, the Wafer Test cavity may not be able to reach its design parameters. It will operate at the correct frequency, and reach field with some powerful RF sources, but will not

operate at high Q at high field.

C. Conclusions

The loss tangent of a HEMEX sapphire crystal was measured at a variety of temperatures and under several different conditions. The best measurement of the sapphire at 4.2 Kelvin was 9.1×10^{-9}, and the best measurement at 2.07 Kelvin was 3.52×10^{-9} by the network analyzer. The best measurement made by the RF system for the same temperature was 5.42×10^{-9}. The 4K measurement is consistent with previous work performed using resonant cavities, but 50 times worse than a measurement performed by calorimetry. There were several discussions about error in these measurements. Some may increase the loss tangent, and other might have hindered measuring a lower loss tangent. One such error, and precaution for the future, is to only clean the sapphire as described by NASA. The structure of the dielectric test cavity may have hindered the correct measurement of the 2 K value through heating of the sapphire and the inability to adequately cool the sapphire directly. This would be remedied in the Wafer Test cavity.

The heating of the sapphire lead to the ability to make heat capacity measurements of the sapphire at low temperatures. There is little data between 2-4 K. The calculations here fit in nicely with pre-existing data at higher temperatures with a standard T^3 dependence.

The Wafer Test cavity has a number of issues to overcome. However if a better loss tangent can be achieved by direct cooling and a cleaner experiment (less internal structure), high Q might be established at high field. A loss tangent held lower than 1×10^{-9} would create the necessary field and high Q with low power requirements. The Wafer Test cavity might be an ideal environment to perform such a second round of

testing of the sapphire's loss tangent because of the separated antennas, large crystal, and lack of internal metal structure.

These experiments have shown that low loss tangent can be achieved in resonant cavities using a large sapphire. New measurements of heat capacity have been presented. It is the hope that future work will improve on processing, design, and implementation of dielectrically loaded cavities for the understanding of material properties.

REFERENCES

[1] Interactions.org, "1st model of KEK 9-cell cavity (ICHIRO cavity)," (2005), http://www.interactions.org/imagebank/images/KE0057M.jpg.

[2] J. Ledbetter, "Single cell cavity - Niobium cavity image MISC 255," (2005), http://www1.jlab.org/ul/jpix/med/MISC_255.jpg.

[3] H. Kamerlingh Onnes, Comm. Phys. Lab. Univ. Leiden, **122**, (1911).

[4] M. Stockner, "Beam loss calibration studies for high energy proton accelerators," Ph.D. dissertation, Vienna University of Technology, (2007).

[5] J. Matricon and D. Saint-James, Physics Letters A, **24**, 5, pp. 241 – 242, (1967).

[6] S. Turner, Ed., *Proceedings of the CERN Accelerator School 1988*, vol. 89, Hamburg, West Germany, (1988). DESY, CERN.

[7] J. R. Delayen and K. W. Shepard, Applied Physics Letters, **57**, 5, pp. 514–516, (1990).

[8] D.C. Mattis and J. Bardeen, Phys. Rev., **111**, 2, pp. 412–417, (1958).

[9] H. Padamsee, J. Knobloch, and T. Hays, *RF Superconductivity for Accelerators - 2nd Edition*, (Wiley-VCH Verlag GmbH & Co., Weinheim, Germany, 2008).

[10] P. McIntyre, "Image," private communication, (2006).

[11] P. Kneisel, "Surface characterization: What has been done, what has been learnt?," in *Proceedings of SRF 2003*, DESY, Germany, pp. 387–392, (2003).

[12] Laboratory for Elementary-Particle Physics, "Multipacting," (2009), http://www.lepp.cornell.edu/Research/AP/SRF/SrfCavitiesAPrimerTwo.html.

[13] D. Lide, *CRC Handbook of Chemistry and Physics - 90th edition*, (CRC Press, Boca Raton, FL, 2010).

[14] L. Cooley, "Image," Superconducting Materials - U.S. Particle Accelerator School, Albuquerque, NM, (2009).

[15] A. Gurevich, Applied Physics Letters, **88**, 1, pp. 012511, (2006).

[16] D. Rubin, K. Green, J. Gruschus, J. Kirchgessner, D. Moffat, H. Padamsee, J. Sears, and Q. Shu, Physical Review B, **38**, 10, pp. 6538–6542, (1988).

[17] C. Nantista, S. Tantawi, J. Weisend, R. Siemann, V. Dolgashev, and I. Campisi, in *Proceedings of 2005 Particle Accelerator Conference*, Knoxville, Tennessee, pp. 4227–4229, (2005).

[18] L. Phillips, G. K. Davis, J. R. Delayen, J. P. Ozelis, and H. Wang, "A sapphire loaded TE_{011} cavity for surface impedance measurements - design, construction, and commissioning status," SRF Workshop 05, (2005).

[19] BinPing Xiao, "Information," private communication, (2009).

[20] C. Reece, "Brief review of RF measurement of SRF samples," SRF Materials Workshop, Batavia, IL, (2007).

[21] J. Hartnett, M. Tobar, D. Cros, J. Krupka, and P. Guillori, IEEE Transactions on Ultrasonics, Ferroelectrics, and Frequency Control, **49**, pp. 1628, (2002).

[22] J. Lu, X. Ren, and Q. Zhang, "A $TE_{011+\delta}$ mode sapphire resonator probe for accurate characterization of microwave surface resistance of HTS thin films," in *Proceedings of Singapore ICCS '94*, Singapore, vol. 3, pp. 959-963, (1994).

[23] H. Halama, IEEE Transactions on Nuclear Science, **18**, 3, pp. 182–192, (1971).

[24] G. Ciovati, R. Flood, C. Grenoble, L. King, P. Kneisel, M. Morrone, and M. Snyder, "Temperature mapping system for single cell cavities," Thermometry, Jefferson National Lab, Newport News, VA, (2007).

[25] J. Krupka, K. Derzakowski, M. Tobar, J. Hartnett, and R. Geyerk, Meas. Sci. Technol., **10**, pp. 387–392, (1999).

[26] J. Jensen, W. Tuttle, R. Stewart, H. Brechna, and A. Prodell, "*Cryogenic Data Handbook*," Material data handbook BNL 10200-R, Brookhaven National Laboratory, (1980).

[27] M. D. Sturge, Proceedings of the Royal Society of London. Series A, Mathematical and Physical Sciences, **246**, 1247, pp. 570–581, (1958).

[28] Anthony Mann, "Ultrastable cryogenic microwave oscillators," in *Frequency Measurement and Control*, Andre Luiten, Ed., vol. 79 of *Topics in Applied Physics*, pp. 37–67. Springer, Berlin, Germany, (2001).

[29] S.N. Buckley, P. Agnew, and G.P. Pells, Journal of Physics D: Applied Physics, **27**, pp. 2203, (1994).

[30] V.B. Braginsky, V.S. Ilchenko, and Kh.S. Bagdassarov, Physics Letters A, **120**, 6, pp. 300 – 305, (1987).

[31] R. Wang, "Information," private communication, (2010).

[32] G. Dick, "Introduction to sapphire microwave frequency sources," Frequency Control Symposium, New Orleans, LA, (2005).

[33] Y. Zhao and M. Cole, in *Proceedings from 2003 Particle Accelerator Conference*, Portland, OR, pp. 2050–2052, (2003).

[34] W. Hartung, J. Bierwagen, S. Bricker, C. Compton, T. Grimm, M. Johnson, D. Meidlinger, D. Pendell, J. Popielarski, L. Saxton, and R. C. York, in *Proceedings of LINAC 2006*, Knoxville, Tennessee, pp. 755–757, (2006).

[35] T. Powers, "Theory and practice of cavity RF test systems," in *SRF Workshop 2005*, Ithaca, NY, (2005), LEP, Cornell University, and NSF.

[36] V.B. Braginsky, V.I. Panov, and A.V. Timashov, Dokl. Akad. Nauk. SSSR, **267**, pp. 74, (1982).

[37] S. Thakoor, D.M. Strayer, G.J. Dick, and J.E. Merereau, Journal of Applied Physics, **59**, pp. 854, (1986).

[38] Blair D.G. and Jones S.K., Journal of Physics D: Applied Physics, **20**, pp. 1559, (1987).

[39] R. Q. Fugate and C. A. Swenson, Journal of Applied Physics, **40**, 7, pp. 3034–3036, (1969).

[40] Eckels Engineering, "Cryocomp," This program computes thermal properties of materials, licensed to Prof: Steven Van Sciver, (2010).

[41] P. Noyes, "Data," private communications, (2010).

[42] A. Sattarov, *Direct Cooling (analytical model)*, Department of Physics and Astronomy, Texas A&M University, 3380 University Dr. East, TI Building, College Station, Texas, (2009).

APPENDIX A

POWER SAVINGS FROM SUPERCONDUCTIVITY

In an empty cavity the geometric design specifies where the fields will be positioned, and is therefore a constant. This is called the geometric factor,

$$G = \frac{\omega\mu_0 \int_V |\mathbf{H}|^2 dV}{\int_S |\mathbf{H}|^2 dS}. \tag{A.1}$$

It defines the field structure in terms of shape only. The same cavity scaled larger will only have its frequency change. Therefore the geometry factor's value scales with size as the frequency. A second factor called the shunt impedance is important as well. It is defined as

$$R_{shunt}(\Omega) = \frac{{E_{acc}}^2 l^2}{P_{diss}} \tag{A.2}$$

and has an associated linac definition

$$r_{shunt}\left(\frac{\Omega}{m}\right) = \frac{{E_{acc}}^2}{\left(\frac{P_{diss}}{l}\right)}. \tag{A.3}$$

The true usefulness of this quantity is not in this form but rather the quantities R_{shunt}/Q_0 and r_{shunt}/Q_0 which are independent of surface resistance, just as the geometric factor.

$$\frac{R_{shunt}}{Q_0} = \frac{{E_{acc}}^2 l^2}{\omega_0 U} \;\&\; \frac{r_{shunt}}{Q_0} = \frac{{E_{acc}}^2 l}{\omega_0 U}. \tag{A.4}$$

In a standard cavity, once the field design has been optimized using the geometric factor and shunt impedance, the only variable that has a bearing on a cavity's success is the surface resistance (ignoring, of course, other material aspects described later).

For a normal conducting cavity the resistance is defined as

$$R_s = \sqrt{\frac{\mu\omega}{2\sigma}} \text{ with } \rho = \frac{1}{\sigma}. \tag{A.5}$$

The resistivity, ρ, of pure annealed copper at room temperature is 16.7×10^{-9} Ohm-m. Using Eq. A.5 it is possible to calculate the resistance at 1.3 GHz with $\mu = \mu_0$. For a copper cavity the surface resistance is 9.3 $m\Omega$. When using a copper linac system the resistance produces enormous amounts of heat and requires huge amounts of power to continuously energize the cavity. On the other hand, superconducting cavities, which operate at superfluid helium temperatures ($\approx$2 K), have resistances a million times less than copper. The dramatic decrease in resistance is what makes superconducting cavities very attractive.

In the simple case of a pill box cavity (i.e. cylinder with two caps on the end) with length, l, and radius, R, the electric and magnetic fields can be calculated analytically. Several developments of the field calculations are available, such as Classical Electrodynamics, by J.D. Jackson or RF Superconductivity for Accelerators, by H. Padamsee, as well as derivations of general solutions for transverse electric (TE) and transverse magnetic (TM) fields.

Keeping in mind the following Bessel function relations

$$J_{-v}(x) = (-1)^v J_v(x), \tag{A.6}$$

$$J_v(x_{vn}) = 0 \text{ for } (n = 1, 2, 3, ...), \tag{A.7}$$

$$J'_v(x) = \frac{1}{2}(J_{v-1} - J_{v+1}), \tag{A.8}$$

the solutions to the pillbox are quite simple. For a pill box in the TM_{010}, all but the E_z and H_ϕ terms go to zero.

$$E_z = E_0 J_0\left(\tfrac{2.40483\rho}{R}\right) e^{i\omega t} \tag{A.9}$$

$$H_\phi = -iE_0\sqrt{\frac{\epsilon_0}{\mu_0}} J_1\left(\tfrac{2.40483\rho}{R}\right) e^{i\omega t} \tag{A.10}$$

The number 2.40483 is the first zero for the lowest order Bessel function. From the

field equations the stored energy and power dissipated is quite straight forward to obtain. It can also be proven the electric and magnetic field independently produce the same stored energy, as Equation 1.4 stated, if integrated over the entire cavity. Using Eq. 1.4

$$U = \frac{\mu_0}{2} {E_0}^2 \frac{\epsilon_0}{\mu_0} \int_0^l \int_0^{2\pi} \int_0^R J_1^2 \left(\tfrac{2.405\rho}{R}\right) \rho d\rho d\phi dz = \frac{\epsilon_0}{2} {E_0}^2 \int_0^l \int_0^{2\pi} \int_0^R J_0^2 \left(\tfrac{2.405\rho}{R}\right) \rho d\rho d\phi dz. \quad \text{(A.11)}$$

This simplifies to

$$U = \pi \epsilon_0 {E_0}^2 l \int_0^R J_1^2 \left(\tfrac{2.405\rho}{R}\right) \rho d\rho = \pi \epsilon_0 {E_0}^2 l \int_0^R J_0^2 \left(\tfrac{2.405\rho}{R}\right) \rho d\rho. \quad \text{(A.12)}$$

Integrating the equations above, using the identity

$$\int z J_v^2(az) = \frac{z^2}{2} [J_v^2(az) - J_{v-1}(az) J_{v+1}(az)] \quad \text{(A.13)}$$

and inserting the limits, it becomes clear that indeed both treatments (E and H) for stored energy produce

$$U = \frac{\pi \epsilon_0 {E_0}^2 l R^2}{2} J_1^2(2.40483). \quad \text{(A.14)}$$

for the TM_{010} mode.

A similar treatment can be performed with the power dissipated (refer to Eq. 1.5). Integrating over the entire surface

$$P_{diss} = \frac{R_s E_0^2}{2} \frac{\epsilon_0}{\mu_0} (\underbrace{\int_0^l 2\pi R J_1^2(2.40483) dl}_{\text{Cylinder Walls}} + \underbrace{2 \int_0^R 2\pi J_1^2 \left(\tfrac{2.40483\rho}{R}\right) \rho d\rho)}_{2 * \text{Endcap}} \quad \text{(A.15)}$$

and reducing the equation to

$$P_{diss} = \frac{\epsilon_0 R_s E_0^2}{2\mu_0} (2\pi R J_1^2(2.40483) l + 2 * 2\pi \frac{R^2}{2} J_1^2(2.40483)), \quad \text{(A.16)}$$

then allows simplification to

$$P_{diss} = \frac{\pi \epsilon_0 R_s E_0^2 J_1^2(2.40483) R}{\mu_0}(l + R). \tag{A.17}$$

This produces a concise form of the dissipated power, where all the quantities can be experimentally measured.

Empowered with Eq. A.14 and Eq. A.17, it is straight forward to obtain the geometric factor for the pillbox cavity.

$$G = \frac{\mu_0 \omega l R}{2(l + R)}. \tag{A.18}$$

To simplify further,the relationship between the l and R must be known. As part of the field solution, the resonant frequency of the cavity independent of length is

$$\omega_{mn} = c\sqrt{\frac{x_{mn}^2}{R^2}}. \tag{A.19}$$

Here x_{mn}^2 is x_{01}^2, whose value is 2.40483 and is the first zero for the zeroth Bessel function. Using Eq. 1.1 (gives length needed for correct phase) and Eq. A.19, a relationship between l and R can be established.

$$l = \frac{\pi R}{2.40483}. \tag{A.20}$$

Inserting this relation into Eq. A.18, the geometric factor is,

$$G = 256.58(\Omega) \tag{A.21}$$

for the pill box cavity. For comparison, the geometry factor for a CEBAF single cell cavity is approximately 273 Ω.

Knowing the fields and their dependences on position and time, it is feasible to calculate the average accelerating gradient. Recalling the electric field points parallel to the axis in the TM_{010} mode, the beam will be positioned on the axis and therefore

Eq. A.9 reduces to

$$E_z = E_0 e^{i\omega t}. \tag{A.22}$$

Therefore

$$<E_{acc}>= \frac{1}{t_{cell}} \left| \int_0^{t_{cell}} E_0 e^{i\omega t} \right| = \frac{E_0}{t_{cell}} \left| 2e^{\frac{i\omega t}{2}} \left(\frac{e^{\frac{i\omega t}{2}} - e^{\frac{-i\omega t}{2}}}{2i\omega} \right) \right| = \frac{2E_0}{\omega t_{cell}} \sin \frac{\omega t_{cell}}{2} \tag{A.23}$$

simplifies, using Eq. 1.1 in the form of $t_{cell} = \pi/\omega$, to

$$<E_{acc}>= \frac{2E_0}{\pi}. \tag{A.24}$$

Now the shunt impedance can be calculated, and more importantly R_{shunt}/Q_0 can be calculated with the use of Eq. A.4, Eq. A.14, Eq. A.19, Eq. A.20, and Eq. A.24.

$$\frac{R_{shunt}}{Q_0} = \frac{149.97l}{R} = 195.92(\Omega), \tag{A.25}$$

and the linac shunt impedance is

$$\frac{r_{shunt}}{Q_0} = \frac{195.92}{l} \left(\frac{\Omega}{\mathrm{m}} \right). \tag{A.26}$$

It is now easy to solve for the power dissipated per unit length.

$$\frac{P}{l} = \frac{{E_{acc}}^2}{\frac{r_{shunt}}{Q_0} Q_0}. \tag{A.27}$$

To find the power needed to produce a 30 MV/m accelerating gradient in a 1.3 GHz single cell pillbox cavity, the dimensions of the cavity must first be known. For a 1.3 GHz cavity with maximum gradient Equations A.19 and A.20 dictate $l = 11.53cm$ and $R = 8.83cm$. To find Q_0, or quality factor, one must just divide $G = 256.58\Omega$ (geometric factor) by R_s (surface resistance). For a normal conductor such as copper, the resistance at room temp is 9.3 $m\Omega$ as Eq. A.5 illustrated. In contrast a superconductor, such as Niobium, generally has a resistance of 20 $n\Omega$. Thus the

superconducting pillbox will have a Q_0 of 1.28×10^{10} and the copper pillbox will have a Q_0 of 2.76×10^4. Clearly the superconductor has a far superior quality factor, but is it more efficient?

With the Q_0s of both cases computed and the relation Eq. A.27, the amount of power necessary to generate a 30 MV/m accelerating gradient in a normal conducting copper pillbox single cell cavity is 19.20 MW/m. For the superconducting Niobium case only 41.37 W/m is required. The power dissipated in copper case is done at room temperature with water cooling, but in the superconducting case the energy is being deposited into the liquid helium bath at 2 K. The Carnot efficiency in cooling is

$$\nu = \frac{T}{300 - T} = .0067, \tag{A.28}$$

where T is 2 K. The efficiencies of cryogenic systems are between 20-30% and efficiency of the room high power klystrons for normal conducting cavities are 50% efficient. The solutions to the pill box cavity make it evidently clear that using superconducting technology reduces the AC power required per meter by a factor of 1865 compared to the normal conducting case. In real accelerating cavities the factor is smaller. In this exercise the holes for the beam to pass were not taken into account. For superconducting cavities, the shunt impedance is reduced because typically the beam tubes are large compared to normal cavities. Even with large beam tubes the superconducting cavity is still more economical choice due to the enormous Q_0. Superconductivity is therefore quite advantageous, and understanding this physical phenomenon and the mechanisms of surface resistance is of the utmost importance to the goals of high energy research.

VITA

Nathaniel Johnston Pogue

Address:

Physics and Astronomy Department

c/o Dr. Peter McIntyre

Texas A&M University

College Station, TX 77843-4242

Email: npogue@physics.tamu.edu

Education:

B.A. in Physics from Carleton College (2003),

M.S. in Physics from Texas A&M University (2005),

Ph.D. in Physics from Texas A&M University (2011).